

UNIVERSITY OF PISA

PHD THESIS

---

**Study of real-time estimation of the  
power attenuation due to rainfall along  
microwave link**

---

*Author:*

Clio Mugnai

*Supervisor:*

Fabrizio Cuccoli

Luca Facheris

*A thesis submitted in fulfilment of the requirements  
for the degree of Doctor of Philosophy*

*in the*

Engineering  
Remote Sensing

June 2016

*“The unexamined life is not worth living”*

Socrate

# *Acknowledgements*

Firstly, I would like to thank my supervisors Fabrizio Cuccoli and Luca Facheris. They inspired me with their enthusiasm and ideas, from the earliest stages of my research.

A big thank you also to Professor Giuli, a kind person, always ready to answer my questions.

I am thankful to all of the members of the laboratory group since I joined, especially my lovely friend Francesca, with me since 10<sup>th</sup> September 2001.

I will also thank my mother, father, brother and my friends for their support.

Finally, my biggest thank you goes to my husband Lorenzo, my love, my best friend, my life.

*Clio*

# Contents

Acknowledgements	ii
Contents	iii
List of Figures	v
List of Tables	ix
Abbreviations	x

Introduction	xii
--------------	-----

<b>1 Rainfall rate estimation methods</b>	<b>1</b>
1.1 Raingauges and disdrometers . . . . .	1
1.1.1 Pros and cons . . . . .	2
1.2 Weather Radar . . . . .	2
1.2.1 Pros and cons . . . . .	4
1.3 Microwave link . . . . .	5
1.3.1 Tomographic Approach . . . . .	6
1.3.2 Pros and cons . . . . .	6
1.4 Satellite systems . . . . .	7
<b>2 Satellite link estimation approach</b>	<b>9</b>
2.1 K <sub>A</sub> -band satellite system . . . . .	9
2.1.1 Eutelsat KA-SAT Satellite . . . . .	10
2.1.2 Tooway Kit . . . . .	10
2.2 Satellite system employment . . . . .	11
2.3 Physical approach . . . . .	14
2.3.1 Attenuation of Earth-Space link . . . . .	14
2.3.2 Rain attenuation $aR^b$ . . . . .	15
<b>3 Measurement System</b>	<b>18</b>
3.1 Test Site . . . . .	18
3.2 Employed devices . . . . .	19
3.3 Data processing software . . . . .	20

<b>4</b>	<b>RET-AB Algorithm</b>	<b>22</b>
4.1	RET-AB 1.0	22
4.1.1	Data Processing Chain	22
4.1.2	Measurement campaign	25
4.1.3	Considerations	26
4.2	RET-AB 2.0	27
4.2.1	Cloud Height	27
4.2.1.1	Metar Bulletins	27
4.2.1.2	LIDAR	28
4.2.2	Temporal Resolution	29
4.2.2.1	Variation of Integration Time	30
4.2.3	Spatial Resolution	30
4.2.3.1	Kriging Technique	30
<b>5</b>	<b>Measurements Campaign and Results</b>	<b>44</b>
5.1	27 December 2014	45
5.2	25 March 2015	60
5.3	4 April 2015	76
<b>6</b>	<b>Conclusions and Further Developments</b>	<b>90</b>
6.1	Limits of the system	91
6.2	Validation of the results	91
6.2.1	Ad-hoc rain gauges network	92
6.2.2	Computation of $a$ and $b$ parameters	92
6.3	Future developments	92
6.3.1	Frequency diversity techniques	92
6.3.2	Investigation of other estimation methods for clouds height	93
6.3.3	Data fusion	93
6.3.4	Other improvements	94

# List of Figures

2.1	KA-SAT coverage over Europe . . . . .	11
2.2	Satellite system scheme . . . . .	12
2.3	Modem GUI interfaces . . . . .	12
2.4	Tooway2 transmitted power (IF) recorded during a rainy day . . . . .	13
2.5	Tooway2 transmitted power (IF) recorded during a rainy and a dry day . . . . .	13
2.6	Geometry of the satellite link . . . . .	14
3.1	Data Acquisition Block Diagram . . . . .	18
3.2	Position of the earth station, dislocation of the rain gauges and direction of the satellite link (green line). Google earth image. . . . .	19
4.1	Data processing chain . . . . .	23
4.2	Cumulated rainfall rate over 15' - 2 May . . . . .	32
4.3	Cumulated rainfall rate over 15' - 25 June . . . . .	33
4.4	Cumulated rainfall rate over 15' - 26 June . . . . .	34
4.5	Cumulated rainfall rate over 15' - 29 June . . . . .	35
4.6	Variation of rain rate depending on $h_R$ - 2 May . . . . .	36
4.7	Variation of rain rate depending on $h_R$ - 25 June . . . . .	36
4.8	Variation of rain rate depending on $h_R$ - 26 June . . . . .	37
4.9	Variation of rain rate depending on $h_R$ - 29 June . . . . .	37
4.10	Variation of rain rate depending on $a$ and $b$ parameters - 2 May . . . . .	38
4.11	Variation of rain rate depending on $a$ and $b$ parameters - 25 June . . . . .	38
4.12	Variation of rain rate depending on $a$ and $b$ parameters - 26 June . . . . .	39
4.13	Variation of rain rate depending on $a$ and $b$ parameters - 29 June . . . . .	39
4.14	An example of METAR report (Firenze Peretola airport) . . . . .	40
4.15	LIDAR plots: Signal and Depolarization . . . . .	40
4.16	Variation of cloud layer $h_R$ . . . . .	41
4.17	Variation of integration time . . . . .	41
4.18	Cumulated rainfall rate recorded by regional rain gauges . . . . .	42
4.19	Comparison of rain rate: measurements by rain gauges vs interpolation with kriging technique . . . . .	43
5.1	Rain rate measured by rain gauges . . . . .	46
5.2	Rainfall rate: variation of cloud layer $h_R$ - Fixed vs METAR vs LIDAR . . . . .	47
5.3	Rain rate measured by rain gauges vs estimated with RET-AB . . . . .	48
5.4	Rain rate measured by rain gauges vs estimated with RET-AB . . . . .	49
5.5	Rain rate measured by rain gauges vs estimated with RET-AB . . . . .	50
5.6	Rain rate measured by Florence University rain gauge vs estimated with RET-AB . . . . .	51

5.7	Rain rate measured by Florence City Center rain gauge vs estimated with RET-AB . . . . .	51
5.8	Rain rate measured by Florence Genio Civile rain gauge vs estimated with RET-AB . . . . .	52
5.9	Rain rate measured by Florence Ximenian Observatory rain gauge vs estimated with RET-AB . . . . .	52
5.10	Rain rate measured by LaMMA Consortium Sesto Fiorentino rain gauge vs estimated with RET-AB . . . . .	53
5.11	Rainfall rate evaluated at three different integration times . . . . .	53
5.12	Comparison of rain rate: estimation with RET-AB vs interpolation with kriging technique . . . . .	54
5.13	Rainfall rate evaluated at three different integration times vs measurement by Florence University rain gauge . . . . .	55
5.14	Rainfall rate evaluated with 7.5' integration times vs measurement by Florence University rain gauge . . . . .	55
5.15	Rainfall rate evaluated at three different integration times vs measurement by Florence City center rain gauge . . . . .	56
5.16	Rainfall rate evaluated with 7.5' integration times vs measurement by Florence City center rain gauge . . . . .	56
5.17	Rainfall rate evaluated at three different integration times vs measurement by Florence Genio Civile rain gauge . . . . .	57
5.18	Rainfall rate evaluated with 7.5' integration times vs measurement by Florence Genio Civile rain gauge . . . . .	57
5.19	Rainfall rate evaluated at three different integration times vs measurement by Florence Ximenian Observatory rain gauge . . . . .	58
5.20	Rainfall rate evaluated with 7.5' integration times vs measurement by Florence Ximenian Observatory rain gauge . . . . .	58
5.21	Rainfall rate evaluated with 7.5' integration times vs measurement by LaMMA Consortium Sesto Fiorentino rain gauge . . . . .	59
5.22	Rainfall rate evaluated with 7.5' integration times vs measurement by LaMMA Consortium Sesto Fiorentino rain gauge . . . . .	59
5.23	Rain rate measured by rain gauges . . . . .	61
5.24	Rainfall rate: variation of cloud layer $h_R$ - Fixed vs METAR vs LIDAR . . . . .	62
5.25	Rain rate measured by rain gauges vs estimated with RET-AB . . . . .	63
5.26	Rain rate measured by rain gauges vs estimated with RET-AB . . . . .	64
5.27	Rain rate measured by rain gauges vs estimated with RET-AB . . . . .	65
5.28	Rain rate measured by Florence University rain gauge vs estimated with RET-AB . . . . .	66
5.29	Rain rate measured by Florence City Center rain gauge vs estimated with RET-AB . . . . .	66
5.30	Rain rate measured by Florence Genio Civile rain gauge vs estimated with RET-AB . . . . .	67
5.31	Rain rate measured by Florence Ximenian Observatory rain gauge vs estimated with RET-AB . . . . .	67
5.32	Rain rate measured by LaMMA Consortium Sesto Fiorentino rain gauge vs estimated with RET-AB . . . . .	68
5.33	Rainfall rate evaluated at three different integration times . . . . .	68

5.34 Comparison of rain rate: estimation with RET-AB vs interpolation with kriging technique . . . . .	69
5.35 Rainfall rate evaluated at three different integration times vs measurement by Florence University rain gauge . . . . .	70
5.36 Rainfall rate evaluated with 7.5' integration times vs measurement by Florence University rain gauge . . . . .	70
5.37 Rainfall rate evaluated at three different integration times vs measurement by Florence City center rain gauge . . . . .	71
5.38 Rainfall rate evaluated with 7.5' integration times vs measurement by Florence City center rain gauge . . . . .	71
5.39 Rainfall rate evaluated at three different integration times vs measurement by Florence Genio Civile rain gauge . . . . .	72
5.40 Rainfall rate evaluated with 7.5' integration times vs measurement by Florence Genio Civile rain gauge . . . . .	72
5.41 Rainfall rate evaluated at three different integration times vs measurement by Florence Ximenian Observatory rain gauge . . . . .	73
5.42 Rainfall rate evaluated with 7.5' integration times vs measurement by Florence Ximenian Observatory rain gauge . . . . .	73
5.43 Rainfall rate evaluated with 7.5' integration times vs measurement by LaMMA Consortium Sesto Fiorentino rain gauge . . . . .	74
5.44 Rainfall rate evaluated with 7.5' integration times vs measurement by LaMMA Consortium Sesto Fiorentino rain gauge . . . . .	74
5.45 The map of the urban area. Rain gauges, Florence airport, Earth station and satellite link are poited out . . . . .	75
5.46 Rain rate measured by rain gauges . . . . .	77
5.47 Rainfall rate: variation of cloud layer $h_R$ - Fixed vs METAR . . . . .	78
5.48 Rain rate measured by rain gauges vs estimated with RET-AB . . . . .	79
5.49 Rain rate measured by Florence University rain gauge vs estimated with RET-AB . . . . .	80
5.50 Rain rate measured by Florence City Center rain gauge vs estimated with RET-AB . . . . .	80
5.51 Rain rate measured by Florence Genio Civile rain gauge vs estimated with RET-AB . . . . .	81
5.52 Rain rate measured by Florence Ximenian Observatory rain gauge vs estimated with RET-AB . . . . .	81
5.53 Rain rate measured by LaMMA Consortium Sesto Fiorentino rain gauge vs estimated with RET-AB . . . . .	82
5.54 Rainfall rate evaluated at three different integration times . . . . .	82
5.55 Comparison of rain rate: estimation with RET-AB vs interpolation with kriging technique . . . . .	83
5.56 Rainfall rate evaluated at three different integration times vs measurement by Florence University rain gauge . . . . .	84
5.57 Rainfall rate evaluated with 7.5' integration times vs measurement by Florence University rain gauge . . . . .	84
5.58 Rainfall rate evaluated at three different integration times vs measurement by Florence City center rain gauge . . . . .	85
5.59 Rainfall rate evaluated with 7.5' integration times vs measurement by Florence City center rain gauge . . . . .	85

---

5.60	Rainfall rate evaluated at three different integration times vs measurement by Florence Genio Civile rain gauge . . . . .	86
5.61	Rainfall rate evaluated with 7.5' integration times vs measurement by Florence Genio Civile rain gauge . . . . .	86
5.62	Rainfall rate evaluated at three different integration times vs measurement by Florence Ximenian Observatory rain gauge . . . . .	87
5.63	Rainfall rate evaluated with 7.5' integration times vs measurement by Florence Ximenian Observatory rain gauge . . . . .	87
5.64	Rainfall rate evaluated with 7.5' integration times vs measurement by LaMMA Consortium Sesto Fiorentino rain gauge . . . . .	88
5.65	Rainfall rate evaluated with 7.5' integration times vs measurement by LaMMA Consortium Sesto Fiorentino rain gauge . . . . .	88

# List of Tables

2.1	KA-SAT features . . . . .	10
3.1	Rain gauge stations . . . . .	19
4.1	Features of the 2014 rain events . . . . .	25
4.2	Features of the IFAC CNR LIDAR . . . . .	28
5.1	Features of the 2015 rain events . . . . .	44

# Abbreviations

<b>ACM</b>	<b>A</b> daptive <b>C</b> oding and <b>M</b> odulation
<b>AGL</b>	<b>A</b> bove <b>G</b> round <b>L</b> evel
<b>CNIT</b>	<b>C</b> onsorzio <b>N</b> azionale <b>I</b> nteruniversitario per le <b>T</b> elecomunicazioni
<b>CNR</b>	<b>C</b> onsorzio <b>N</b> azionale di <b>R</b> icerca
<b>CPE</b>	<b>C</b> ustomer <b>P</b> remises <b>E</b> quipment
<b>DSD</b>	<b>D</b> rop <b>S</b> ize <b>D</b> istribution
<b>GUI</b>	<b>G</b> raphical <b>U</b> se <b>I</b> nterface
<b>HTS</b>	<b>H</b> igh <b>T</b> roughput <b>S</b> atellite
<b>ICAO</b>	<b>I</b> nternational <b>C</b> ivil <b>A</b> viation <b>O</b> rganization
<b>IF</b>	<b>I</b> ntermediate <b>F</b> requency
<b>IFAC</b>	<b>I</b> stituto <b>F</b> isica <b>A</b> pplicata <b>C</b> arrara
<b>LIDAR</b>	<b>L</b> ight <b>D</b> etection <b>A</b> nd <b>R</b> anging
<b>METAR</b>	<b>M</b> ETeorological <b>A</b> ir <b>R</b> eport
<b>NOC</b>	<b>N</b> etwork <b>O</b> perating <b>C</b> enter
<b>NWS</b>	<b>N</b> ational <b>W</b> eather <b>S</b> ervice
<b>QoS</b>	<b>Q</b> uality of <b>S</b> ervice
<b>RADAR</b>	<b>R</b> Adio <b>D</b> etection <b>A</b> nd <b>R</b> anging
<b>RaSS</b>	<b>R</b> and <b>S</b> urveillance <b>S</b> ystems
<b>RET-AB</b>	<b>R</b> ainfall rate <b>E</b> sTimation <b>A</b> ttenuation <b>B</b> ased
<b>RF</b>	<b>R</b> adio <b>F</b> requency
<b>SNMP</b>	<b>S</b> imple <b>N</b> etworkize <b>M</b> anagement <b>P</b> rotocol
<b>SNR</b>	<b>S</b> ignal <b>N</b> oise <b>R</b> atio
<b>TCP</b>	<b>T</b> ransmission <b>C</b> ontrol <b>P</b> rotocol

*To my family. . .*

# Introduction

The problem of rainfall monitoring is a topic task in areas where precipitations are characterized by high intensity and very fast development. Tuscany is a region interested by flood and logistic problems due to strong intensity storms especially in autumn. Some events characterized by floods can be cited:

- Florence, 1966
- Maremma, 2012
- Siena, 2015

The 1966 flood of the Arno River in Florence killed 101 people and damaged or destroyed millions of masterpieces of art and rare books. It is considered the worst flood in the city's history since 1557. In august 2015, a very fast and strong storm of rain and hail, named "*bomba d'acqua*", hit some quarters of Florence: residential, commercial, and public buildings, as well as critical infrastructure such as transportation, water, energy, and communication systems have been damaged or destroyed. Wind and water can be tremendously destructive and deadly.

The main problem connected to flood or other natural events is the fact that citizens are not prepared and aware to deal with that kind of emergency; furthermore, regional authorities are not able to face off the situation, because the emergency measures in place are not enough to handle such critical situations.

All of these problems are related to the time delay characterizing the alarm to citizens, caused by the lack of instrumentations for real time monitoring and warning alert. The topic task is to find a rainfall method that can permit to monitor in real time risk areas so that, in case of hazard, citizens can be alerted earlier.

Nowadays rain gauges, weather radar, microwave networks and satellite sensing are the most employed approaches to the task of rainfall monitoring. Unfortunately, all of these methods show substantial weakness that, in different ways, limit their employment in

any scenario. For example, the beam of the weather radar can be partially or totally blocked by surrounding reliefs within regions characterized by a particularly complex orography. Data gathered through a rain gauges network are generally affected by long sampling time (typically over 15 min.), geographically restricted validity and scarce accuracy, especially in case of weather event marked by mixed hydrometeors. For these and many other reasons, such approaches are not always suitable, most of all in areas where precipitations are characterized by high intensity and fast development. An alternative approach to the estimation of rainfall exploits the rain-induced attenuation along terrestrial and satellite microwave links: these methods are more suitable when real-time data over large areas are required, especially whenever multiple links that cover the same region are available. Actually, if multiple links forming a dense network are simultaneously available (generally this is true in urban areas), then it is possible to apply tomographic inversion algorithms to obtain a real time estimation of rainfall rate fields over a large area. Although the attenuation of a microwave link is not entirely due to rain, and generally the precipitation events are characterized by a simultaneous multiple status of water, from the point of view of both the probability of occurrence and the severity of effect, the rain scattering is however the most important of the hydrometeor phenomena, especially for operative frequencies above 10 GHz. In literature, many publications relative to the relation between the attenuation of microwave signals and the rain rate can be found.

In the last two years a novel method for rainfall monitoring has been proposed [1], [2]: it is based on the employment of an opportunistic commercial kit for satellite internet services, operating in K<sub>A</sub>-band. Since the signals within this band are particularly affected by hydrometeors fading, in order to guarantee a continuity of the service in all-weather conditions, the employed device needs to carry out a continuous adjustment of the uplink transmitted power in function of the intensity of the signal received from the satellite. This mechanism, that gives to the service a certain weather independency, is the basic principle of the proposed low-cost digital rain gauge. This power-control technique, essential for K<sub>A</sub>-band satellite internet applications, can be exploited to measure in real time the signal fading induced by hydrometeors along the Tropospheric segment of the Earth-space link.

In the first chapter section the actual rainfall rate estimation methods (i.e. rain gauges, weather radar, microwave networks and satellite systems) are described, focusing on pros and cons of each one. Then, chapter 2 outlines the estimation approach: the considered system, the geometry of the satellite-link scenario and the adopted physical/mathematical model that associates the power attenuation of the microwave link to the rain rate are illustrated; the sensors that provide the cumulated rainfall are employed to validate the results. In chapter 3 the measurement system is explained: test site, employed

devices and software. Chapter 4 presents the proposed algorithm, named ***Rainfall rate EsTimation - Attenuation Based (RET-AB)***, highlighting the digital signal processing carried out on the gathered data and the first measurement campaign held in 2014: the collected data of three different rain events are processed and compared with the cumulated rainfall values from the Regional Monitoring Service. Some considerations lead to the definition of the second version of RET-AB. In chapter 5 are shown the results obtained during the second measurement campaign, where gathered data are processed with the improved algorithm (RET-AB 2.0). The last chapter is dedicated to the interpretation of the results and to some consideration about the algorithm and its potentialities as a real time tool for the remote sensing of rainfall.

# Chapter 1

## Rainfall rate estimation methods

This chapter investigates the different methods of rainfall rate estimation using common measurement instruments such as raingauges, weather radar, microwave links and satellite systems.

### 1.1 Raingauges and disdrometers

A rain gauge is a meteorological instrument to measure precipitation, in millimetres, in a certain time period. The rain gauge was defined by NWS in the beginning of the 20th century. It consists of a funnel graduated cylinder, which fits inside a larger container. If the rainwater overflows the graduated inner cylinder, the larger container will catch it. Some gauges are calibrated to allow the amount of rainfall to be read directly in the graduated cylinder; with others it must be calculated from the depth of water in the container and the dimensions of the funnel [3].

Nowadays, the tipping bucket rain gauge is the most common instrument (it is the one owned by regional authorities): it consists of a funnel that collects the precipitation into a small container. After a pre-set amount of precipitation falls, the lever tips, dumping the collected water and sending an electrical signal. Since this kind of gauge is digital, the amount of water is electronically recorded or transmitted to a remote collection station.

Rain gauges are widely installed in every meteorological station. It is possible to assume that one millimetre of measured precipitation is the equivalent of one litre of rainfall per square meter.

### 1.1.1 Pros and cons

The main advantage of rain gauge is its portability. Thanks to limited dimensions it can be installed everywhere (far from obstacles blocking the rain). The disadvantages are:

- it is affected by time delay (the measurements are collected at least every 10 minutes);
- it is not possible to characterize the precipitation (rain, snow, hail);
- the measurements are not too much accurate, providing misleading information about the real intensity of a storm (especially in case of snowfall or heavy rain events);
- the cumulative measured values are point-like (the amount of rain is referred to a localized area);
- the costs of handling and maintenance are high, especially in case of a dense network of sensors;
- the data should be verified by the operator before the release.

## 1.2 Weather Radar

RADAR technology is utilized in many fields since the World War II. In recent years, this technique has been employed also in remote meteorological observation: the backscattered energy is converted to rainfall intensity, providing indirect measurements of amount of precipitation. They operate in C and S band; recently X-band radars have been developed and installed on aircrafts because of their limited size.

Weather radar measures the power returns, identified as the *reflectivity factor*  $Z$ . This will be converted to *rain rate*  $R$  by using the empirical relation  $Z - R$ .

The meteorological radar equation [4] is the measure of the received power from a distribution of meteorological targets:

$$P_R = \frac{P_T G_{max}^2 \pi^3 \theta \varphi h |K|^2 Z}{1024 \ln(2) \lambda^2 r^2}$$

where:

- $P_R$  is the received power

- $P_T$  is the transmitted power
- $G_{max}$  is the antenna gain
- $\theta$  is the horizontal antenna beam width
- $\varphi$  is the vertical antenna beam width
- $h$  is the pulse length
- $|K|$  is the dielectric constant
- $r$  is the range
- $\lambda$  is the wavelength
- $Z$  is the reflectivity factor

Radar reflectivity factor is expressed in  $[mm^6m^{-3}]$  and defined as:

$$Z = \frac{\sum_i D_i^6}{V}$$

It is the sum of all drop diameters within a unit volume; it can contain many different sizes of raindrops, whose distribution is known as *Drop Size Distribution*  $N(D)$ . Radar reflectivity can be expressed as:

$$Z = \int_0^\infty D^6 N(D) dD$$

By using the measured  $Z$  it is possible to calculate the rain rate, [5]:

$$Z = aR^b$$

$a$  and  $b$  are parameters whose values may vary with precipitation type and operative frequencies [6].

The main problem concerning the inversion of the power-law equation is the characterization of hydrometeors. In fact, when the radar beam encounters hail the reflectivity will be affected, because it tends to have much larger diameters than rain drops. A similar problem occurs in case of snow and ice, where reflectivity can be modified by the dielectric constant or by the larger size of such particles. Another particular situation is related to snow flakes: reflectivity increases considerably when the drops have the size of snow but the gains the dielectric constant of water.

In order to reduce such problems and improve the rainfall estimation the dual-polarization technology has been developed for weather radar [7]. By employing this technique, rainfall rate estimations could be improved. The *differential reflectivity* ( $Z_{DR}$ ) is defined as the ratio of reflectivity at horizontal and vertical polarizations:

$$Z_{DR} = 10 \log \frac{Z_{HH}}{Z_{VV}}$$

This parameter is independent of drop concentration and gives information on the size of the drops. With knowledge of  $Z_{DR}$  it is possible to discern water for ice drops, hence allowing more accurate rainfall rate estimation. All the polarimetric parameters, measured by dual-polarization radar, are listed below:

- Reflectivity  $Z_{HH}$
- Differential Reflectivity  $Z_{DR}$
- Linear Depolarization Ratio  $LDR$
- Specific Differential Phase  $K_{DP}$
- Correlation Coefficient  $\rho_{HV}$

Such parameters can be employed to hydrometeor classification.

### 1.2.1 Pros and cons

Several factors may limit the advantages brought by range resolution and instantaneous sampling, that may lead to an incorrect interpretation of the real situation and to a dangerous underestimate or even a missing detection of the risk induced by precipitation.

- precipitations are sampled at an excessive height: that is due to the distance of the radar site and/or the particular territorial orography;
- distance may limit the resolution in the cross-range (azimuth) direction, preventing the observers from appreciating at full the real importance of critical localized events;
- the possibility of loss of power, due to orography, can reduce the intensity of precipitation;
- the minimum height above ground allowing radar visibility may become considerable, due to orography.

### 1.3 Microwave link

In recent years some researchers have proposed terrestrial microwave links as a low-cost method for regional rainfall monitoring. Nowadays, commercial microwave radio links form a dense cellular communication network, offering a great potential for the use of this system in combination with other measurement devices, such as rain gauges or weather radars [8], [9], [10].

Mobile phone network is composed by a system of antennas (transmitters and receivers): when the electromagnetic waves pass between them, the precipitation creates an attenuation of signal (decreasing of received signal level means increasing of rainfall intensity). A part of the energy of electromagnetic waves is absorbed or scattered by the raindrops, so the relative decreasing of the power of the signal per unit of distance, known as *specific attenuation* (measured in  $[dB/km]$ ), could be used to estimate intensity of the rainfall between transmitting and receiving antennas (measured in  $[mm/h]$ ). Records on transmitted and received power are collected at a control center of the service provider. Commercial links operate at frequencies between 10 GHz and 40 GHz, so the wavelength  $\lambda \leq 3cm$  is roughly in the same order of the magnitude of raindrop diameter  $D \leq 5mm$  and losses due to rain are the main cause of signal attenuation (after free space losses). Hence, attenuation by hydrometeors can be evaluated using the Mie solution to Maxwell's equations. The relation between rain rate  $R$  and attenuation  $A$  can be approximated by the aforementioned power law [5].

Some studies proposed tests in order to evaluate the goodness of this cost-effective rainfall monitoring [11].

- Netherland, October-November 2003: data are collected using two links operating at 38 GHz during eight rain events. The number of links the commercial networks in Netherland (territory of 35,000 km<sup>2</sup>) is more or less of 12,000, with an average length of links of 3-4 km, so the relative density is approximately 1 km/km<sup>2</sup> [12].
- Southern Germany, July-October 2010: data are collected for five commercial links and compared with those provided by rain gauges and weather radar. The overall performance is good with correlation (0.8 with rain gauges and 0.84 with weather radar) even if some detection errors remain [13], citechw2.

In the three case studies listed above, the results of the measurements outlines that microwave links can offer a great potential to improve continuously measurements of terrestrial rainfall, especially in combination with existing monitoring systems.

### 1.3.1 Tomographic Approach

Other studies proposed a tomographic approach to reduce uncertainties in individual link and improve accuracy of the measurements.

The basic idea of this remote sensing approach for rainfall rate estimation in real time is to exploit the correlation between the specific attenuation, affecting the electromagnetic waves propagating in rainfall, and the rainfall intensity. Total attenuation measurements made along multiple terrestrial paths forming a network then could be exploited to provide an estimate of the rainfall field over the area containing that network. Since the wavelength are in the order of magnitude of centimeters, the uncertainties in the power law relation do not exceed approximately 10%. Operative frequencies of radiobase network were 18, 23 and 35 GHz and microwave path link was not longer than 15 km. The primary objective of the network is the definition of an efficient and robust strategy of reconstruction and tracking of rainfall fields, based on a stochastic solution search technique and followed by a finite sequence of optimization and control phases. This is possible thanks to the topology of the urban radiobase station networks, more and more dense, that can permit the tomographic inversion and reconstruction of rainfall field. Such algorithm has been tested many times on simulated specific attenuation maps based on true polarimetric weather radar data (data gathered by the POLAR55 C polarimetric radar located in Rome) [14], [15].

### 1.3.2 Pros and cons

The main advantages deriving from exploitation of microwave links for indirect measurements of rainfall are:

- the effective-cost to create a system of measurement is quite to zero, because all the devices are already present in the territory;
- the available dense network permit to monitor the rainfall precipitations over a wide area;
- the network is available everywhere, so there are not problems due to obstacles or complex orography;
- it is possible to obtain high spatial resolution measurements;
- it is possible to obtain high temporal resolution measurements [16].

On the contrary, this method have also disadvantages:

- uncertainties the accuracy of electronic system for attenuation measurement;
- uncertainties due to inverse tomographic reconstruction;
- uncertainties due to water vapour and scintillation effects [17];
- uncertainties due to drop size distribution (leading to a not perfect calculation of  $a$  and  $b$  parameters in power law relation) [18], [19].

But, the main disadvantage for the research is related to the lack of attenuation measurements: in Italy, cellular communication companies do not provide those data and it is impossible to evaluate the goodness of the algorithms, as tomographic inversion, that could be used for a real time monitoring.

## 1.4 Satellite systems

The last method for rainfall measurements is represented by meteorological satellites [20]. The primary scope of satellite rainfall monitoring is to provide information on rainfall occurrence, amount and distribution over the globe. This is due to the fact that the distribution of rain gauges and weather radars is not so wide to cover the also the oceans and other parts of the world not provided with those devices.

There are two types of meteorological satellites:

- Geostationary satellites
- Polar orbiting satellites

The most employed is the first one. Geostationary satellites orbit around the earth at 35,000 km of altitude above the equator. They complete one orbit in 24 hours, synchronized with earth's rotation. This is its main advantage: they have a high time scale resolution. The coverage area extends to an angle of  $81^\circ$  from the sub satellite point, corresponding to over 40% of the earth surface [21].

Satellite systems can operate in two bands of frequencies:

- $K_A$  band: 12-18 GHz
- $K_A$  band: 27-40 GHz

Similar to weather radars and microwave links, rainfall rate is obtained through indirect measurements: in this case attenuation of signal along the slant path is used. Since the satellites operate at frequency above 10 GHz, rain drops are the first cause of signal attenuation, due to absorption and scattering, with other less significant effects, due to atmospheric gases (oxygen and water vapour) and non-precipitating water (clouds) [22], [23]. The attenuation can then be exploited to be inverted to retrieve rainfall rate, by applying the power law relationship [5].

The system set up is quite simple. It is composed by a satellite dish antenna and a receiver: such devices can be installed both in urban areas and complex terrain area.

Various rain estimation algorithms have been developed in recent years using satellite data operating in  $K_U$  and  $K_A$  [24], [25].

The first one was developed in Pennsylvania in 2014. It employs a direct tv transponder, continuously broadcasting  $K_U$ -band signal, and a meter to gather attenuation data. Results from signal processing and comparison with radar measurements show a good agreement between the retrieved rainfall rate along the link. Another relevant study proposes estimation of path-averaged rain rate from  $K_U$  band signals received from geostationary satellite and testing of feasibility of measurements using those devices. Also this study outlines that rainfall intensity estimated by satellite system and by weather radar is on the same order of magnitude [26].

By all the previous considerations it is possible to affirm that satellites can be exploited for the estimation of rainfall as a low-cost ground based microwave system.

The only limited thing is the terrestrial receiver: in order to collect power data along the path, this device has to record such values. This kind of receiver is quite expensive. For this reason the algorithm described in the following chapters is based on exploitation of  $K_A$ -band satellite link, because receiver has a very low cost and the gathered data can be acquired and processed in real time.

## Chapter 2

# Satellite link estimation approach

This chapter will focus on the description of the satellite system and on the physical approach adopted to retrieve the rain rate from satellite link attenuation.

### 2.1 K<sub>A</sub>-band satellite system

The main objective of the thesis is the real time estimation of rainfall rate through the opportunistic employment of a commercial K<sub>A</sub>-band satellite link for DSL services [27]. The instrumentation consists of: *Eutelsat KA-SAT Satellite* and *Surfbeam 2 system*.

The main building blocks of the K<sub>A</sub>-SAT satellite network which is used in this activity are:

- Tooway kit - the satellite kit is based on Surfbeam2 technology. It provides interconnection between the CPE (Customer Premises Equipment) and the teleport infrastructure.
- Eutelsat KA-SAT - the latest generation of HTS (High Throughput Satellite) satellite, which provides bidirectional full IP K<sub>A</sub>-band services over Europe and the Mediterranean Basin.
- Skylogic Teleport - the terrestrial segment of the network architecture. It controls and manages the Ka-band satellite beams through the interconnected teleports (70 Gbps fiber ring).
- Opensky NoC - placed in the Skylogic premises and interconnected through a gigabit Ethernet to the Teleport Hub. While the Teleport Hub is responsible for

the satellite layer the Opensky NoC provides services and bearer control at IP level.

### 2.1.1 Eutelsat KA-SAT Satellite

The Satellite KA-SAT, owned by Eutelsat, operates in  $K_A$  frequencies band and it has an orbital position of  $9^\circ$ East. It provides broadband Internet access service. It can guarantee a full Europe coverage with 82 spotbeams connected to a network of ten ground stations and a capacity of 70 Gbps. It was launched in December 2010 and it is operative since May 2011. Table 2.1 summaries KA-SAT main features:

KA-SAT Satellite	
Orbital Position	$9^\circ$ East
Nr. of spotbeams	82
Bandwidth per spot	237MHz
Throughput per spot	475Mbps
Total Throughput	70Gbps

TABLE 2.1: KA-SAT features

The frequencies used for the data communication between the KA-SAT satellite and the Teleport HUB (ViaSat SurfBeam2 hub system) are:

- 27.5 – 29.5 GHz for the uplink (hub  $\rightarrow$  satellite)
- 17.7 – 19.7 GHz for the downlink (satellite  $\rightarrow$  hub)

### 2.1.2 Tooway Kit

The Tooway kit includes a parabolic satellite antenna and a ViaSat SurfBeam 2 modem. It guarantees a high speed connectivity and a sophisticated quality of service (QoS), thanks to the Adaptive Coding and Modulation (ACM) on the forward link for the network capacity optimization, the built-in TCP and web acceleration system and the security countermeasures against theft-of-service and theft-of-subscriber. However the main interesting feature for this activity is the automatic power control and rate adaptation on the return link, which assure high availability even during fades.

The satellite terminal parameters, such as the transmitted power and the SNR level, can be easily monitored through the modem Web GUI, which allows both a local and an SNMP-based remote management and control of the terminal. The frequencies used by the ViaSat SurfBeam 2 modem are:

- 29.5 – 30 GHz for the uplink (modem  $\rightarrow$  satellite)
- 19.7 – 20.2 GHz for the downlink (satellite  $\rightarrow$  modem)



FIGURE 2.1: KA-SAT coverage over Europe

## 2.2 Satellite system employment

The whole system is located at the Department of Information Engineering of the University of Florence. The antenna is installed on the roof and, by a coaxial cable, it is connected to the modem (as simple sketch of the system is shown in Figure 2.2).

The modem management software provides some information about the connection data, that can help the user to monitor, through two graphical interfaces (see Figure 2.3), the main parameters useful to guarantee a high QoS.

The parameters values that are provided by they interface are:

- Transmitted IF Power
- Transmitted RF Power
- Received Power
- Signal to Noise Ratio

This system can be exploited to obtain data relating the abovementioned parameters in order to evaluate and process them.

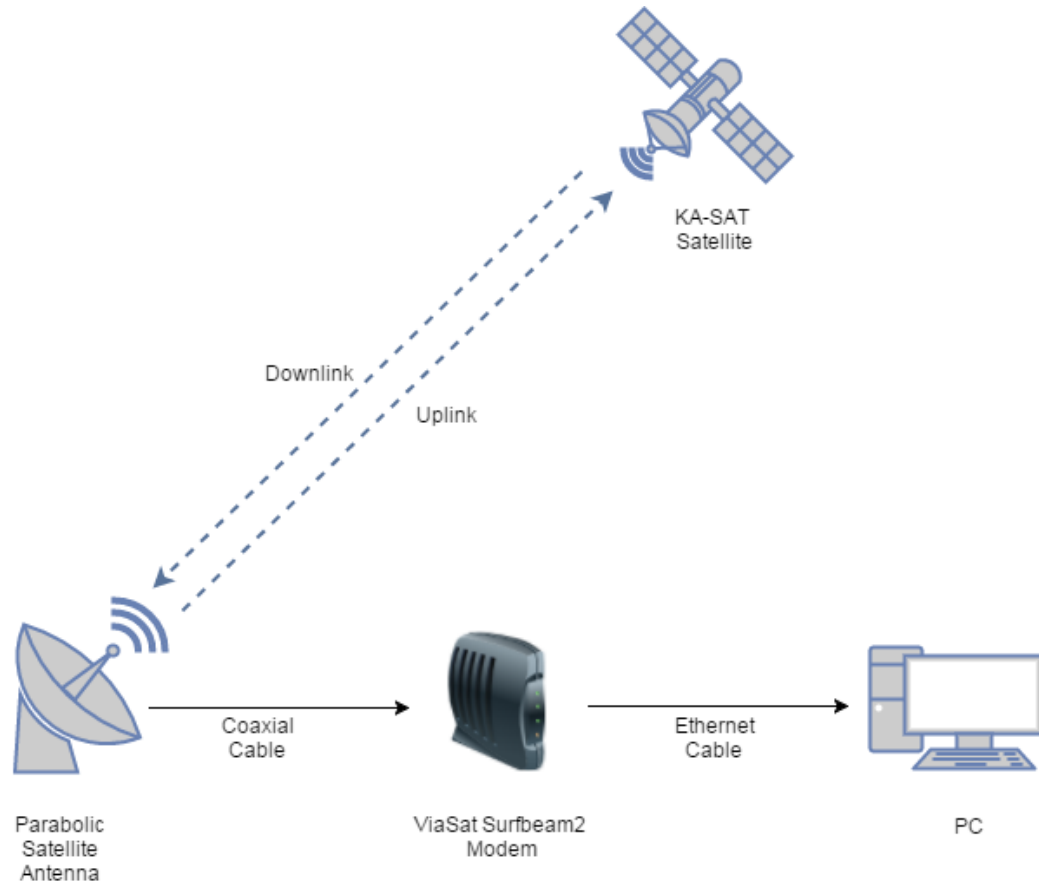


FIGURE 2.2: Satellite system scheme

Every value, continuously displayed on the GUI, can be acquired by a Python script. With this tool it is possible to select and store automatically every single parameter value about every 20 seconds in a first approach; by improving the script the sampling time has been reduced to 10 seconds. Python collects values until it is stopped manually and sorts them in rows and columns before saving them in a text file, so they could be easily imported in matlab or excel to be processed.

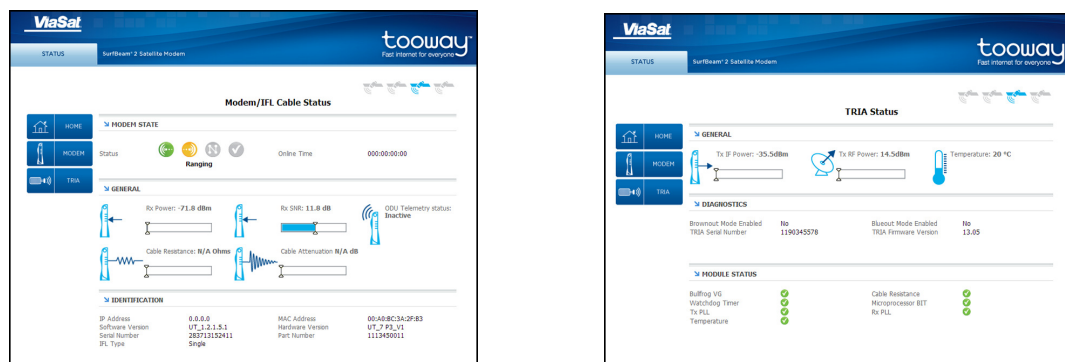


FIGURE 2.3: Modem GUI interfaces

In Figure 2.4 it is shown a 24-hour raw data relating to transmitted power, collected by the satellite receiver. It can be noticed a significant power increase between 14:00 and 20:00. This power variation is due to rain activity.

In fact, by comparing the transmitted power values during two different days, as shown in Figure 2.5 where the blue line is referred to a typical dry day, while the red one represents the data collected during a rainy day, the rain activity appears quite evident at a first visual exam.

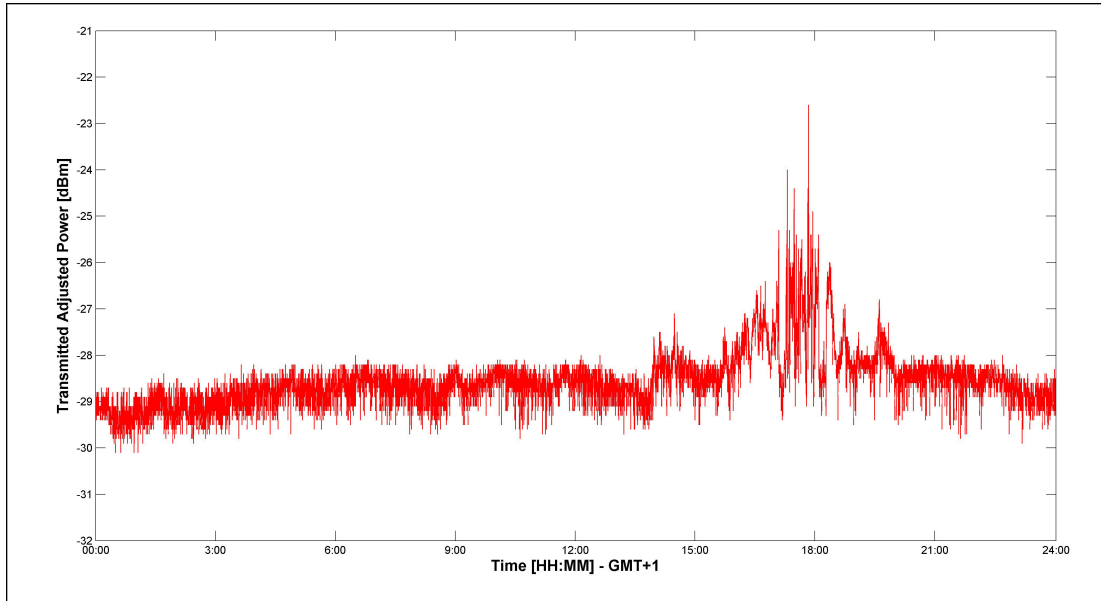


FIGURE 2.4: Tooway2 transmitted power (IF) recorded during a rainy day

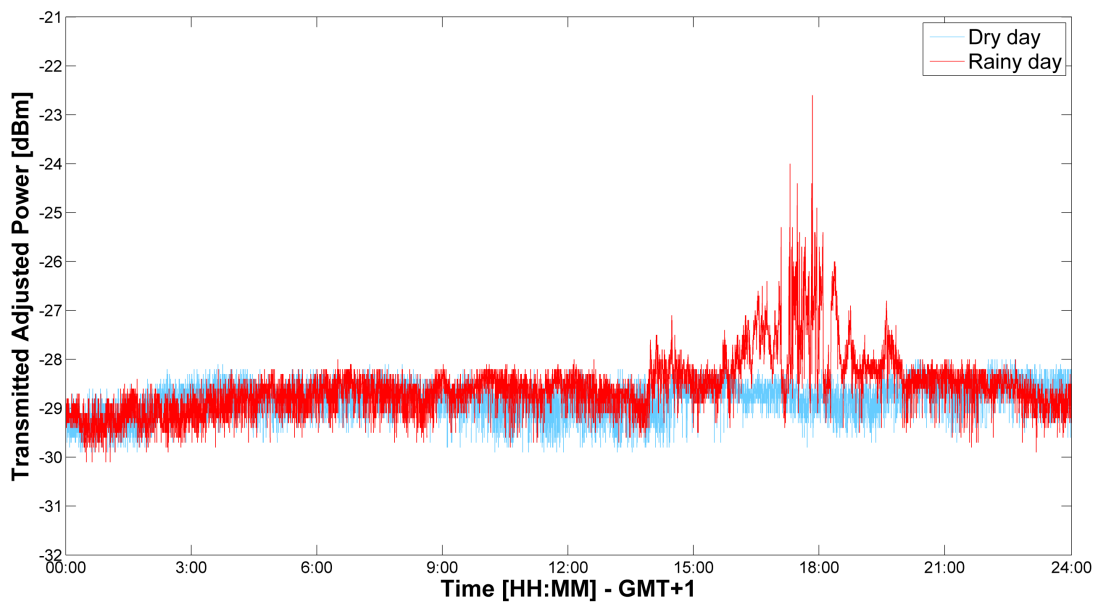


FIGURE 2.5: Tooway2 transmitted power (IF) recorded during a rainy and a dry day

## 2.3 Physical approach

The model adopted for the satellite link is outlined in Figure 2.6. It has been designed according to ITU recommendation [28].

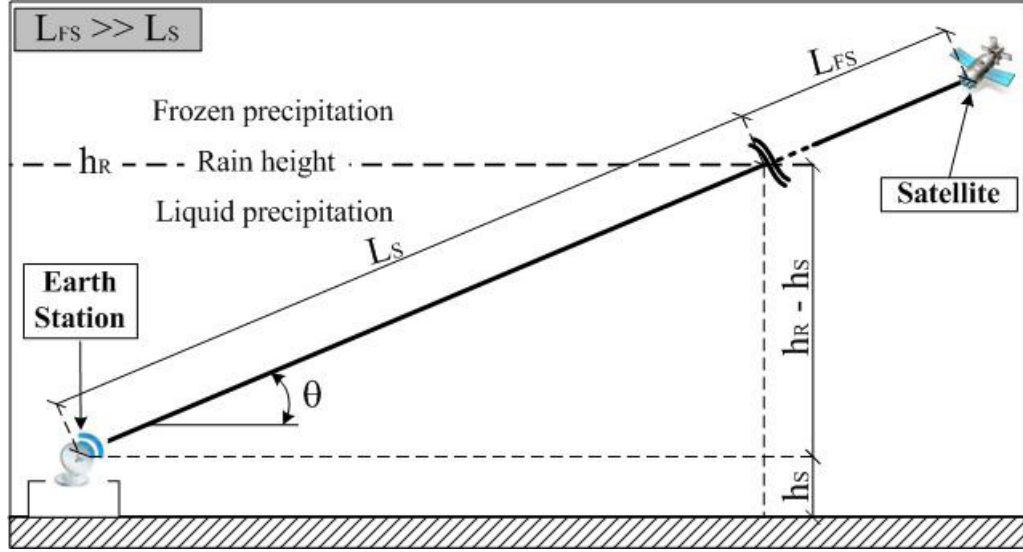


FIGURE 2.6: Geometry of the satellite link

The main parameters that characterize the geometry are:

- $h_S$ : height above mean sea level of the Earth station (about 0.12 km for our system);
- $h_R$ : mean annual rain height at the coordinate of the Earth station [km];
- $\Theta$ : elevation angle of the satellite link ( $39.45^\circ$ );
- $\varphi$ : latitude of the Earth station ( $43.80^\circ$ );
- $L_S$ : slant-path length of the satellite link below  $h_R$  [km];
- $L_{FS}$ : length of the satellite link above  $h_R$  (in free space) [km].

### 2.3.1 Attenuation of Earth-Space link

In general, an Earth-Space link is typically characterized by several effects, listed below:

- Possible loss of the signal due to beam divergence within the link;
- Decrease in effective antenna gain due to phase decorrelations across the antenna's aperture;

- Rapid fading (scintillation) due to small scale variations in the refractive index;
- Bandwidth limitations due to multi-scattering or multipath effects;
- Ionospheric effects such as Faraday rotation, dispersion, Iono-scintillation, etc.;
- Interfaces between the considered Earth station and different stations.

In the adopted model these effects are assumed to be implicitly accounted for the employed satellite-web system or they are neglected since they are not relevant to the effectiveness of the digital pluviometer.

Therefore, K<sub>A</sub>-band satellite link is characterized by a propagation loss given by the sum of several contributions [29], [30] (function of frequency, geographic location and elevation angle) such as:

- Attenuation by atmospheric gasses;
- Attenuation by rain, other kind of hydrometeors and clouds;
- Fading and multipath effects;
- Focusing and defocusing;
- Decrease in the antenna gain due to wave-front incoherence;

ITU recommendation [28] suggests that only the first three effects listed above can be considered at elevation angles above 10°. Moreover, it is possible to assert that, below 60 GHz, the attenuation due to snow or ice is very small and, hence, can be neglected [31].

After all these assumptions, rainfall can be considered as the only cause of attenuation and this phenomenon occurs mainly below the bright band (0°C isotherm) [32]: in fact, below this threshold, down to the surface, the rain intensity, on the average, does not vary with height [33] [34].

### 2.3.2 Rain attenuation $aR^b$

The adopted model for the attenuation of a link due to hydrometeors is the one suggested by *Olsen and Hodge* [5] and recommended by the ITU [28]. Such attenuation can be calculated applying Mie Scattering solution to Maxwell's Equations.

In the frequency range of microwave links (from about 5 to 50 GHz), electromagnetic

waves interact with raindrops when propagating through rainfall, because their wavelengths are of the order of magnitude of the raindrop sizes [35]. The specific attenuation  $A$  [dB/km] affecting the link can be expressed as a function of the Drop Size Distribution  $DSD$ :

$$A = \frac{1}{\ln 10} \int_0^\infty \sigma_E(\lambda, D) N(D) dD$$

where

- $D$  [mm] is the equivolumetric spherical drop diameter;
- $\sigma_E(D)$  [cm<sup>2</sup>] denotes the extinction cross-section due to a drop of diameter  $D$ ;
- $N$  identifies the DSD;
- $N(D)dD$  [m<sup>3</sup>] is the number of drops per unit volume.

Similarly, the rainfall intensity  $R$  [mm/h] can be expressed as a function of the DSD:

$$R = 6\pi 10^{-4} \int_0^\infty D^3 v(D) N(D) dD$$

where  $v(D)$  [m/s] is the terminal fall velocity of a raindrop of diameter  $D$ . It is worth noting that  $R$  does not depend on the wavelength of the link because it is a flux of water, totally independent of the interaction between microwaves and hydrometeors.

Because the two integrands above are similar at frequencies used for microwave links,  $R$  and  $A$  are almost linearly related [5]:

$$A = aR^b$$

where the  $a$ ,  $b$  parameters are functions of frequency  $f$ ,  $DSD$  and temperature  $T$  [5], [18].

The values assigned to the parameters  $a$  and  $b$  can be derived from the ITU recommendation [36]. Considering:

- Operative frequency  $f=30$  GHz;
- Circular polarization;

- Rain temperature  $T$ .

the values of  $a$  and  $b$  result respectively 0.2261 and 0.9354.

Considering the intense Mediterranean rainfalls and, consequently, their characteristic DSD, for a microwave link operating at frequency of about 30 GHz there is a proportionality between the path-averaged rain rate and the one-way path-averaged specific attenuation, independently from the length of the link. Since the employed frequency is 29.5 GHz this proportionality will be respected. Besides, as outlined, it is possible to affirm that in absence of precipitation, clear-air effects, such as tropospheric scintillation, can be neglected. The same assumption is valid for any potential decreasing of the antenna gain due to small-scale irregularities in the refractive index structure of the atmosphere. In addition, the beam spreading losses, at the operative latitude and elevation angles, can be not considered.

## Chapter 3

# Measurement System

This chapter outlines the measurement system, describing the test site and the different devices employed in the processing chain.

### 3.1 Test Site

The experimental system was installed at the Department of Information Engineering of the University of Florence (see map [3.2](#)).

The microwave signal from the KA-SAT geostationary satellite is received by the parabolic antenna connected to ViaSat SurfBeam2 modem (described in [2.1](#)) as shown in figure [3.1](#).

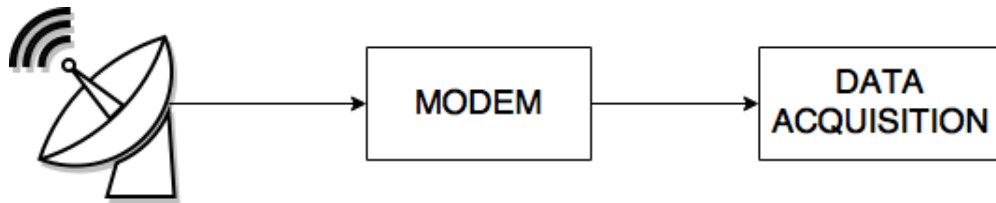


FIGURE 3.1: Data Acquisition Block Diagram

The microwave link is characterized by:

- Earth station latitude  $43.798^\circ$ ;
- Earth station longitude  $11.2526^\circ$ ;
- Elevation angle  $39.4^\circ$ ;
- Azimuth angle  $183.2^\circ$ .



FIGURE 3.2: Position of the earth station, dislocation of the rain gauges and direction of the satellite link (green line). Google earth image.

## 3.2 Employed devices

Independent rain observations have been considered in order to evaluate the performances of the whole system. For this purpose, five rain gauges covering the urban area of Florence have been exploited. The exact position and nature of the rain gauges are provided in table 3.1.

Station Name	Lat [deg]	Lon [deg]	Alt [m a.s.l.]	Device Type
Florence University	43.799	11.251	105	Tipping Bucket Rain gauge
Civil Protection	43.779	11.258	50	Tipping Bucket Rain gauge
Ximenian Observatory	43.774	11.255	66	Tipping Bucket Rain gauge
Florence City Center	43.772	11.265	48	Tipping Bucket Rain gauge
LaMMA Observatory	43.819	11.202	48	Tipping Bucket Rain gauge

TABLE 3.1: Rain gauge stations

Thanks to the competent Regional authorities, it has been possible the employment of the cumulative rainfall data recorded every 15 minutes, during the considered meteorological events, by the devices listed above.

The map in figure 3.2 shows the projection on the surface of the employed satellite link from the Department of Information Engineering of the University of Florence and the position of five automatic rain gauges covering the urban area. One rain gauge, barely visible in the picture, referred to as “Florence University”, is located in proximity of the

ground station, while the rain gauge “LaMMA Observatory” (Laboratorio Monitoraggio e Modellistica Ambientale) located at the outskirts of the city, in the upper-right corner.

### 3.3 Data processing software

The data relating to power from/to satellite are displayed in real time on the graphical interface of the Surfbeam2 modem.

These values need to be collected to be processed. For this purpose two software platforms have been used.

#### Python

Python is a widely used general-purpose, high-level programming language. Python supports multiple programming paradigms, including object-oriented, imperative and functional programming or procedural styles. It features a dynamic type system and automatic memory management and has a large and comprehensive standard library. It is a simple programming language especially used for automation and testing.

In this specific case, the script have to identify the values of interest from two web pages, collect those and, for each sample, insert the date and the timestamps, values and store them into a spreadsheet (to be easily imported in Matlab for the following steps).

The dataset is composed by values relating to four parameters: Transmitted IF Power, Transmitted RF Power, Received Power, Signal to Noise Ratio At first, the script could collect one dataset every 20 seconds (4320 values per day for each parameter). Later, by improving the script, it was able to acquire and store one data set every 10 seconds, so it will be possible to handle an amount of 8640 values per day. In either case, the acquisition delay is about 10 seconds: this time delay is sufficient to guarantee the real time collection of values.

#### Matlab

MATLAB (MATrix LABoratory) is a numerical computing environment and a programming language developed by MathWorks. It allows matrix manipulations, plotting of functions and data, implementation of algorithms, creation of user interfaces, and interfacing with programs written in other languages. MATLAB was first adopted by researchers in control engineering, but quickly spread to many other domains. It is now also used in education, in particular the teaching of linear algebra, numerical analysis, and is popular amongst scientists involved in image processing.

In this specific research, MATLAB is used for data manipulation, processing and analysis. In fact, data collected by Python script are then imported in MATLAB, which can permit to handle and analyze them and create graphs in order to evaluate the quality of the proposed method. The data processing requires a low computational cost so the time delay is limited to few tenths of a second.

## Chapter 4

# RET-AB Algorithm

In this chapter the algorithm for real time rainfall rate estimation is presented.

The proposed algorithm is named *Rainfall rate EsTimation - Attenuation Based (RET-AB)*.

In 2014 a first version of the algorithm was implemented and tested with a measurement campaign. Then, during the first part of 2015, the algorithm has been improved thanks to the considerations and the limits observed by evaluation tests.

The following sections include the description of data processing chain, the measurement campaign held in 2014 and the evolution of the algorithm.

### 4.1 RET-AB 1.0

In this section the first version of the algorithm is described, including the data processing chain, which The proposed algorithm has been tested during a measurement campaign in spring-summer 2014. Such analysis was suitable to verify the feasibility of the whole system and identify the parts to be improved to reach a high level of reliability of real time rainfall rate estimation.

#### 4.1.1 Data Processing Chain

The data processing chain is composed by five steps, as outlined in the block diagram in figure 4.1. These blocks represent the way to retrieve the cumulated rainfall rate along the link between the earth station and the geostationary satellite. The geometry of the link is represented in figure 2.6.

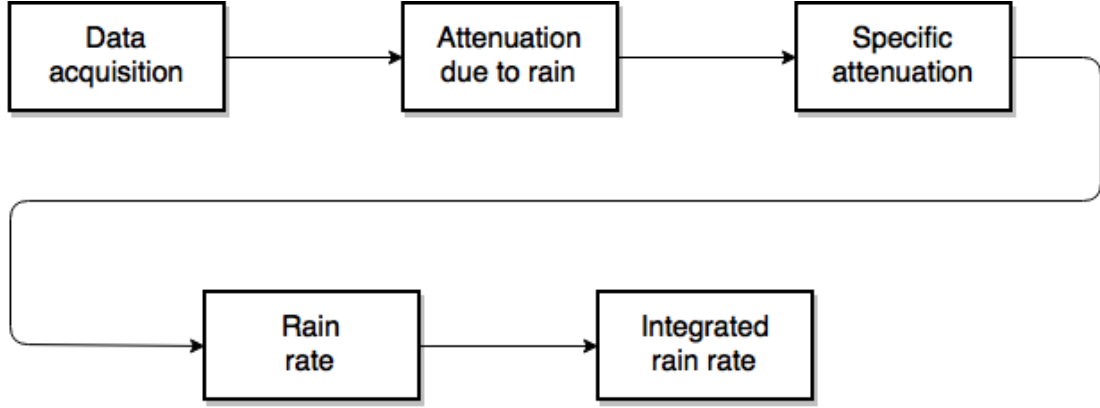


FIGURE 4.1: Data processing chain

The first step is the *data acquisition*. Transmitted and received power data to/from satellite are collected and stored in a spreadsheet document by a Python script. Then, this document can be imported in MATLAB in order to obtain the values of interest and the corresponding timestamps.

The overall attenuation along the satellite link is calculated as the ratio between the transmitted and the received power:

$$A_{TOT} = \frac{P_{TX}}{P_{RX}}$$

The retrieved value of  $A_{TOT}$  accounts for many factors:

$$A_{TOT} = A_{FS} + A_{TROP}$$

where

$A_{FS}$  is the propagation loss along the free space path and  $A_{TROP}$  is the tropospheric ones.

The first parameter is the attenuation evaluated along the free space path ( $L_{FS}$ ). This contribution is independent on the weather event: so it can be considered as a reference level. In fact, it is assumed that during a dry day, there is no attenuation due to rain:

$$A_{TOT} = A_{FS}$$

The last parameter depends by several contribution:

$$A_{TROP} = A_{RAIN} + A_{SCINT} + A_{CLOUD} + A_{VAP} + A_{OX}$$

- $A_{RAIN}$  is the attenuation contribution due to rain (the parameter of interest)
- $A_{SCINT}$  is the attenuation contribution due to scintillation
- $A_{CLOUD}$  is the attenuation contribution due to clouds
- $A_{VAP}$  is the attenuation contribution due to water vapour
- $A_{OX}$  is the attenuation contribution due to oxygen

At the frequencies of K<sub>A</sub> band, as recommended by ITU, the contributions due to scintillation, vapour, oxygen and clouds can be neglected and rain can be considered the only cause of tropospheric attenuation [28], [29], [30]. Furthermore, it has been assumed a homogeneous geographical distribution of the rain within the Tropospheric region crossed by the satellite link.

For this reason, to obtain only the *attenuation due to rain*, it will be necessary to subtract from the overall attenuation the one measured during a previous dry day.

$$A_{RAIN} = A_{TOT} - A_{FS}$$

Then, to calculate the instantaneous *specific attenuation* introduced by rain event, the previous value should be divided for the length of the slant path beyond the rain height (denoted with  $L_S$  in figure 2.6).

$$A_{SPEC} = \frac{A_{RAIN}}{L_S}$$

In a first approach  $L_S$  has been assumed to be constant because, the rain height has been supposed constant (the variability of this parameter will be discussed in section 4.2.1). Following the ITU recommendations [28]:

$$L_S = \frac{h_R - h_0}{\sin \Theta}$$

- $h_R = h_0 + 0.36$
- $h_0 = 2.5$  km

- $h_S = 120$  m

The *rainfall rate* is derived from the specific attenuation by inverting the Olsen and Hodge power law

$$A = aR^b$$

Finally, the *integrated rainfall rate* is obtained by integrating the rain rate over 15 minutes with the trapezoidal approximation. This last step is useful to compare the retrieved results with data recorded from the network of rain gauges from the Regional Monitoring Service, which are collected every 15 minutes.

#### 4.1.2 Measurement campaign

The first measurement campaign was held in 2014. With the described method it was possible to collect and process data regarding to four different rain events that occurred between May and June. The main features of these events are summarized in table 4.1.

Date	Duration	$RR_{MAX}$ (LINK) [mm/h]	$RR_{CUM}$ (LINK) [mm]
2 May	10 h	30.15	19.74
25 June	1 h 15'	5.65	4.59
26 June	2 h 15'	12.98	9.49
29 June	1 h 45'	70.58	45.54

TABLE 4.1: Features of the 2014 rain events

The following figures (4.2, 4.3, 4.4 and 4.5) show the 15 minutes cumulative rainfall of the four considered meteorological events, including the measures recorded by rain gauges.

The first event (figure 4.2) presents a longer temporal scale than the others. In fact, in spite it was characterized by two separated peaks at respectively 15:45 and 19:45, it also exhibited a certain time continuity. The other three events (4.3, 4.4 and 4.5 June 2014) have a relatively reduced time scale of about 1-2.5 hours.

The black bar is referred to the values estimated by the system and the other bars are the ones recorded by rain gauges. It should be noticed that data of the sensor belonging to the Ximenian Observatory are missing: that is due to the fact that it is not automatized and it was unable to collect its measurements during the considered events.

By a first analysis it appears quite clearly that the processed data are in agreement with those provided by the three rain gauges displaced within the city center. On

the contrary, during the second and third rain events, the values from the rain gauge “LaMMA Observatory”, located about 5 km outside of the city center, seem to disagree with those provided by the other three rain gauges and from those elaborated by our system. This is probably due to the excessive distance of the rain gauge from the area covered by the link, relatively to the dimension of the area interested by the precipitation and/or to the time-scale dynamics of the considered meteorological events.

It should also be noticed that the last meteorological event (see figure 4.5 and table 4.1) is relative to a quite intense rainfall, extraordinary in terms of rainfall rate for the considered area, as shown by the values of the 15 minutes cumulated rainfall on the y-axes: it brought several consequences in the city center causing inconveniences to the people (such as closed streets and/or falling trees). For all these reasons, this could be a “key-event” for this purpose as people should be alerted in real time in order to prevent car accidents or avoid other problems connected to the fast storm arrival.

### 4.1.3 Considerations

By analyzing the produced graphs, it was noticed that the model parameter that more affect the results is the height of the 0°C isotherm, that is the altitude of the clouds layer  $h_R$ .

In order to evaluate the influence of this parameter on the data processing, a variation of  $h_R$  of  $\pm 500$  meters has been considered, defining three different models for each considered meteorological event. The results of the processed data relating to three different altitudes of rain are shown in figures 4.6, 4.7, 4.8 and 4.9.

As expected, if the height of the zero degree isotherm decreases the cumulated rainfall measured by the system increases and vice versa. In fact, by reducing the length of the link interested by the precipitation, but keeping the same attenuation values, it is supposed a higher intensity of the rainfall.

The bias is more evident for the higher values of cumulated rainfall (figures 4.6 and 4.9), that leads to an error up to 10 mm in the 15 minutes cumulated rainfall. Also for scarce amounts of rain, the variation is consistent and it cannot be ignored. Therefore, it is necessary to employ an estimation of the rain height as accurate as possible.

Another important factor to take into account is the different nature of precipitation event: in fact, the DSD can vary from a rain event to another. The wrong characterization of Drop Size Distribution (drop concentration and shapes) leads to not negligible errors in the evaluation of the parameters  $a$  and  $b$  in the A-R power law.

In the following figures 4.10, 4.11, 4.12 and 4.13 is shown how a variation of  $a$  and  $b$  parameters can affect the rain rate estimation.

In spite of cloud height altitude, by analyzing the last results, it appears clear that the exact modeling of precipitation does not influence too much the estimation of cumulated rainfall. For this reason, the main parameter to be investigated is the height of the precipitation.

## 4.2 RET-AB 2.0

After the measurement campaign, some considerations came up and they have been useful in order to improve the algorithm.

### 4.2.1 Cloud Height

The main problem to a correct estimation of rainfall rate along a link is connected to the height of the precipitation. By the investigation of possible methods to reach this purpose, two approaches have been followed in order to retrieve the best values of rain height.

These approaches are not expensive and they do not require additional devices to be installed on the roof of the department.

The two selected methodologies are: data collected and published with METAR bulletins and data measured by LIDAR.

#### 4.2.1.1 Metar Bulletins

**METAR (METeorological Air Report)** bulletins are weather messages generated by observation stations, usually located close to the airport, and used by pilots during the pre-flight briefing.

The messages could be generated once an hour (military airport station) or half-hour (civil airport). The code is standardized by the International Civil Aviation Organization (ICAO) and it includes information that would be of interest to pilots or meteorologists: for example data for the temperature, wind speed and direction, precipitation, cloud cover and heights, lightning and visibility.

The sensor of a weather station records data, which are encoded in METAR format in order to generate the report to be emitted. Nowadays METAR are available online.

In figure 4.14 is shown a METAR bulletins whose information refers to Firenze Peretola airport.

METAR reported in figure 4.14 contains a lot of information (as described above). The more interesting for the retrieval of cloud height are *FEW(050)* because *FEW* means the presence of few clouds and *050* is equal to 5000 ft AGL, that is the altitude of clouds is 5000 feet above the airport sensor.

In RET-AB algoirthm collects the level of altitude in a vector to be used during the processing steps to calculate the lenght of  $L_S$ .

#### 4.2.1.2 LIDAR

LIDAR is an optical remote sensing technology that measures properties of scattered light to find range and/or other information of a distant target. The prevalent method to determine distance to an object or surface is to use laser pulses. The range to an object is determined by measuring the time delay between transmission of a pulse and detection of the reflected signal [37].

At IFAC CNR in Sesto Fiorentino a LIDAR is installed. Thanks to an agreement between CNR and CNIT-RaSS it has been possible to obtain data about cloud height. The IFAC CNR LIDAR was designed and built at IFAC in 2002, it is operating 24 hours per day. A pyrex window equipped with a power window for the laser beam makes the all-weather operation of the LIDAR possible. The LIDAR software takes care of the acquisition of the LIDAR data and of the meteorological and housekeeping data. The same software produces time-lapse daily videos from a night-vision webcam. All the above data are pre-processed automatically, and the colour plots for the WWW site are automatically updated every 10 minutes. The IFAC LIDAR is the first and sole online-LIDAR in Italy [38].

The main specifications of the LIDAR are summarized in table 4.2.

IFAC CNR LIDAR	
Laser	Quantel Brilliant B
Telescope	Refractive, 10 cm diameter, f/3
Channels	3 channels - 532 nm, 1064 nm
Range Resolution	7.5 m (vertical)
Measurement Range	50 - 14000 m a.g.
Time Resolution	5 minutes

TABLE 4.2: Features of the IFAC CNR LIDAR

The LIDAR takes measurements continuously and an automatic software processes data to analyze the atmosphere and detect clouds [39]. The algorithm estimates the optical depth of cloud by finding a point characterized by consistent change in the signal, which is represented in a backscattering matrix. It will be then converted into an intensity matrix and, by calculating the maximum gradient, it retrieves the cloud edges, leading to cloud detection. The produced plot (see figures 4.15) is a false-colour scale representing the intensity of the backscattered laser light  $PR^2$ , where  $P$  is the LIDAR signal and  $R^2$  is the range, while the *Depolarization* shows only the presence of particles (i.e. aerosols and clouds). A high intensity of backscattered laser light (highlighted by the rectangle) returns the presence of cloud and the corresponding value of altitude.

The main limit of this device is connected to rain: in fact, in case of rain the LIDAR signals are disturbed by the drops falling on the window, and it must be considered useless (it happened in the 2015 measurement campaign: during the event of 25 June the LIDAR was down and it was not possible to process data with the provided parameter).

RET-AB algorithm processed data from LIDAR to extract the altitude of clouds. It retrieves the values of  $h_R$  by analyzing the backscattered matrix and selecting the level of high intensity, suggesting the presence of clouds. Then, by selecting the corresponding indices of timestamps in a second matrix it is possible to obtain the interest measures of  $h_R$ , used by the algorithm to evaluate the length of  $L_S$ .

In figure 4.16 is compared the variation of rain height. The green line is referred to LIDAR estimation, the red is the one retrieved from METAR and the blue line is the value of  $h_R=2.5$  km assumed constant in the first version of algorithm.

### 4.2.2 Temporal Resolution

Another important aspect to pay attention to is the temporal resolution. In a first approach the estimation temporal resolution has been set up to 15 minutes in order to compare the results with the data provided by sensor displaced along the urban area of Florence.

But, especially during fast and strong events, the rain intensity can vary quickly and there could be a considerable variation between two sensors installed nearby. For this reason it has been useful the possibility to change the resolution, depending on the application and the real time context.

#### 4.2.2.1 Variation of Integration Time

RET-AB algorithm includes the function to select the integration time. During the processing the user can choose this parameter, which can be modified from 1 minute up to 24 hours. Figure 4.17 shows how the rain rate is estimated, depending on three different integration times: the blue line refers to 7.5 minutes, in fact there are slow variations of rain rate estimation while the other two represent longer integration time (15 minutes the red line and 30 minutes the green one) where changes occur quickly.

#### 4.2.3 Spatial Resolution

The last parameter to be considered for the improvement of the algorithm is the spatial resolution. In fact, it could occur a remarkable difference of values of rainfall rate recorded by sensors. That is due to the fact that weather stations are displaced along the urban area of Florence, not so close to the projection of the link (especially the sensor at LaMMA Consortium which is almost 5 km out of the city center, as highlighted by red peaks in figure 4.18). For this reason, a technique to improve the spatial resolution was needed in order to better compare the estimated rainfall intensity with the one provided by authorities.

##### 4.2.3.1 Kriging Technique

The chosen method of regression for spatial interpolation is kriging. It is a geo-statistical technique whose results permit to merge local rain gauges data and to extend their measurements to the region interested by the sat-link [40].

The basic idea is to predict the value of a function at a given point by computing a weighted average of the known values of the function in the neighborhood of the point. The weights, assigned to known values, reflect the proximity of samples to the estimation location (it is supposed that the nearest points have higher weights). They are calculated by using semivariogram, a function describing the degree of spatial dependence between known values at two locations and their relative positions.

With this method it will be possible to take into account mainly the rain gauges installed in proximity of link (i.e. Florence University and Civil Protection, see figure 3.2).

Figure 4.19 shows the bars representing the different values of rain rate measured by the five rain gauges while the blue line is referring to the result of kriging interpolation.

---

In a future scenario, this technique could be exploited to extend the rain rate measured along the satellite link to the surrounding area [\[41\]](#).

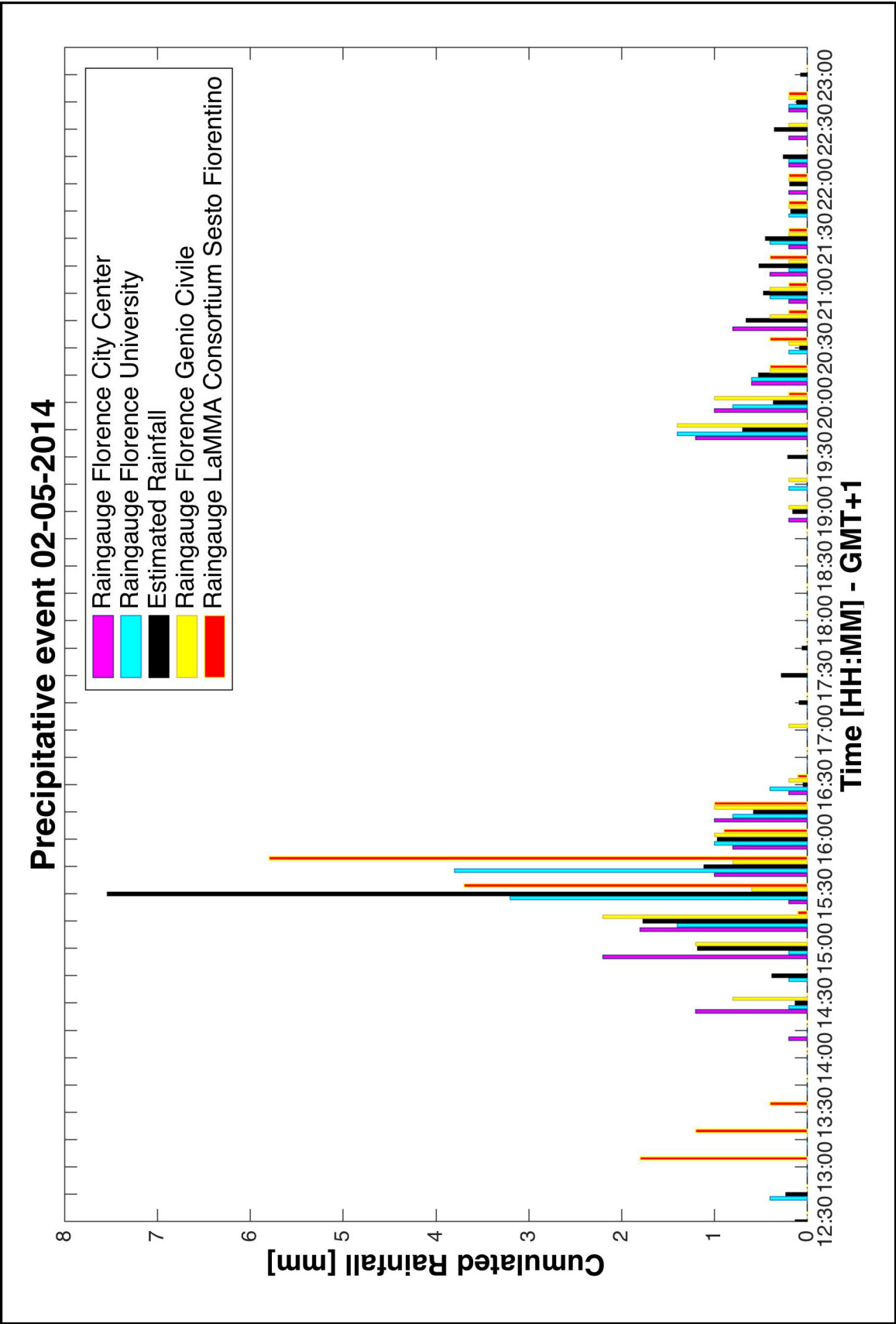


FIGURE 4.2: Cumulated rainfall rate over 15' - 2 May

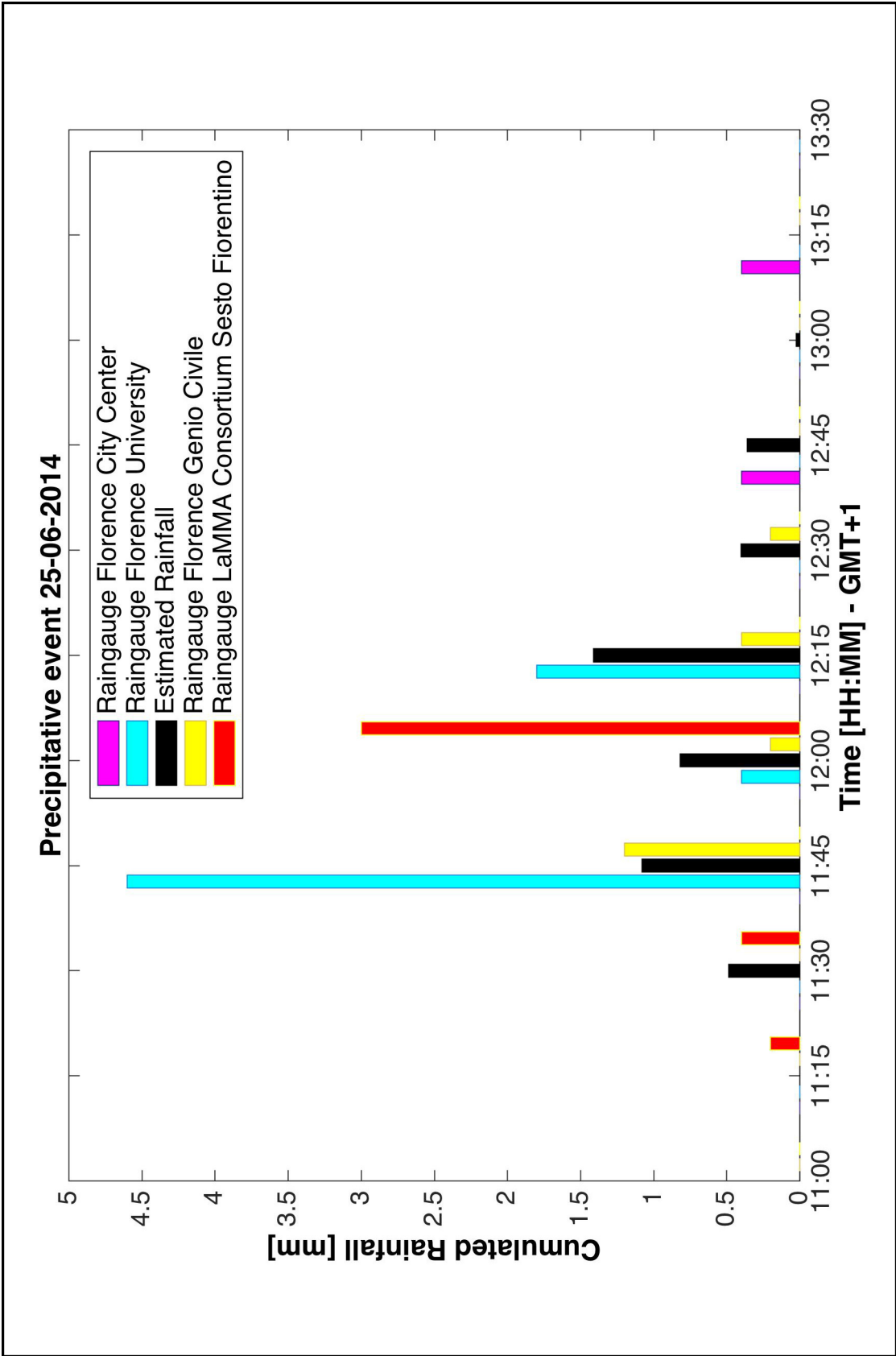


FIGURE 4.3: Cumulated rainfall rate over 15' - 25 June

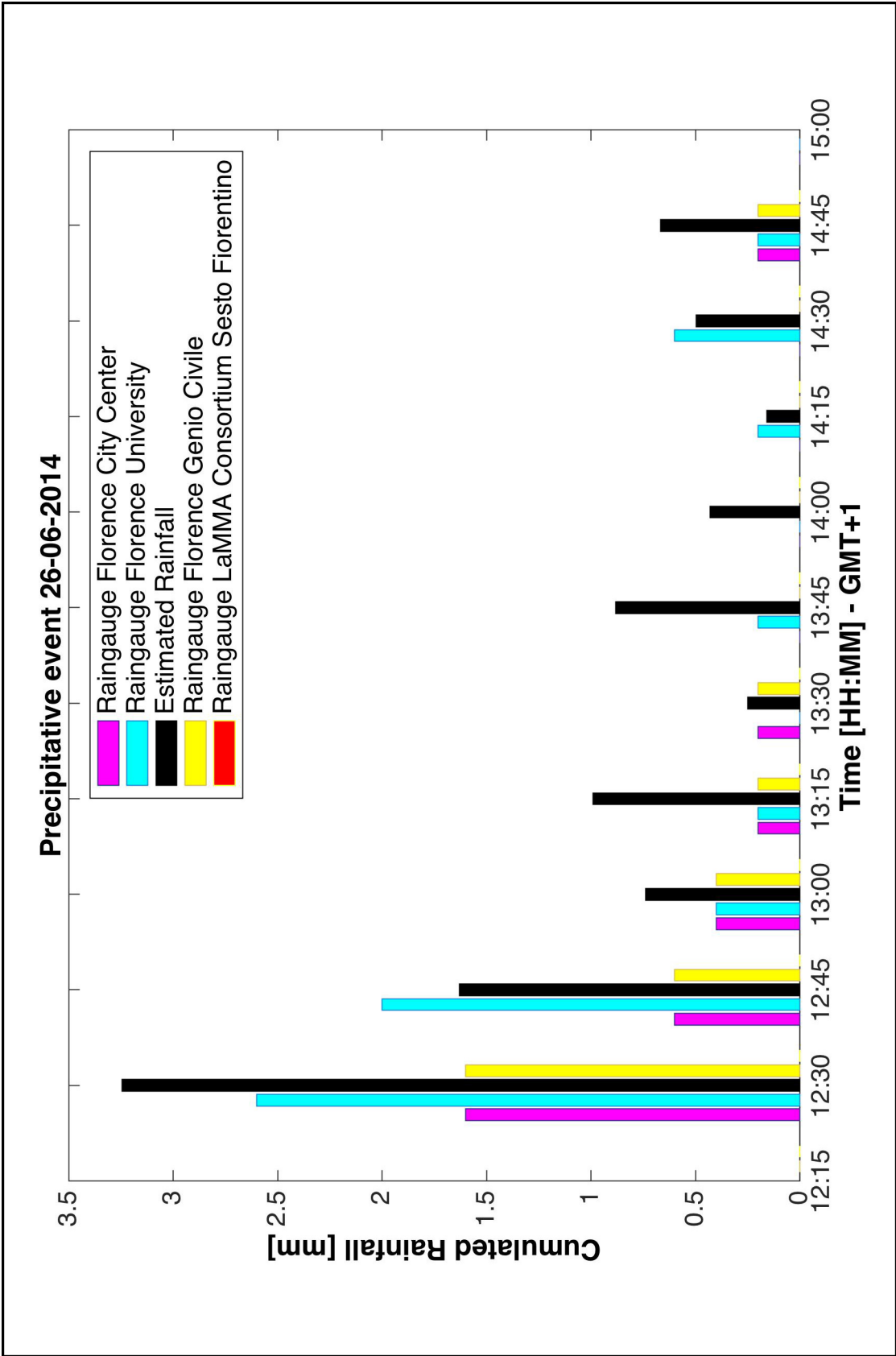


FIGURE 4.4: Cumulated rainfall rate over 15' - 26 June

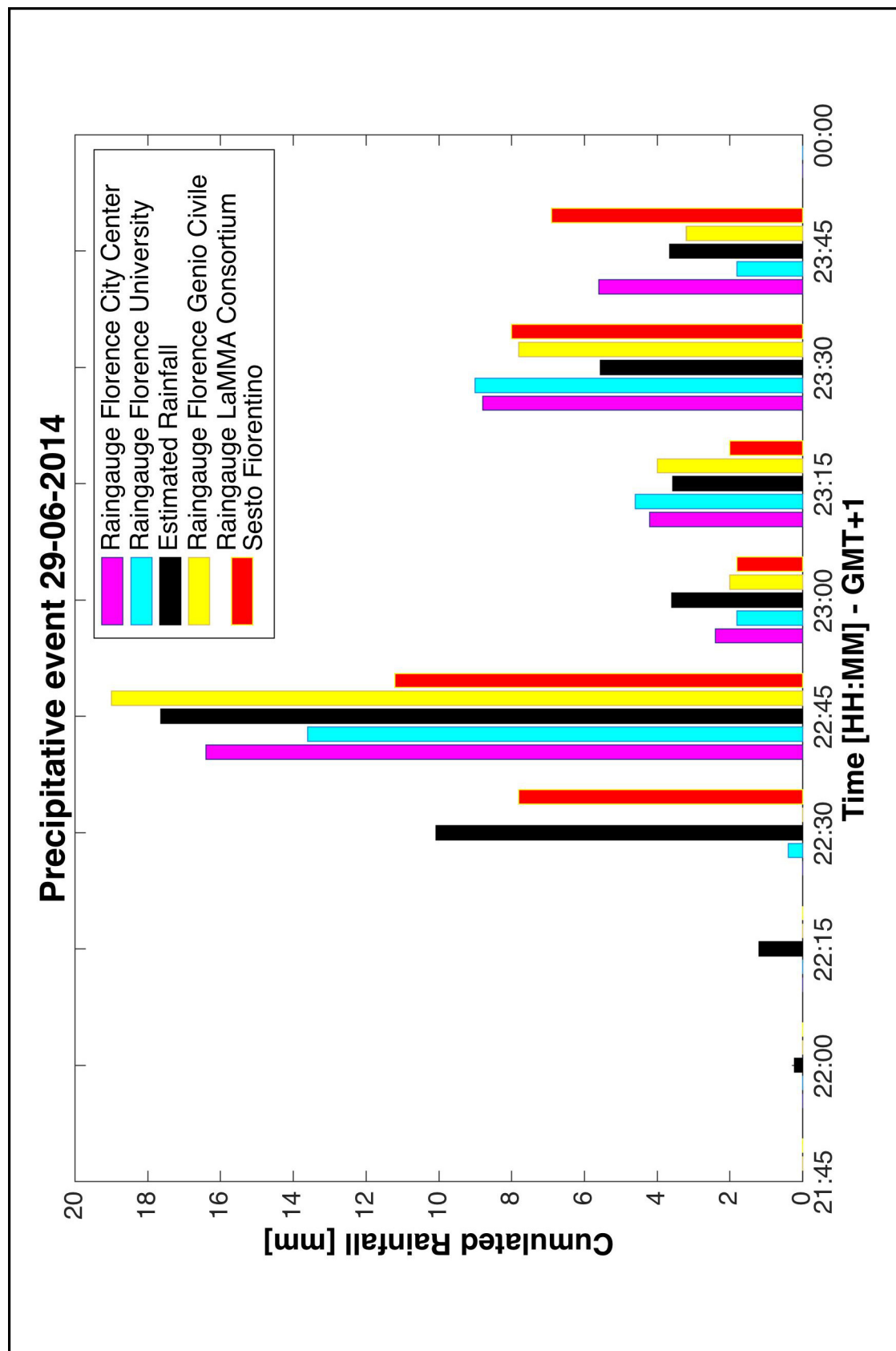
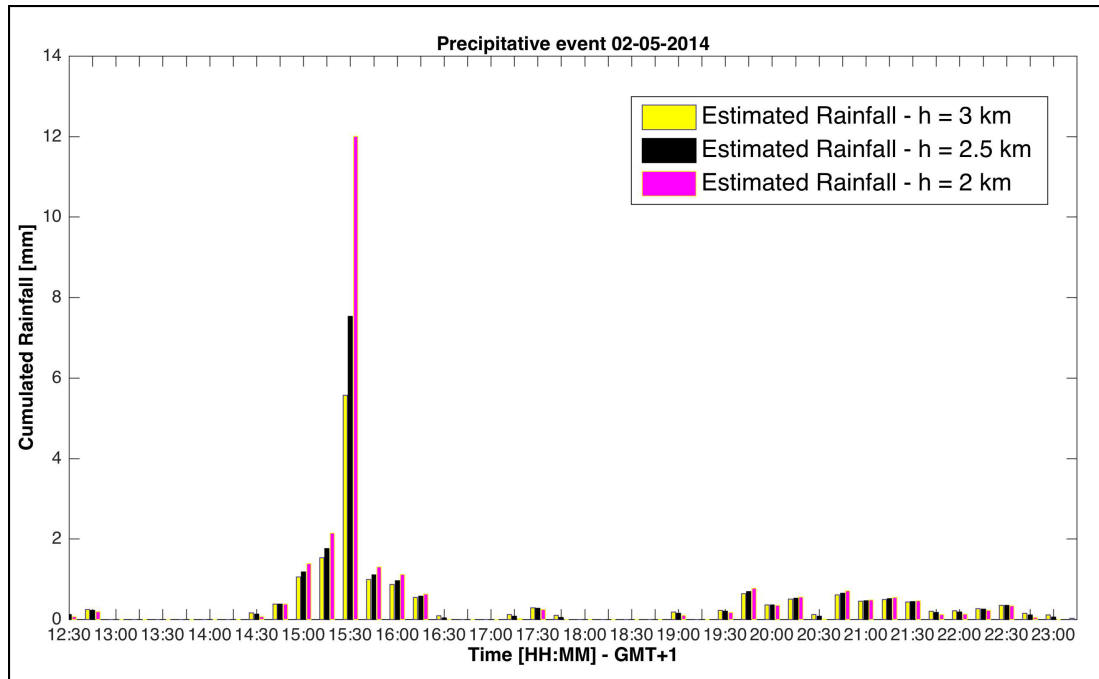
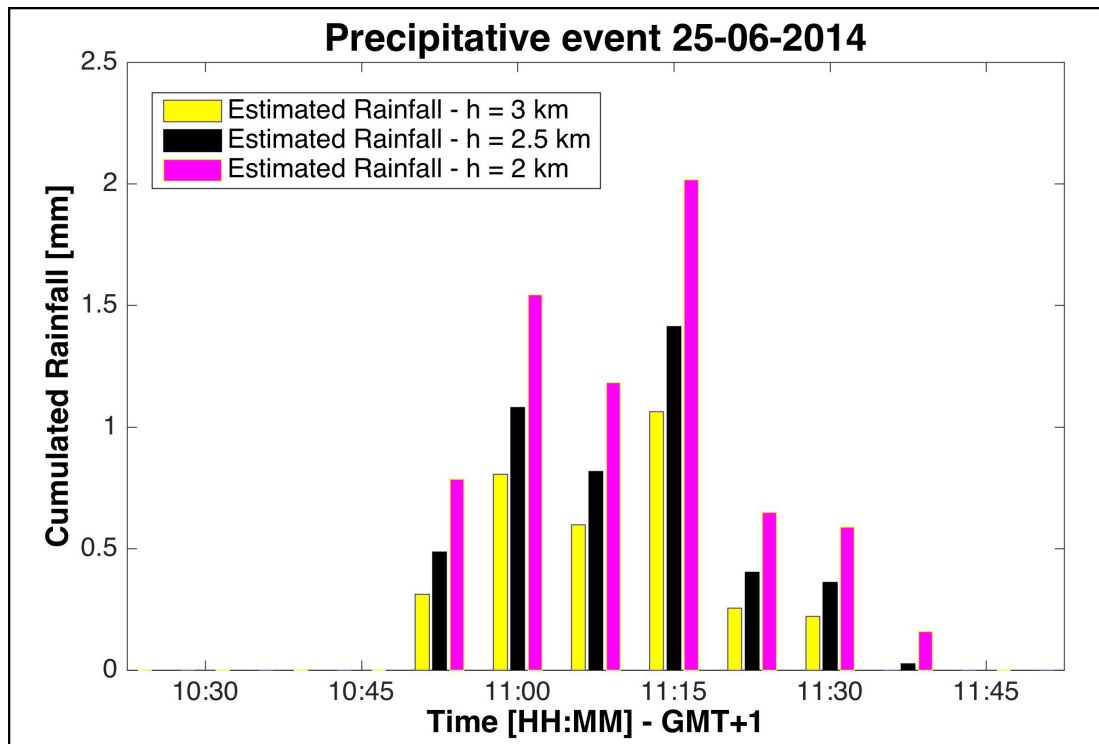
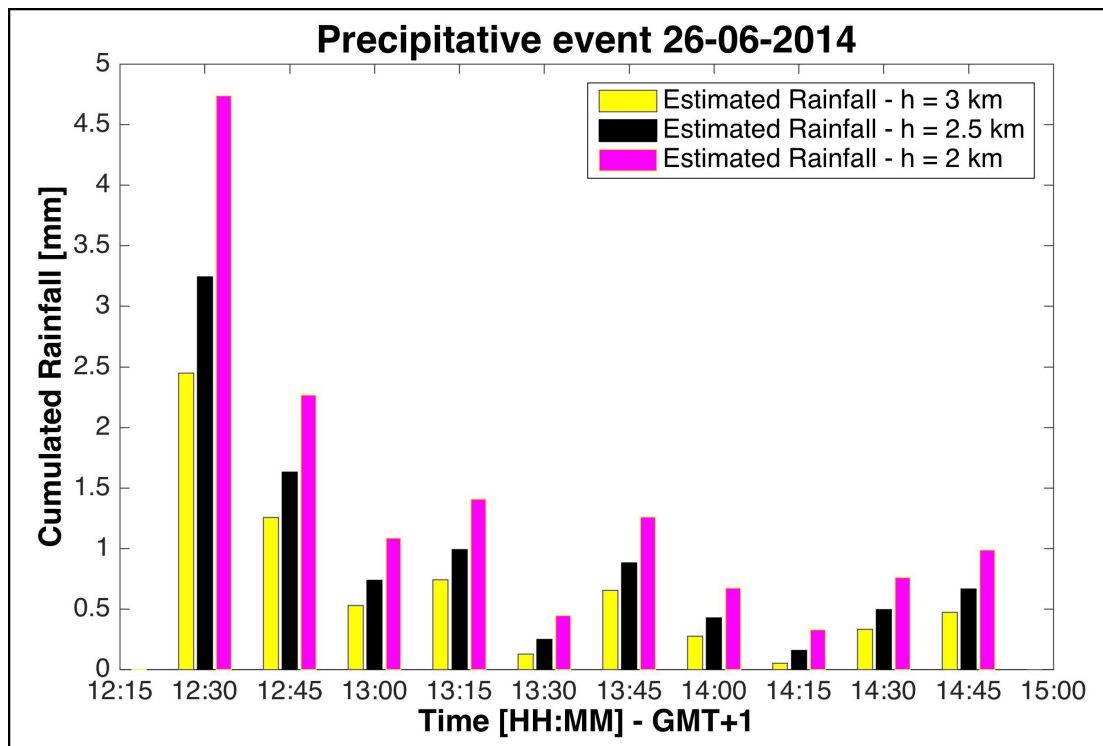
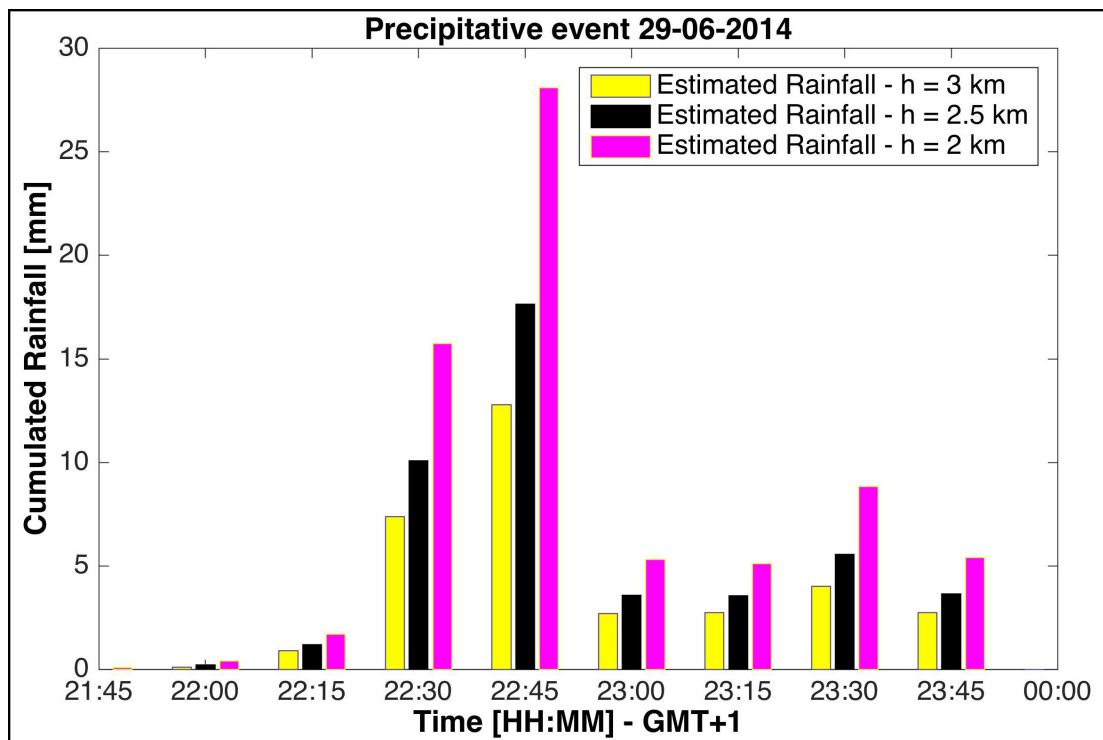
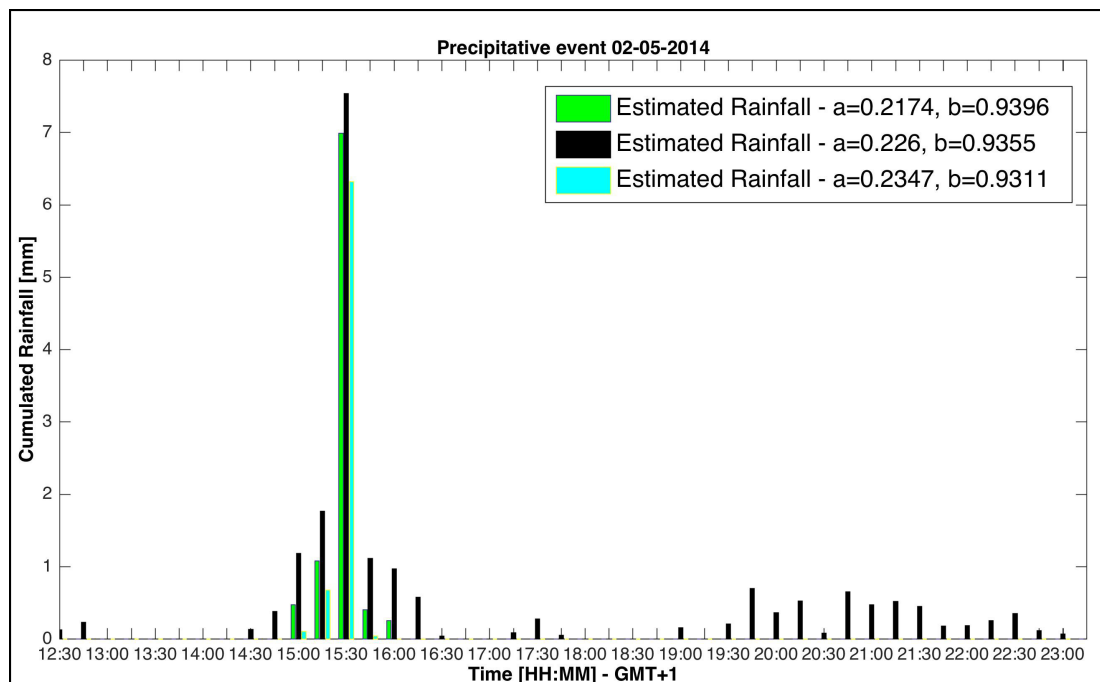
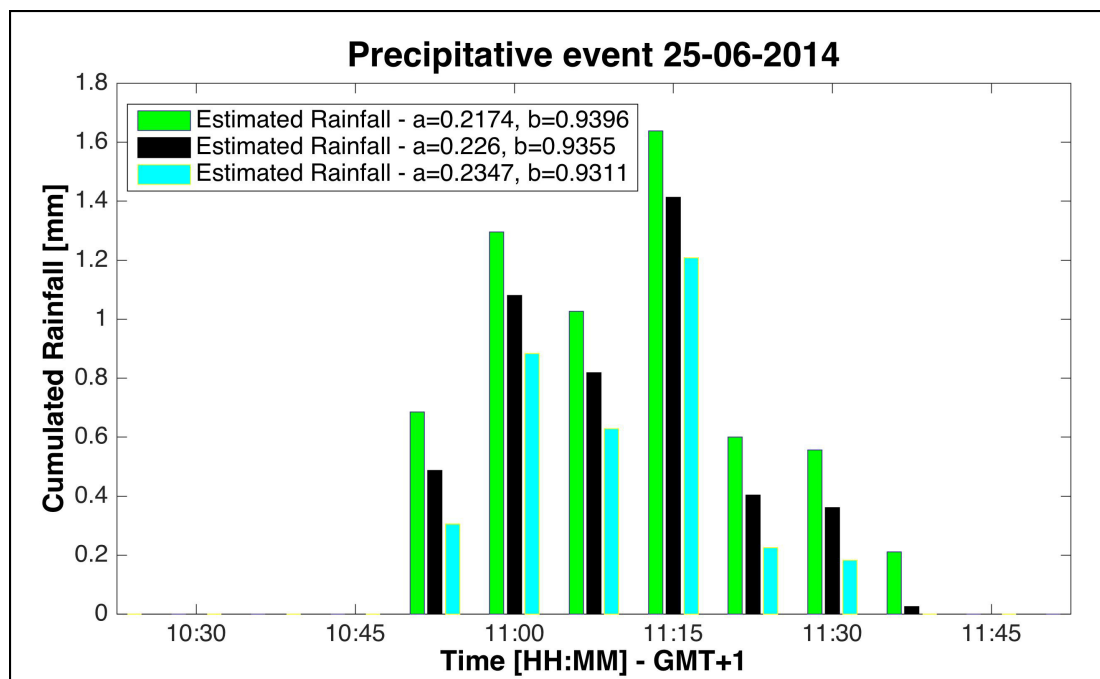
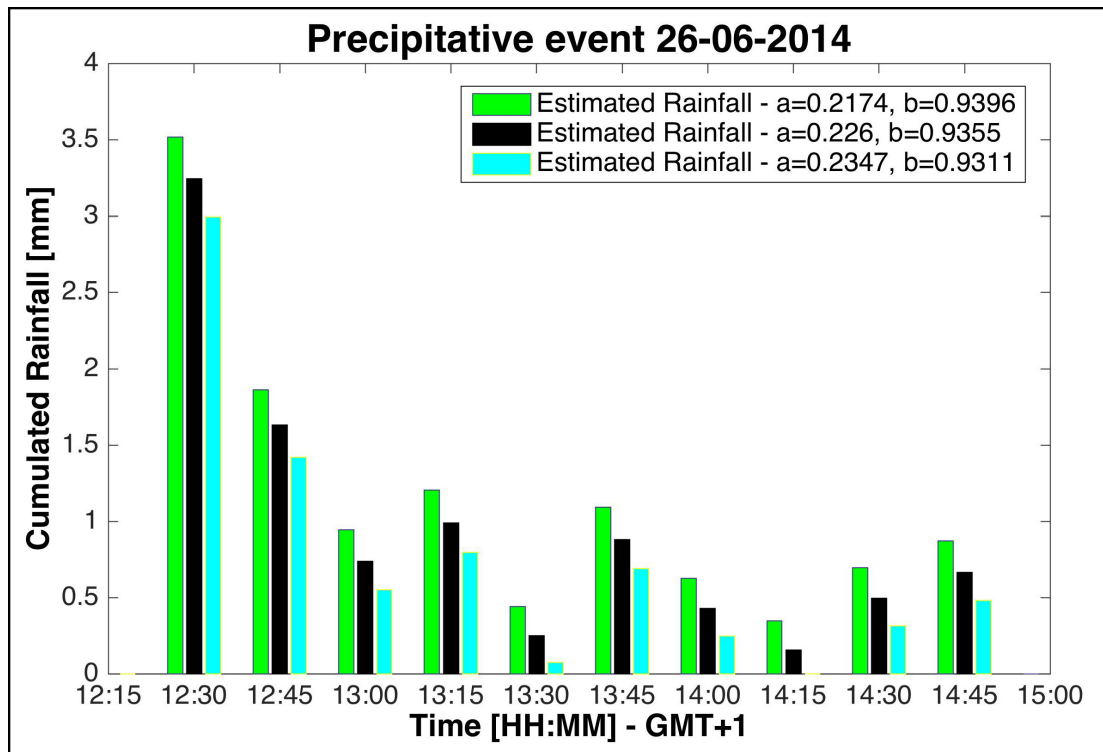
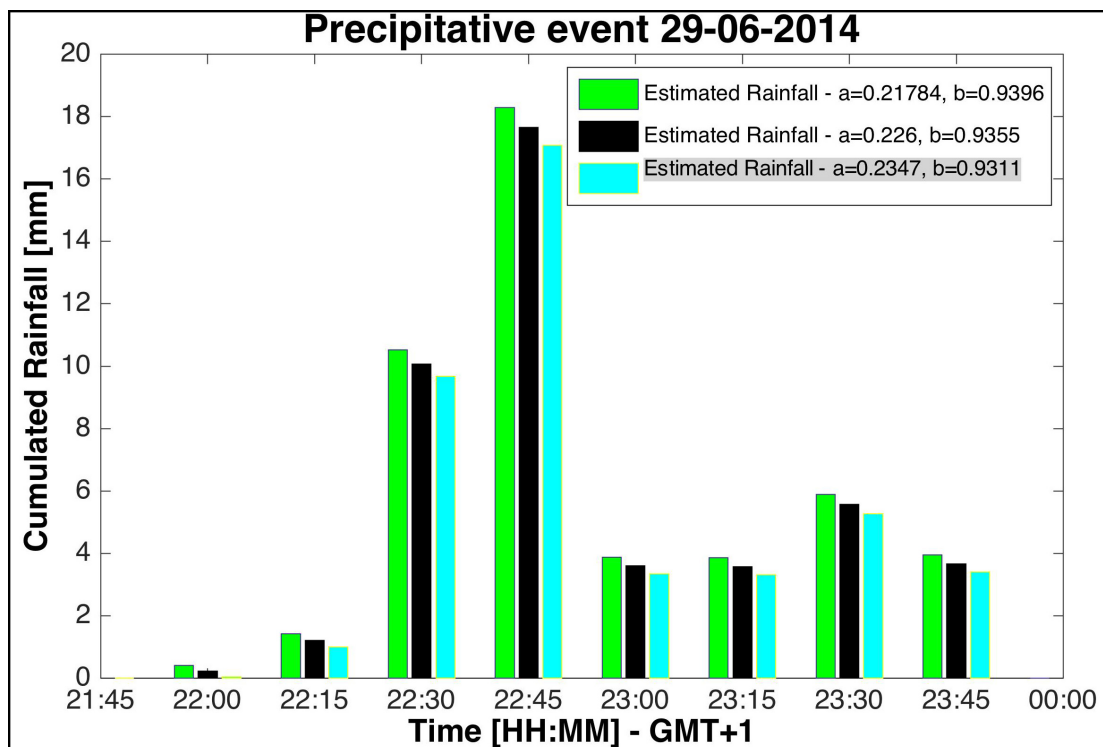


FIGURE 4.5: Cumulated rainfall rate over 15' - 29 June

FIGURE 4.6: Variation of rain rate depending on  $h_R$  - 2 MayFIGURE 4.7: Variation of rain rate depending on  $h_R$  - 25 June

FIGURE 4.8: Variation of rain rate depending on  $h_R$  - 26 JuneFIGURE 4.9: Variation of rain rate depending on  $h_R$  - 29 June

FIGURE 4.10: Variation of rain rate depending on  $a$  and  $b$  parameters - 2 MayFIGURE 4.11: Variation of rain rate depending on  $a$  and  $b$  parameters - 25 June

FIGURE 4.12: Variation of rain rate depending on  $a$  and  $b$  parameters - 26 JuneFIGURE 4.13: Variation of rain rate depending on  $a$  and  $b$  parameters - 29 June

**METAR - FIRENZE PERETOLA**

**LIRQ 170820Z 00000KT 9999 FEW050 01/M02 Q1016**

FIGURE 4.14: An example of METAR report (Firenze Peretola airport)

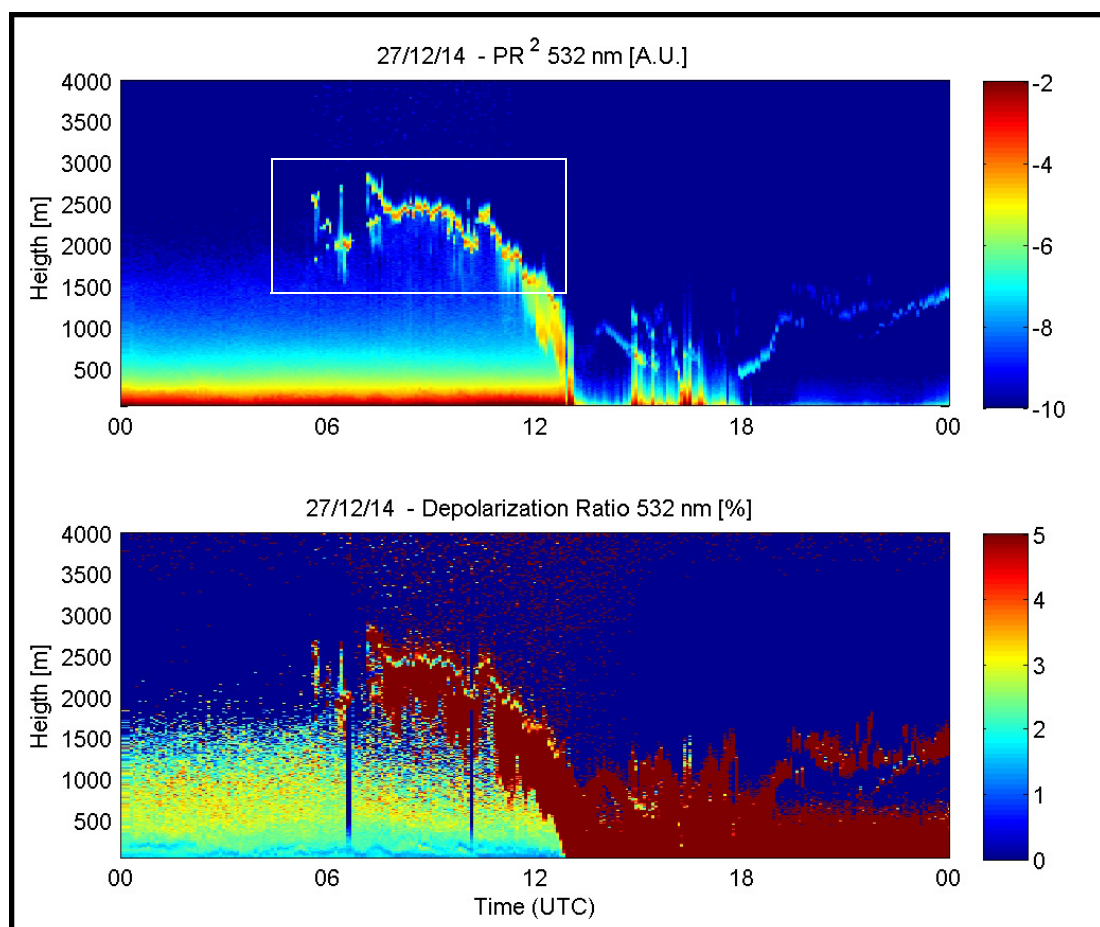


FIGURE 4.15: LIDAR plots: Signal and Depolarization

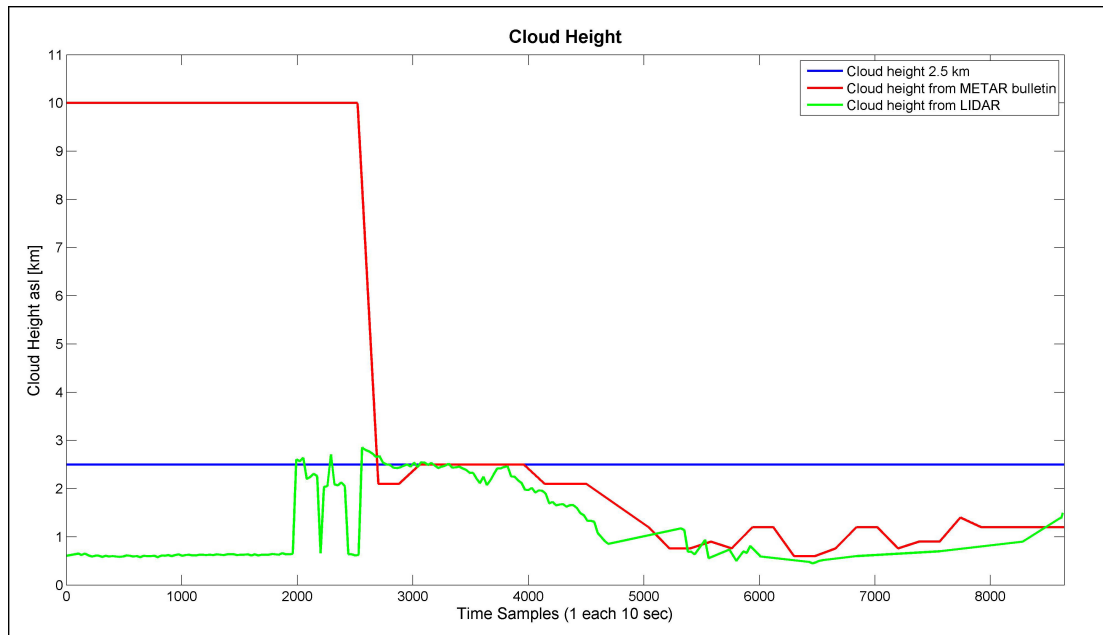
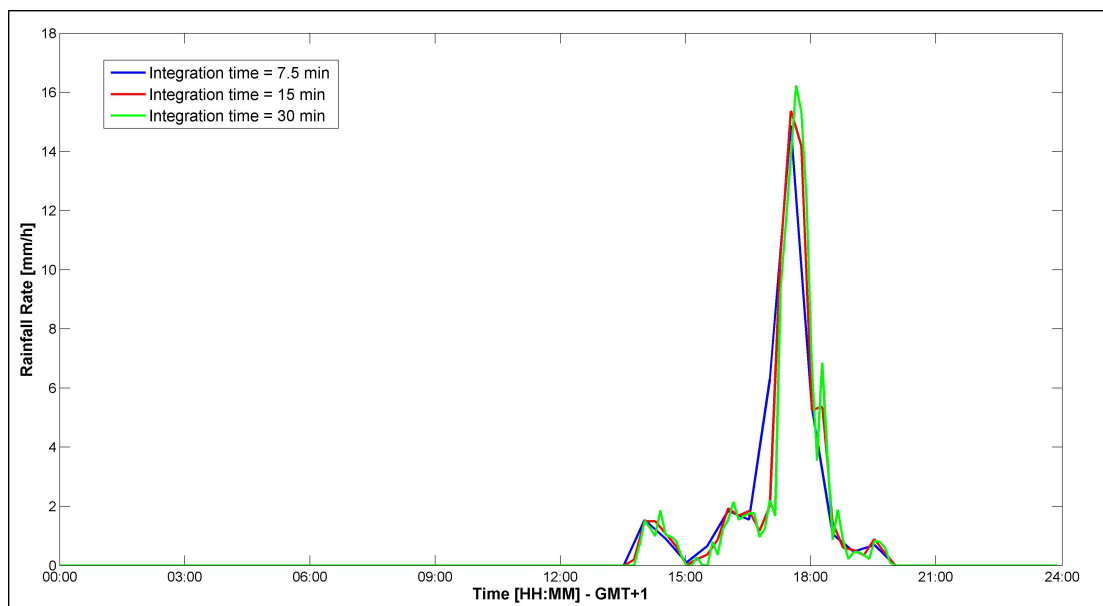
FIGURE 4.16: Variation of cloud layer  $h_R$ 

FIGURE 4.17: Variation of integration time

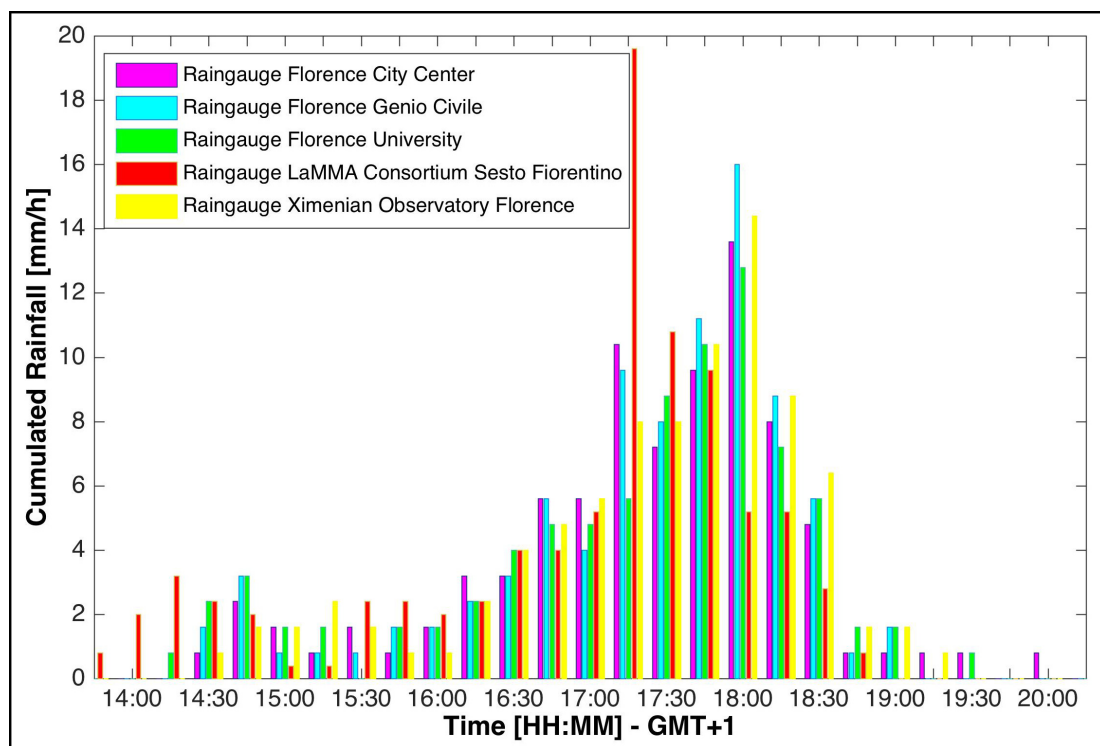


FIGURE 4.18: Cumulated rainfall rate recorded by regional rain gauges

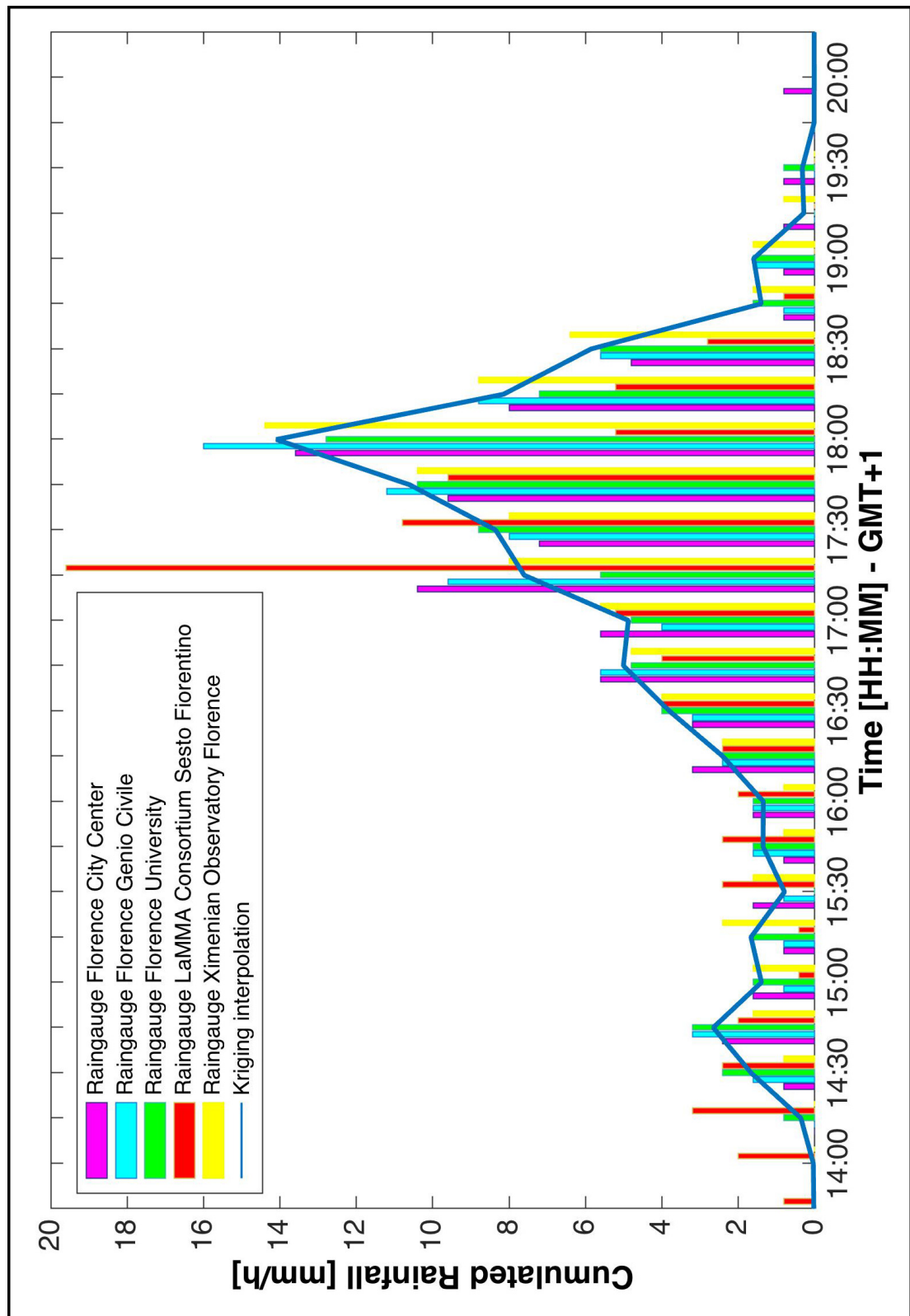


FIGURE 4.19: Comparison of rain rate: measurements by rain gauges vs interpolation with kriging technique

## Chapter 5

# Measurements Campaign and Results

This chapter shows the results obtain by a new measurement campaign, by adopting the new techniques, described in the previous chapter, to improbe the RET-AB algoorhthm.

This second measurement campaign was held between December 2014 and April 2015. During this period, three significant events have been recorded:

- 27 December 2014
- 25 March 2015
- 4 April 2015

The main features of these events are summarized in table 5.1.

Date	Duration	$RR_{MAX}$ ( $h_R$ from METAR) [mm/h]	$RR_{CUM}$ ( $h_R$ from METAR) [mm]	$RR_{MAX}$ ( $h_R$ from LIDAR) [mm/h]	$RR_{CUM}$ ( $h_R$ from LIDAR) [mm]
27 December	6 h	15.38	17.5	22.7	29.5
25 March	16 h	4.27	17.82	8.57	32.6
4 April	10 h 30'	11	27.6	NA	NA

TABLE 5.1: Features of the 2015 rain events

By collecting power data, it was possible to process them and retrieve the rainfall rate. The main feature of the system is the reduced computational load, achieving a quasi-real-time estimation.

## 5.1 27 December 2014

The first event had a strong intensity and significative data have been collected between 14:00 and 20:00, even if the strongest peaks are concentrated between 17:30 and 18:30. During the storm LIDAR was working and it could record cloud data, hence a comparison with METAR data has been possible. Figures 5.1, 5.4, 5.5 and 5.3 show the values of cumulated rain recorded by regional rain gauges with and without the rainfall rate estimated by RET-AB algorithm. In figure 5.2 the results of processing algorithm are compared: since the  $h_R$  is lower when obtained by METAR bulletins, the corresponding amount of rain is higher. Furthermore, LIDAR usually records lower values of cloud altitude and, consequently, higher amount of rain over the one processed with METAR data.

By splitting figures 5.4 and 5.5 is it possible to compare in detail every single measure of rain gauge with the value of rainfall rate retrieved by the algorithm (with altitude from METAR and LIDAR).

Figures 5.6, 5.7, 5.8, 5.9, 5.10 show an agreement of the trend between data from rain gauges and retrieved by the algorithm: in particular, data processing with  $h_R$  calculated by METAR bulletins are quite consistent instead of the one processed with LIDAR data. The red peak at 17:15 from LaMMA means a high concentration of rain in the area of Sesto Fiorentino, out of Florence (figure 5.10). Considering the principles of kriging, the above-mentioned peak, is now attenuated (figure 5.12), because of the position of the sensor (almost 5 km out of the link).

Since the new algorithm permit to choose the time integration, figure 5.11 outlines the difference between three integration times (7.5', 15' and 30').

To better understand the advantages of a real time estimation, the following figures (5.13 - 5.22) show the benefits by using a real time algorithm such as RET-AB, instead of measurement devices affected by time delay as rain gauges. This advantage is more clear in figures where only the 7.5' integration is superimposed on the rain gauges data (5.14, 5.16, 5.18, 5.20, 5.22). In fact, the peak of rainfall rate could be detected earlier with a faster integration.

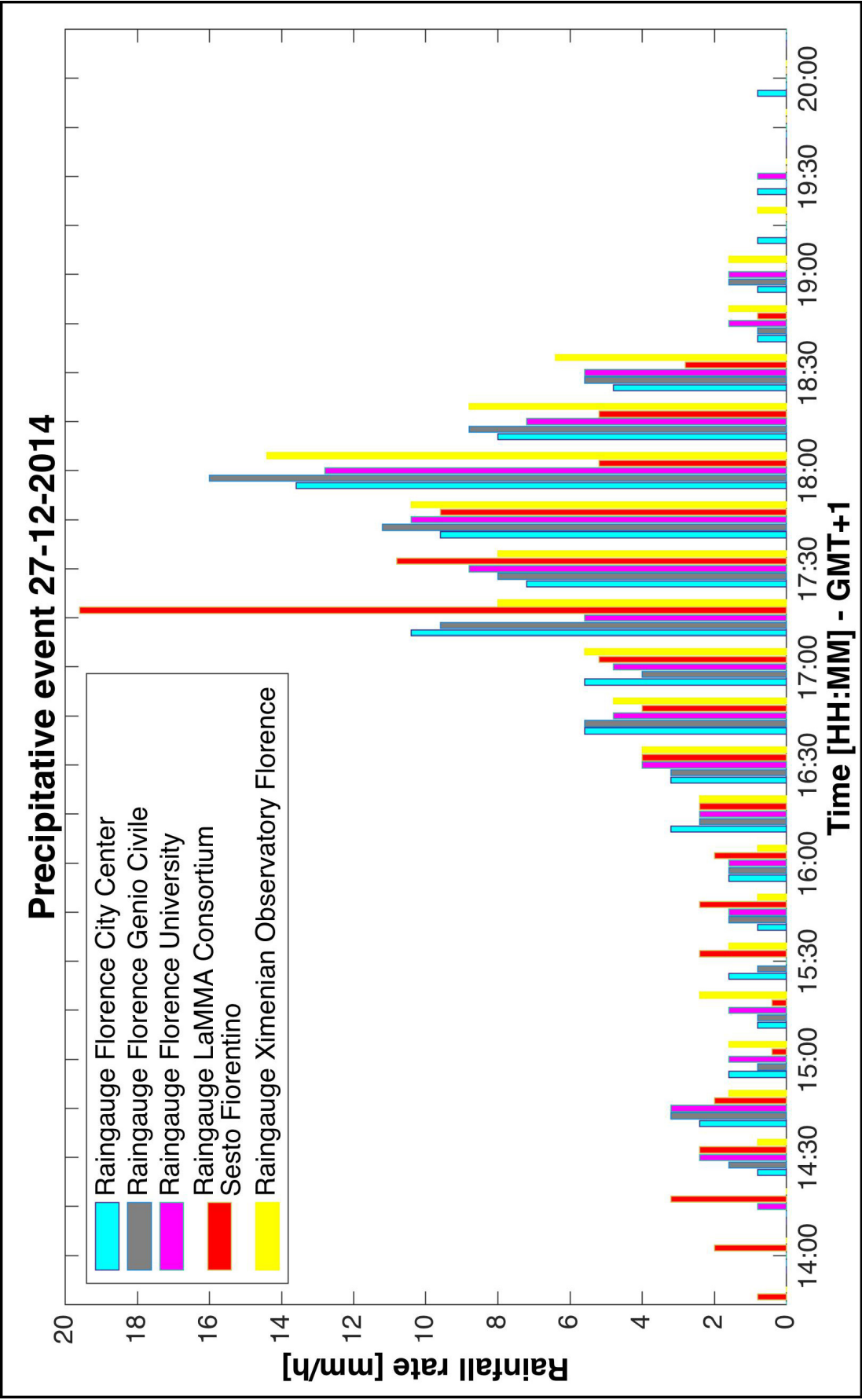
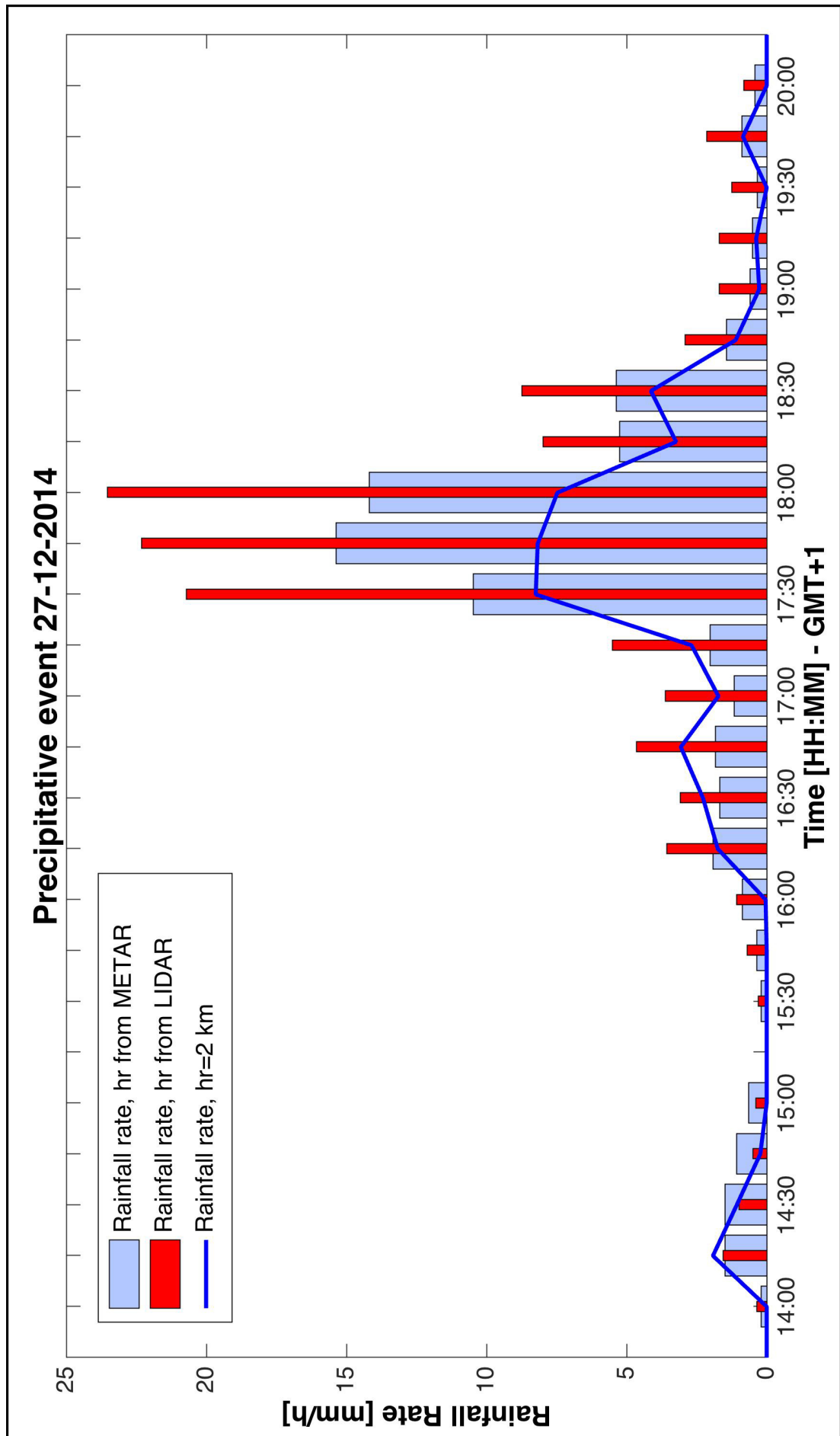


FIGURE 5.1: Rain rate measured by rain gauges

FIGURE 5.2: Rainfall rate: variation of cloud layer  $h_R$  - Fixed vs METAR vs LIDAR

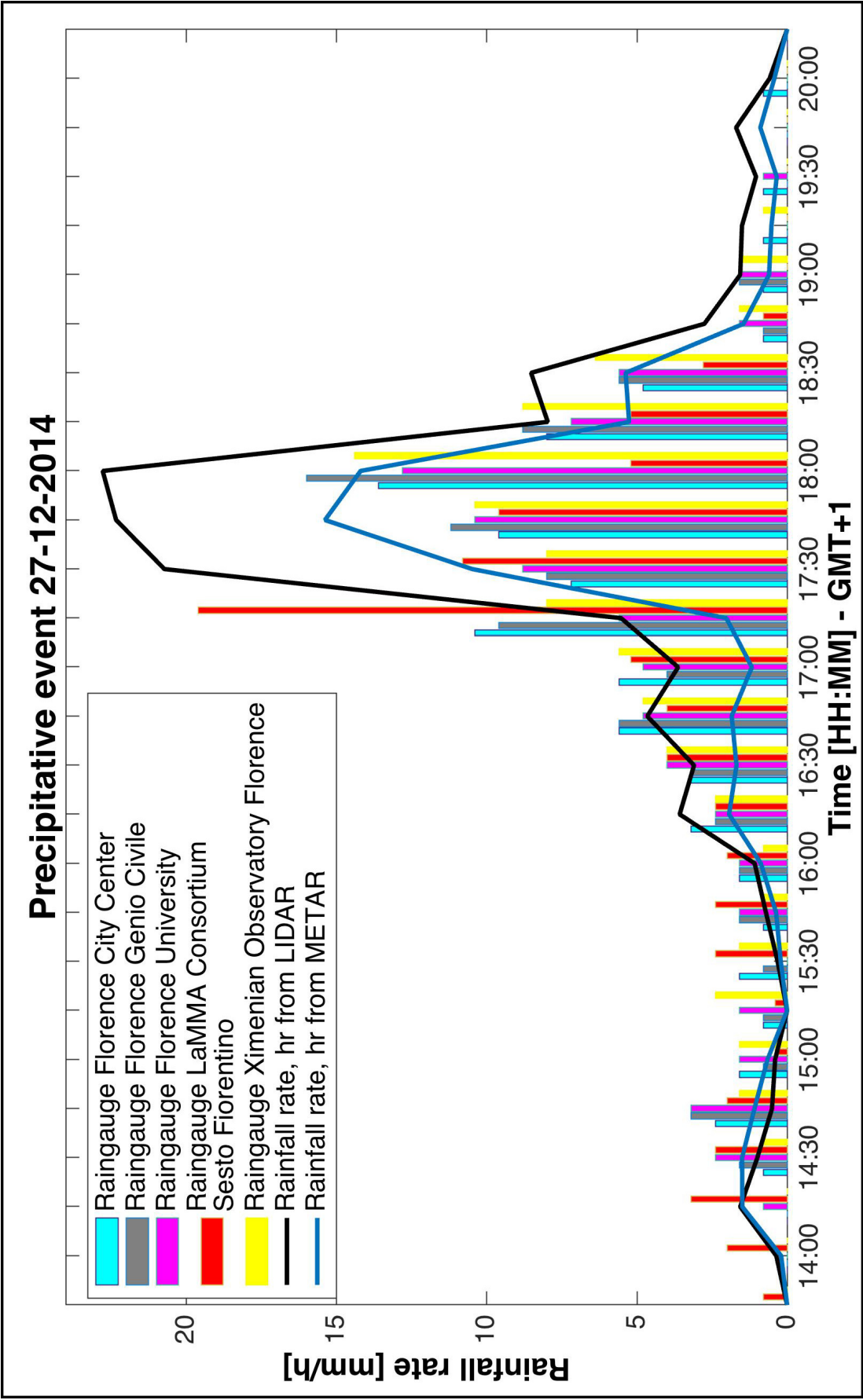


FIGURE 5.3: Rain rate measured by rain gauges vs estimated with RET-AB

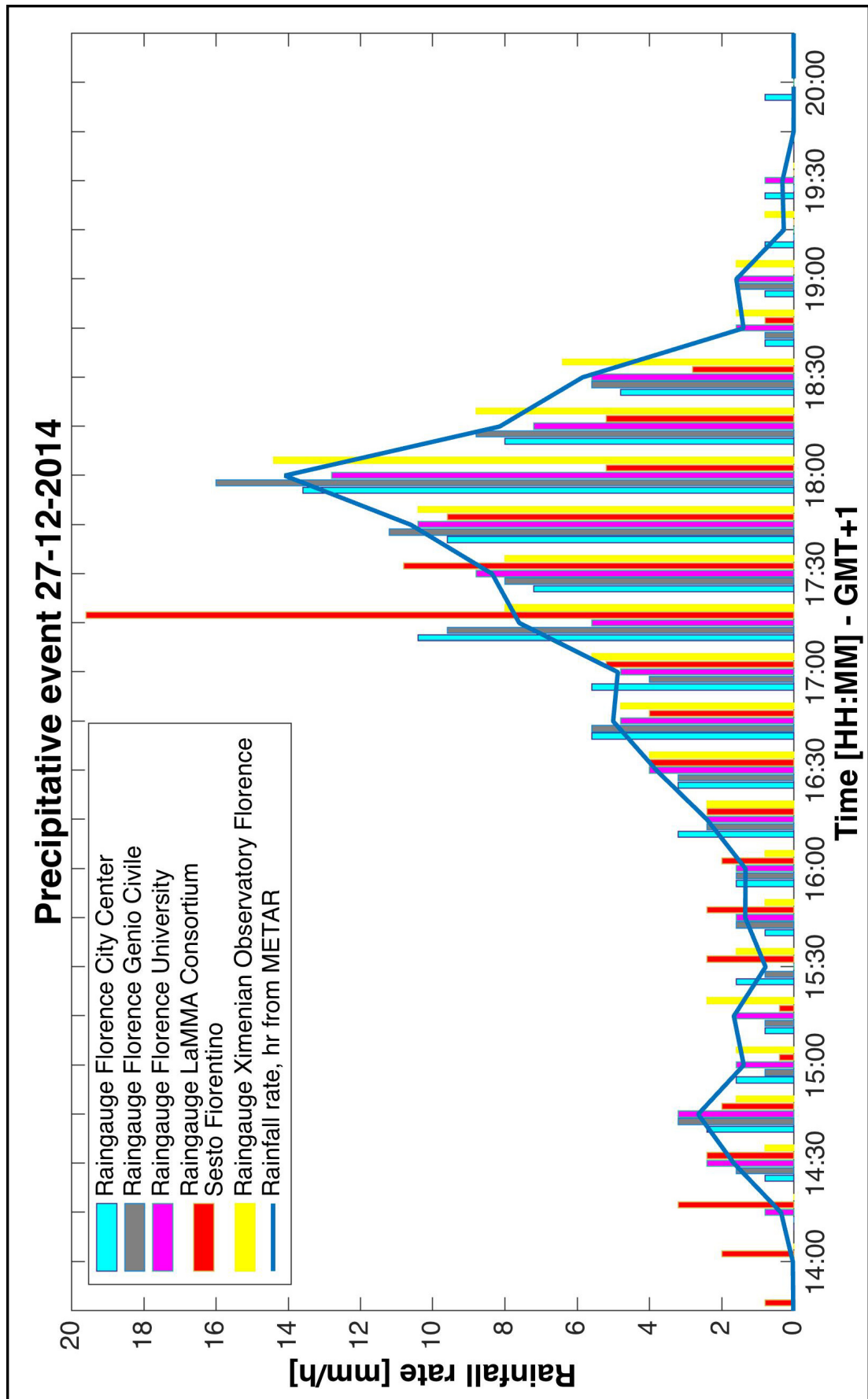


FIGURE 5.4: Rain rate measured by rain gauges vs estimated with RET-AB

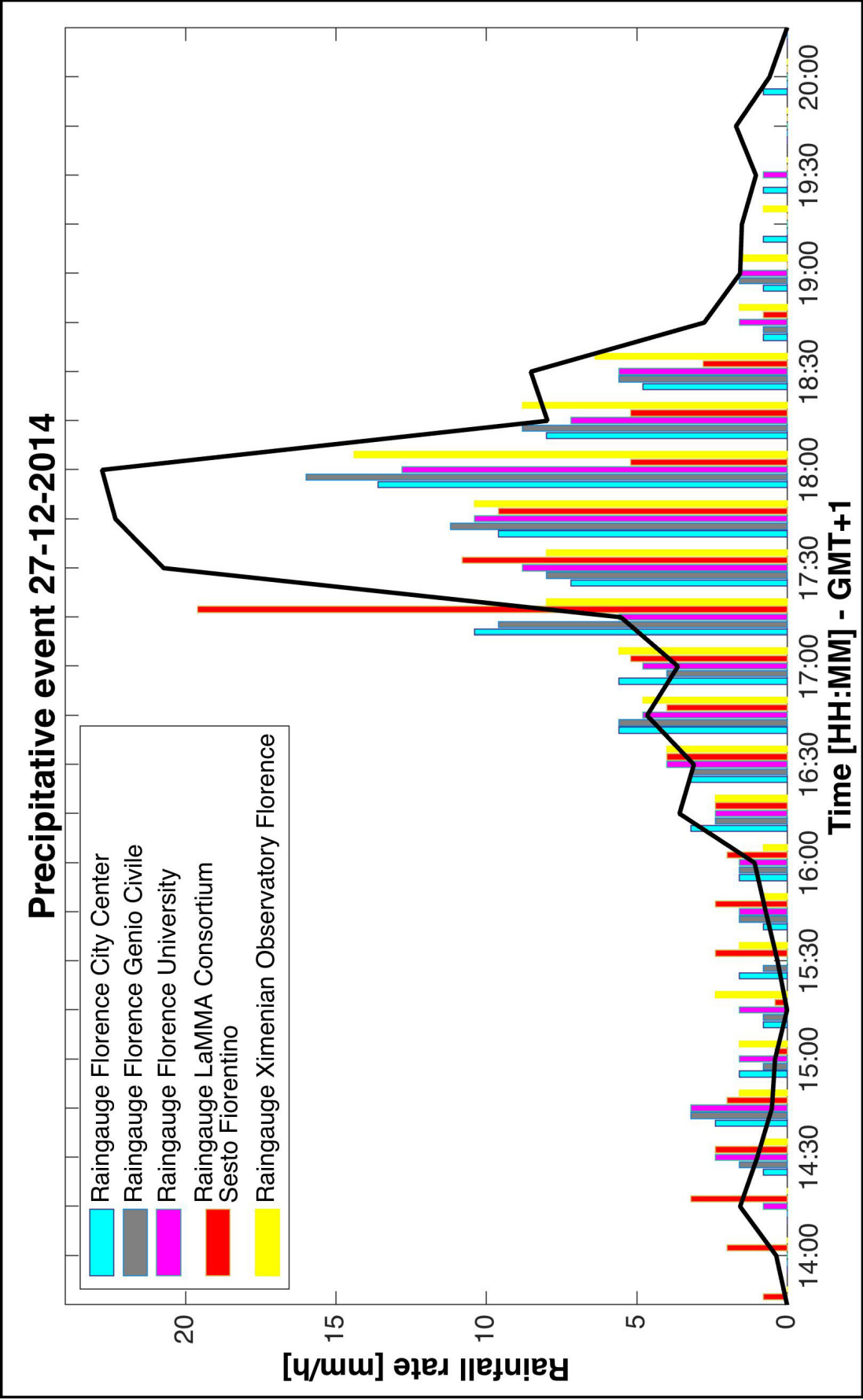


FIGURE 5.5: Rain rate measured by rain gauges vs estimated with RET-AB

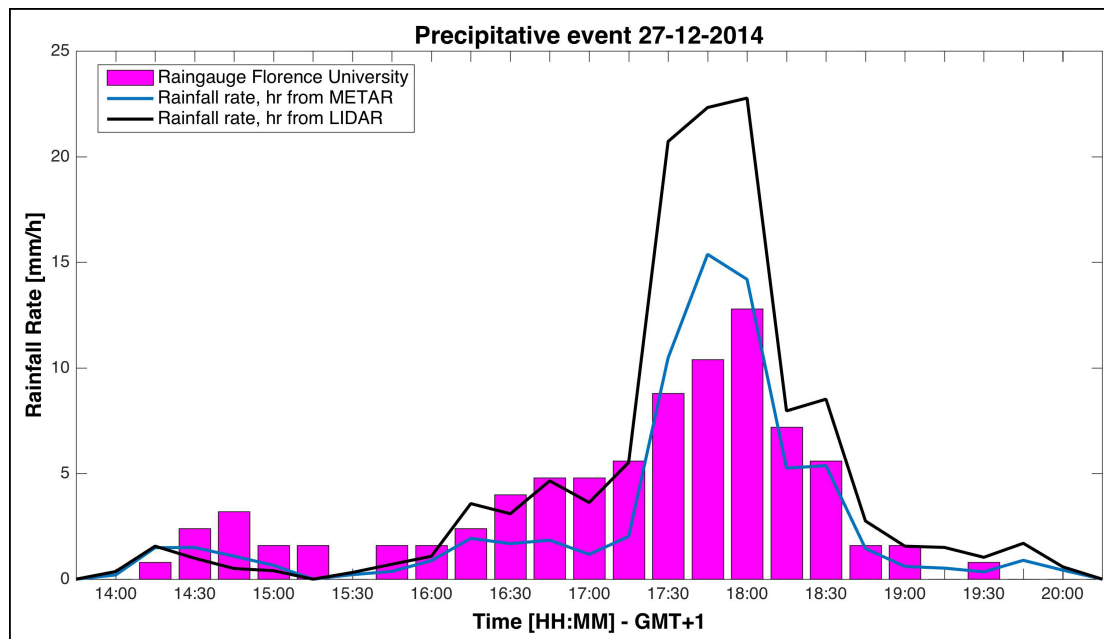


FIGURE 5.6: Rain rate measured by Florence University rain gauge vs estimated with RET-AB

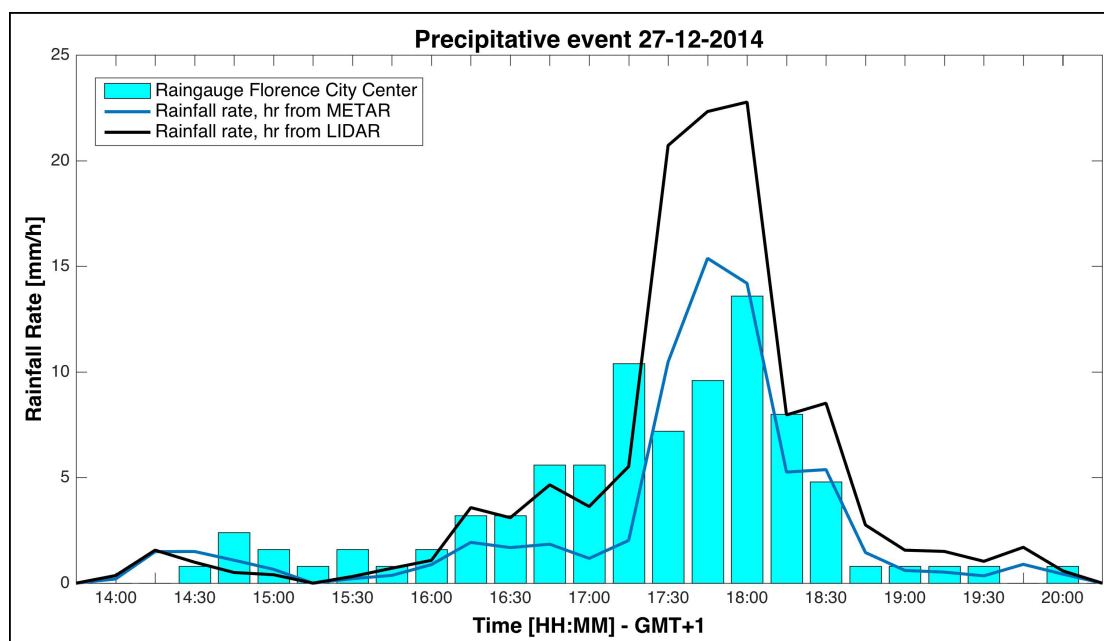


FIGURE 5.7: Rain rate measured by Florence City Center rain gauge vs estimated with RET-AB

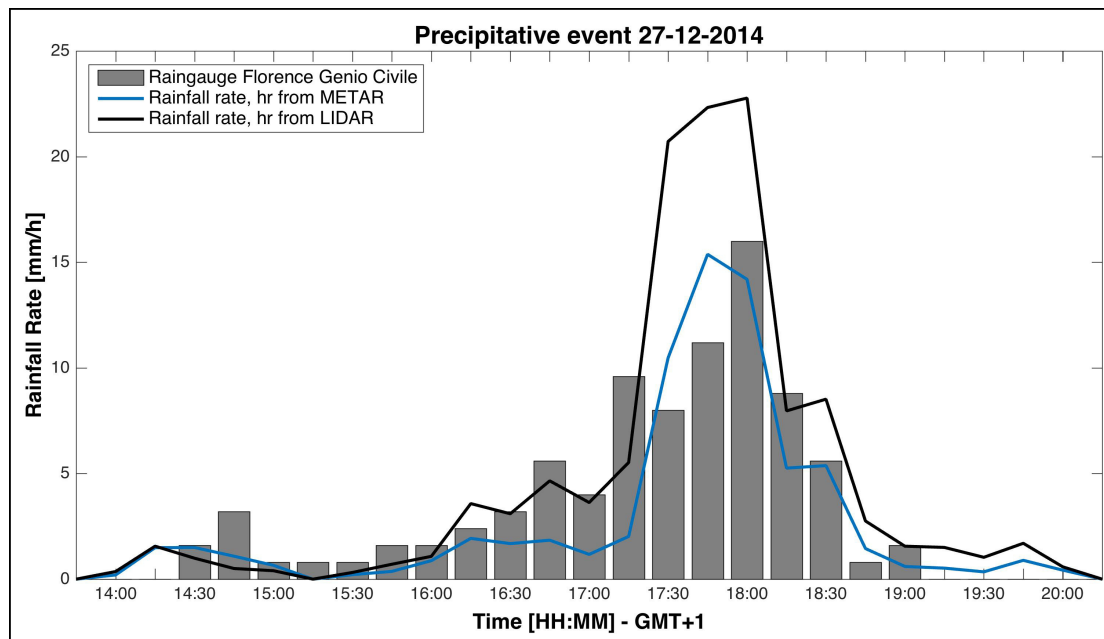


FIGURE 5.8: Rain rate measured by Florence Genio Civile rain gauge vs estimated with RET-AB

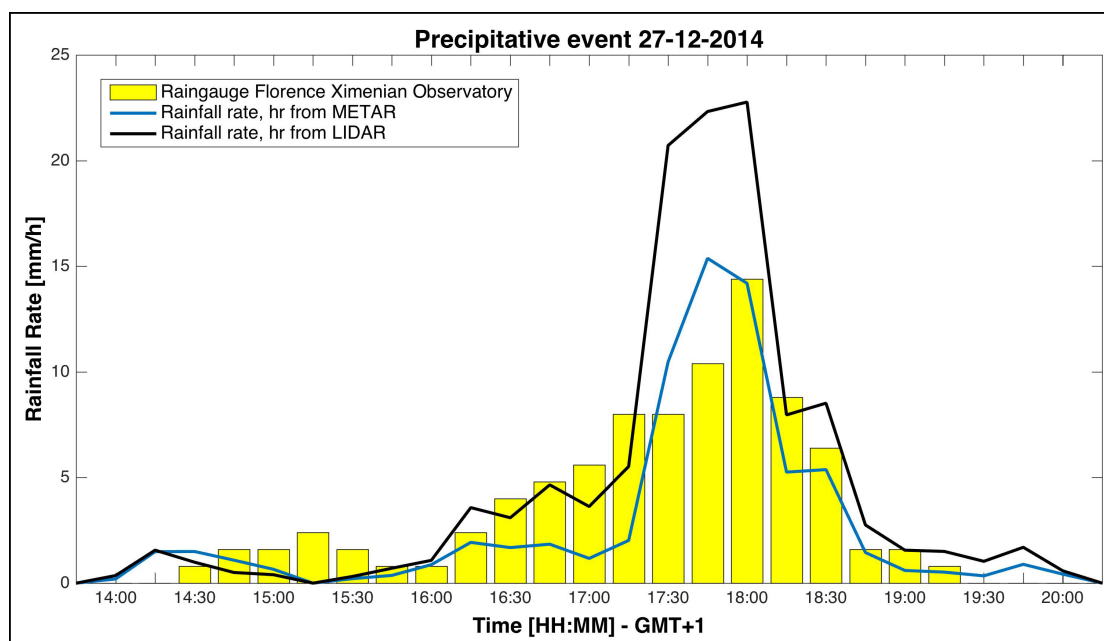


FIGURE 5.9: Rain rate measured by Florence Ximenian Observatory rain gauge vs estimated with RET-AB

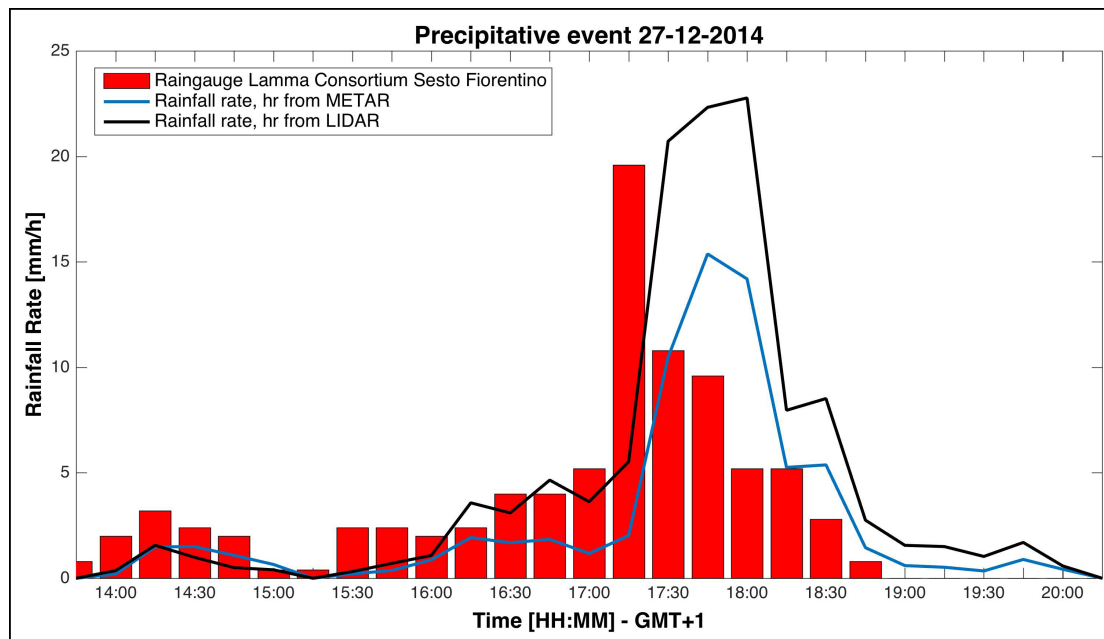


FIGURE 5.10: Rain rate measured by LaMMA Consortium Sesto Fiorentino rain gauge vs estimated with RET-AB

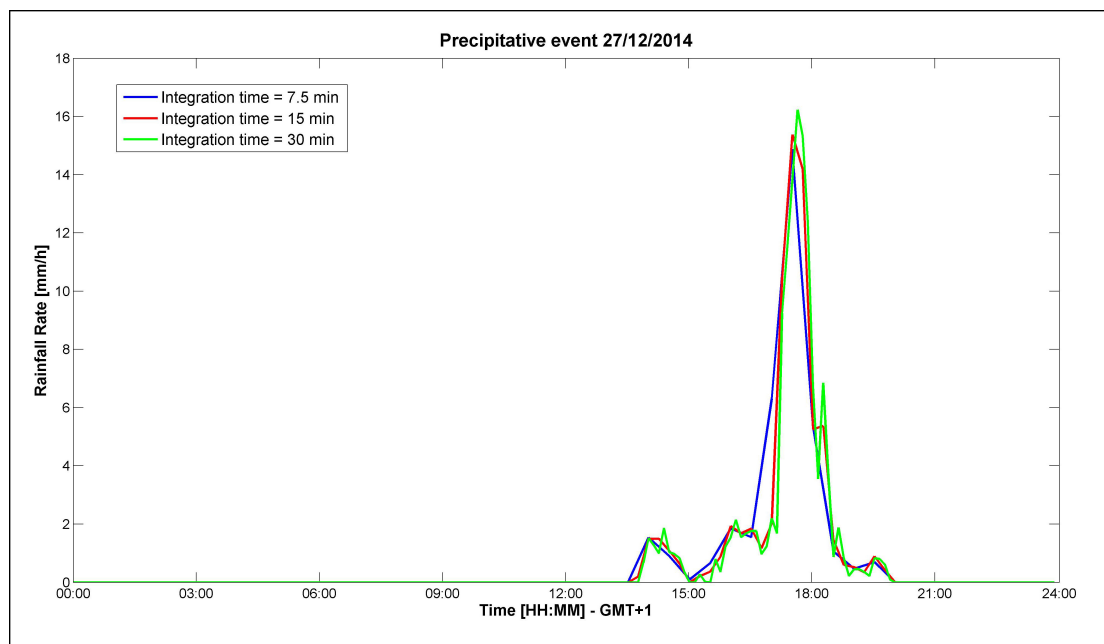


FIGURE 5.11: Rainfall rate evaluated at three different integration times

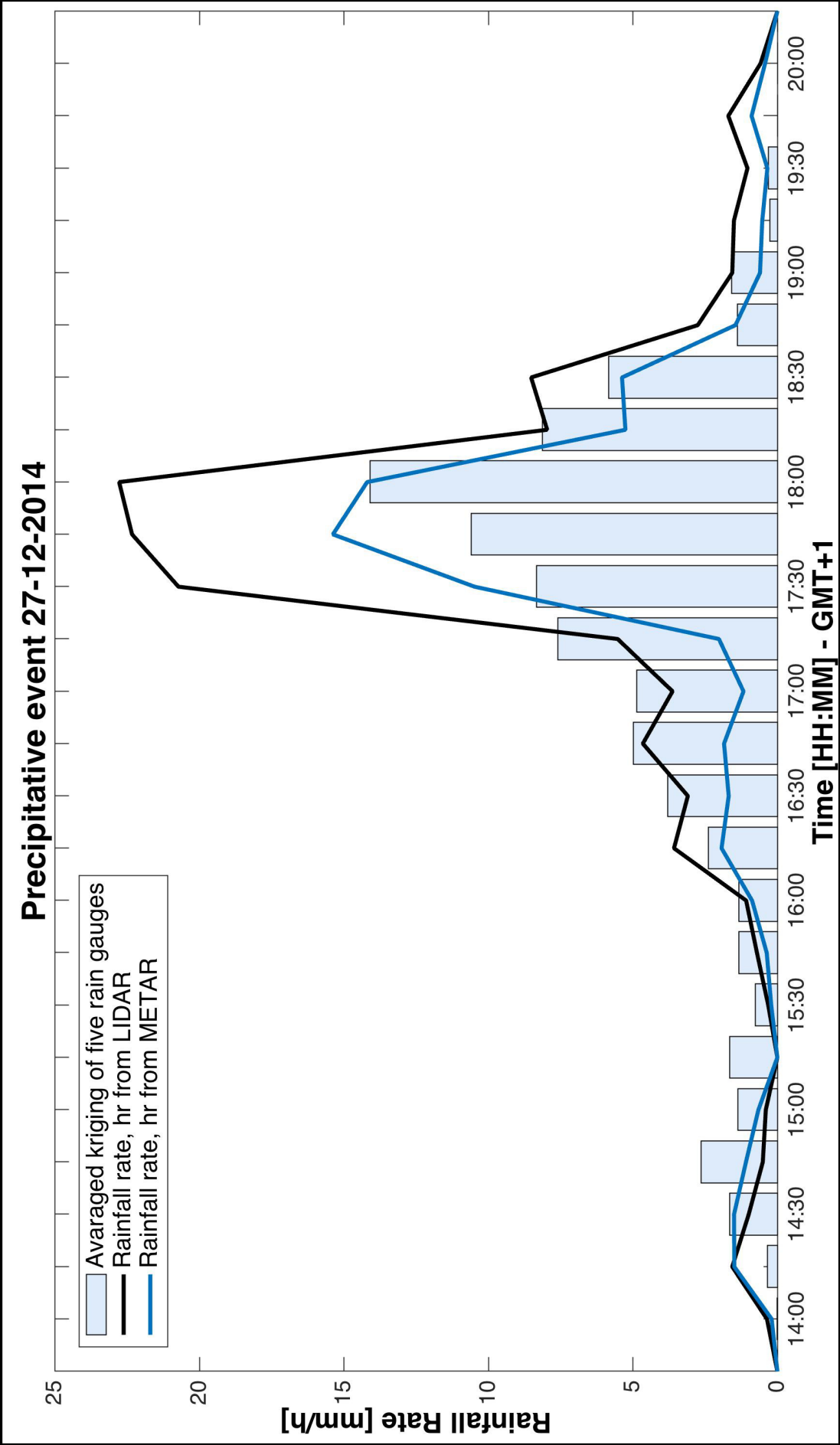


FIGURE 5.12: Comparison of rain rate: estimation with RET-AB vs interpolation with kriging technique

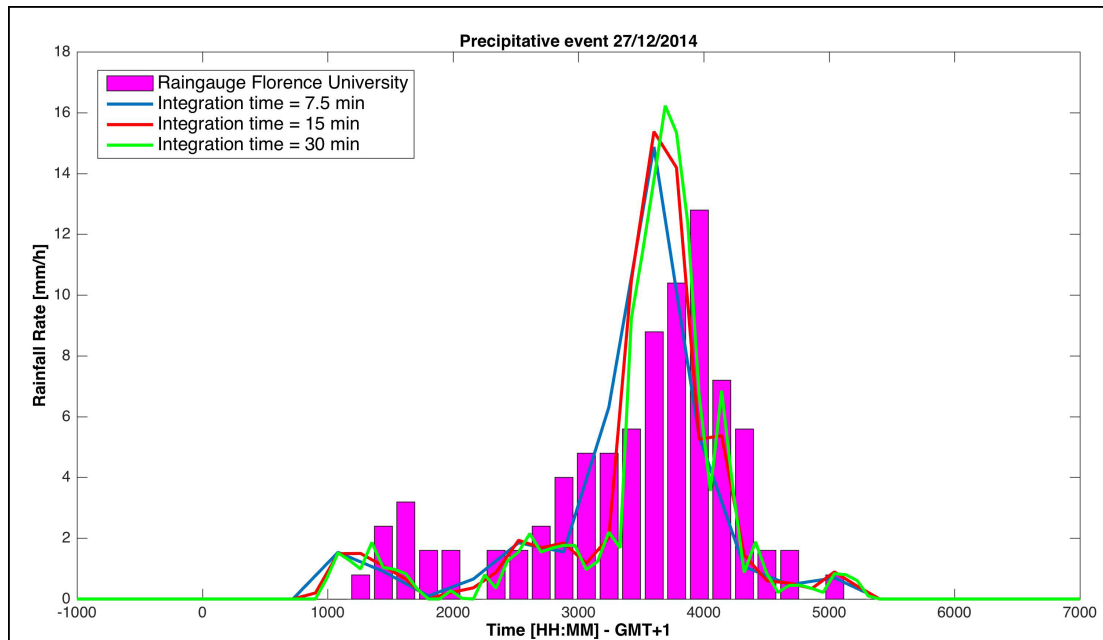


FIGURE 5.13: Rainfall rate evaluated at three different integration times vs measurement by Florence University rain gauge

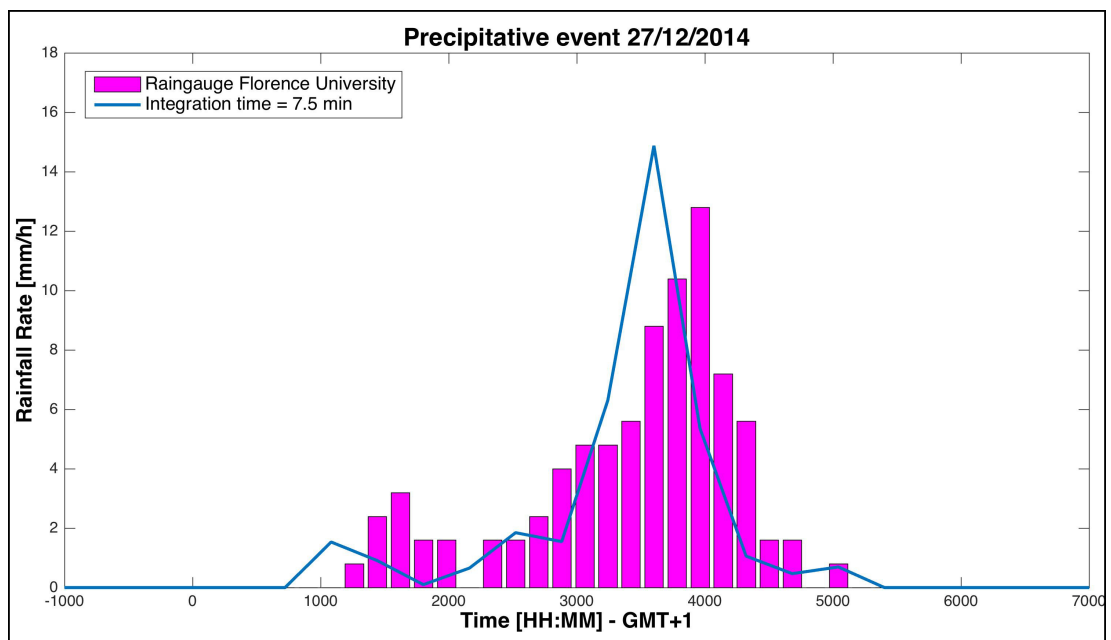


FIGURE 5.14: Rainfall rate evaluated with 7.5' integration times vs measurement by Florence University rain gauge

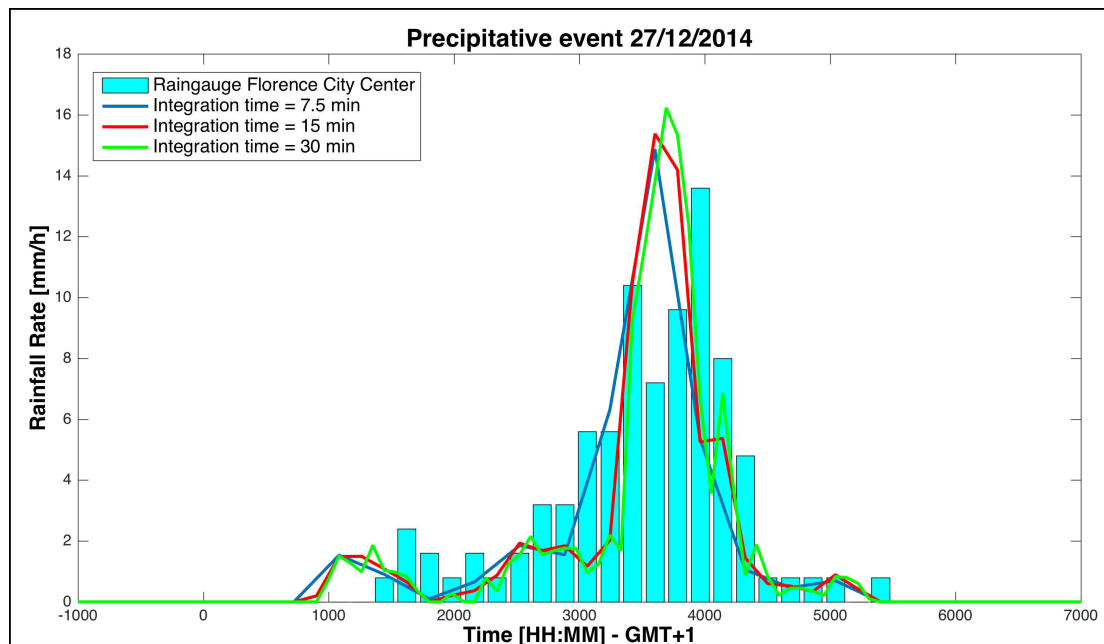


FIGURE 5.15: Rainfall rate evaluated at three different integration times vs measurement by Florence City center rain gauge

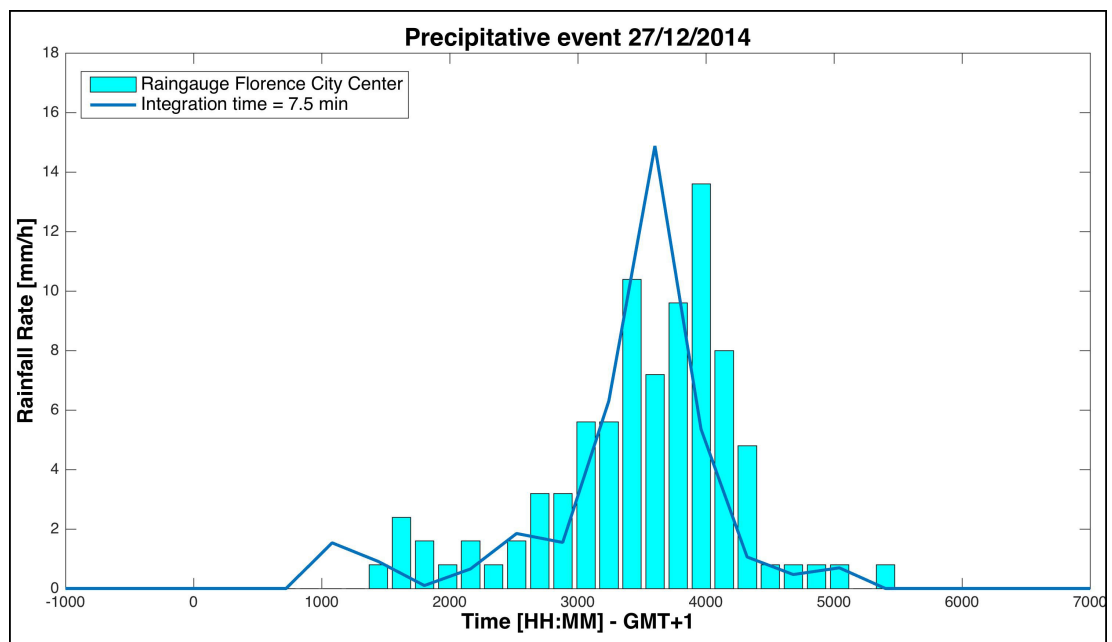


FIGURE 5.16: Rainfall rate evaluated with 7.5' integration times vs measurement by Florence City center rain gauge

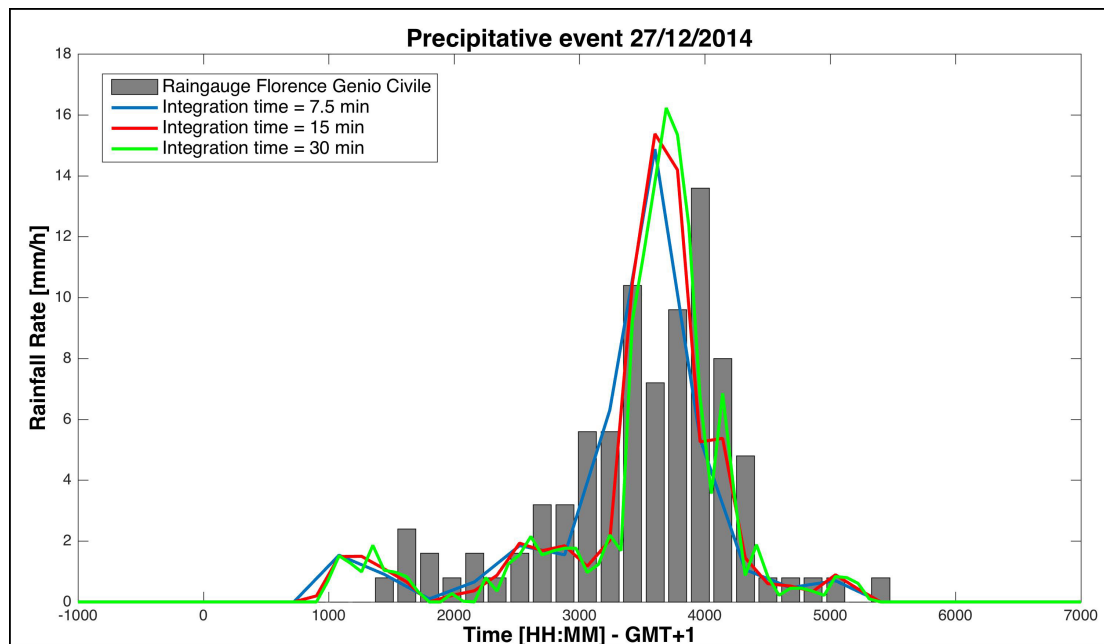


FIGURE 5.17: Rainfall rate evaluated at three different integration times vs measurement by Florence Genio Civile rain gauge

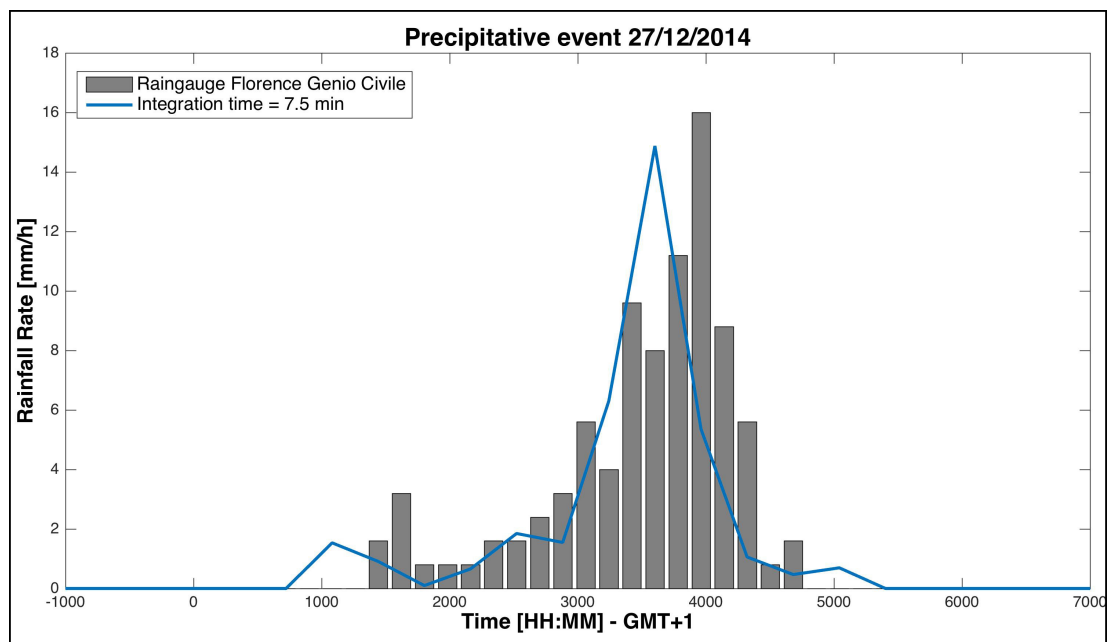


FIGURE 5.18: Rainfall rate evaluated with 7.5' integration times vs measurement by Florence Genio Civile rain gauge

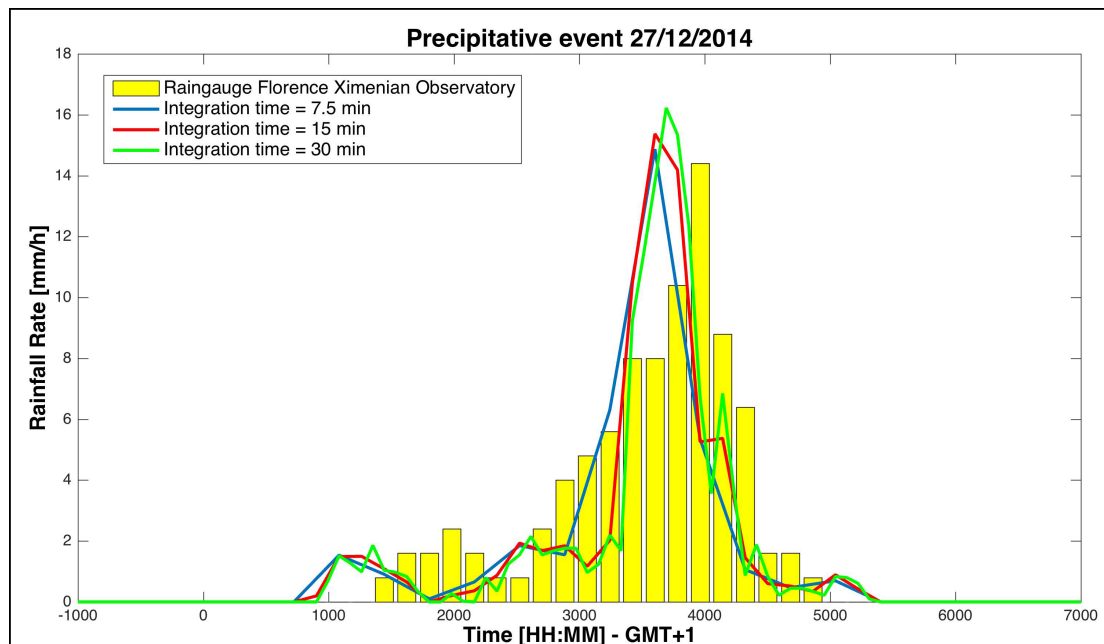


FIGURE 5.19: Rainfall rate evaluated at three different integration times vs measurement by Florence Ximenian Observatory rain gauge

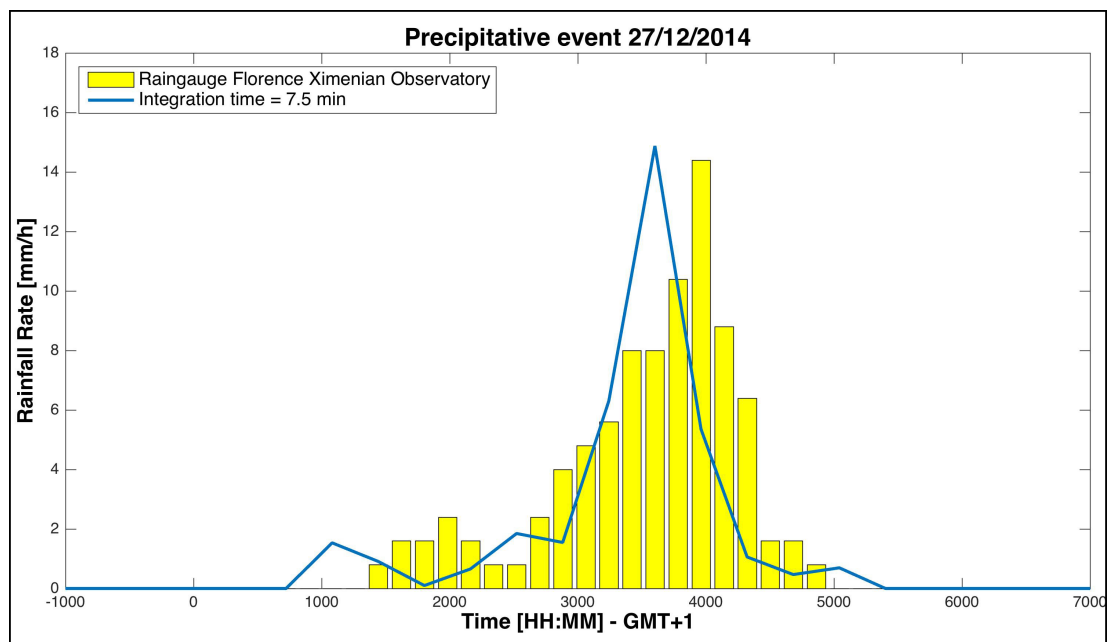


FIGURE 5.20: Rainfall rate evaluated with 7.5' integration times vs measurement by Florence Ximenian Observatory rain gauge

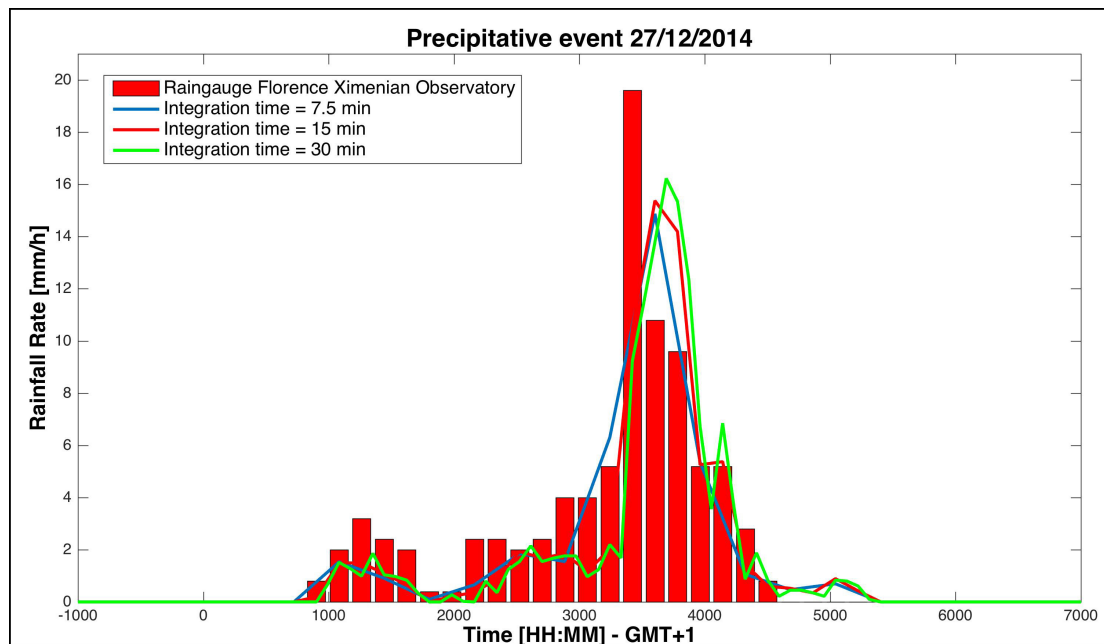


FIGURE 5.21: Rainfall rate evaluated with 7.5' integration times vs measurement by LaMMA Consortium Sesto Fiorentino rain gauge

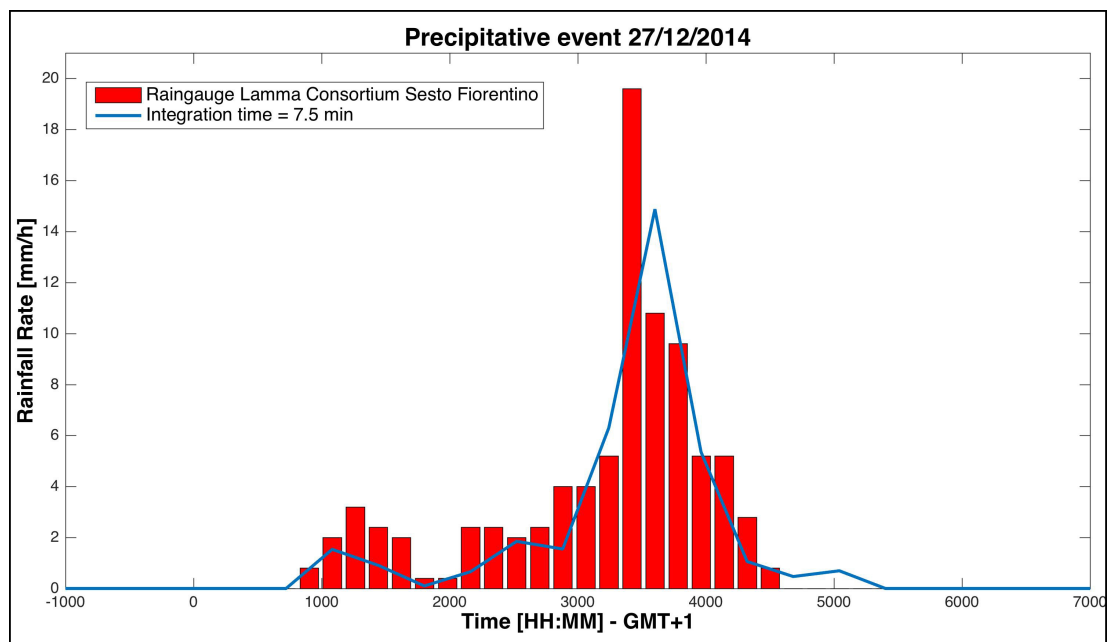


FIGURE 5.22: Rainfall rate evaluated with 7.5' integration times vs measurement by LaMMA Consortium Sesto Fiorentino rain gauge

## 5.2 25 March 2015

The second event is the longest one, since relevant data are reported from 7:00 to 23:45. Also during this day LIDAR was active and a comparison with METAR is shown [5.24](#), [5.26](#), [5.27](#) and [5.25](#); those figures report the retrieved data superimposed on the bars representing the measurement by regional sensors.

Like the first event, LIDAR has recorded lower values of cloud altitude, causing an increase of rainfall rate, in respect on the ones referring to METAR bulletins measurements.

Figures [5.26](#) and [5.27](#) compare in detail data of every single rain gauge with the amount of rain estimated with RET-AB (considering the altitude relating to METAR and LIDAR).

Three particular situations verified, in particular:

- the first peak in the morning is recorded by rain gauges at different times (at 8:45 in figure [5.29](#), at 9:00 in [5.32](#) and at 9:15 in [5.28](#), [5.30](#) and [5.31](#));
- the same problem occurs with the peaks around 18:00 and 20:00, both collected by rain gauges at different times.

Figures [5.28](#), [5.29](#), [5.30](#), [5.31](#), [5.32](#) show that estimated rainfall rate trends data from rain gauges: differently from the previous situation, in this case, data processing with  $h_R$  the calculated by METAR are more conform to rain gauges measurements. Another particular situation is an underestimation around 20:00: this problem could be connected to the absence of clouds out of Florence City Center, in the north west area respect to the link where airport sensor and LIDAR are installed (it appears clearly by seeing the map [5.45](#)). In fact, in the area of Sesto Fiorentino the amount of rain measured by Lamma rain gauge is lower than the other devices: it mean a rapid evolution of the precipitation, maybe combined with by strong wind.

Figure [5.33](#) outlines the difference between three integration times (7.5', 15' and 30'), detailed in [5.35](#) - [5.44](#).

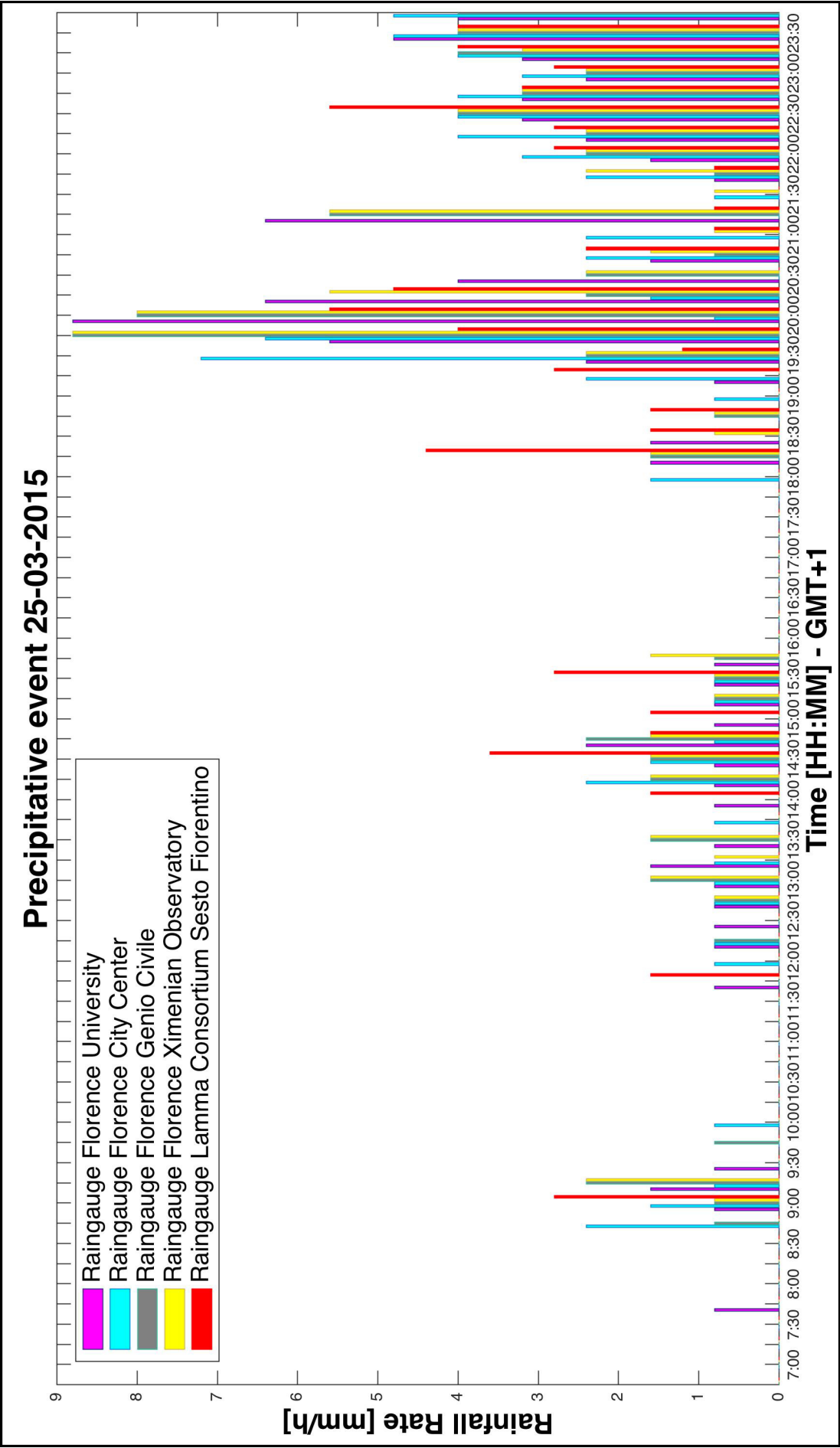


FIGURE 5.23: Rain rate measured by rain gauges

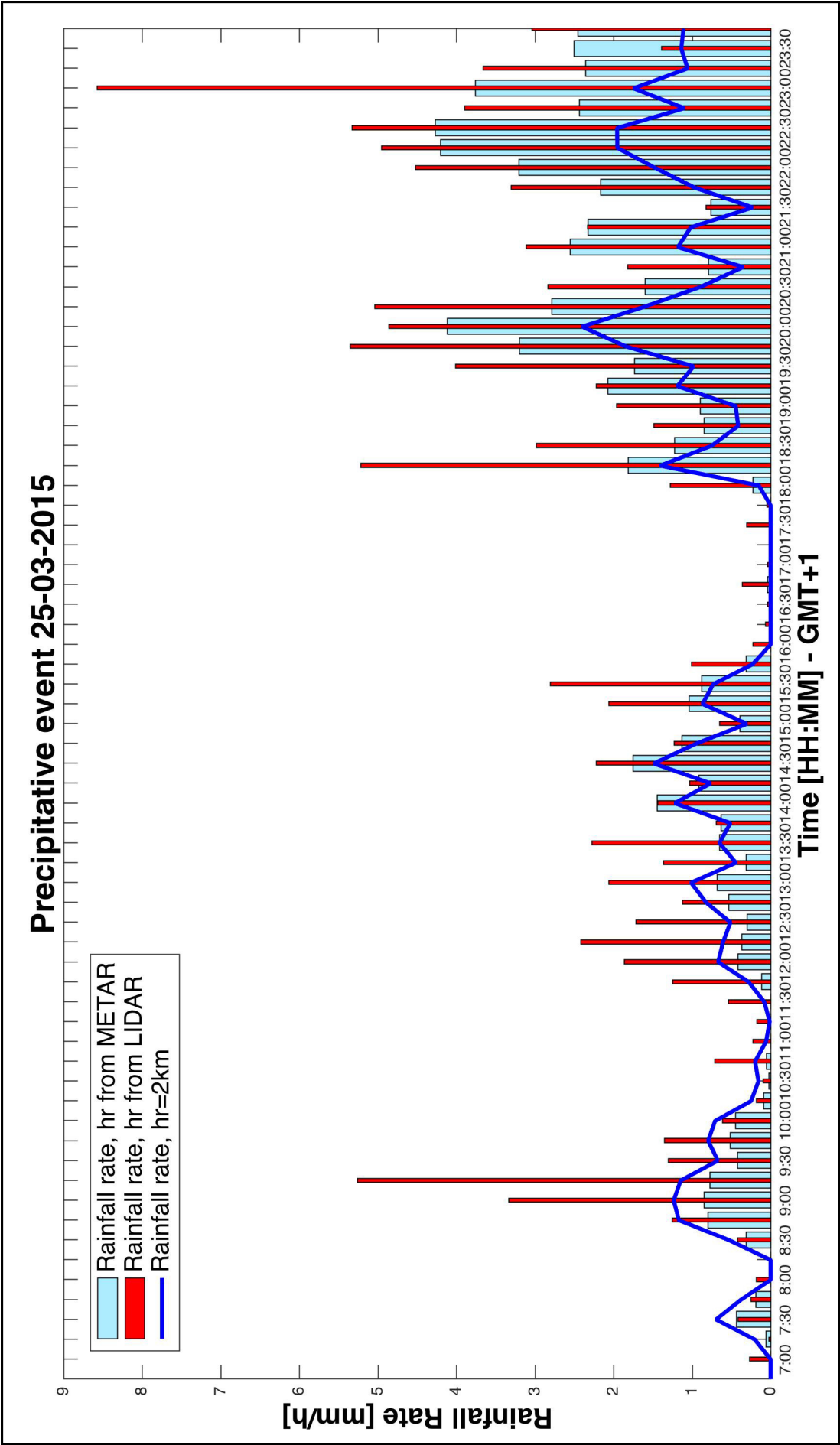


FIGURE 5.24: Rainfall rate: variation of cloud layer  $h_R$  - Fixed vs METAR vs LIDAR

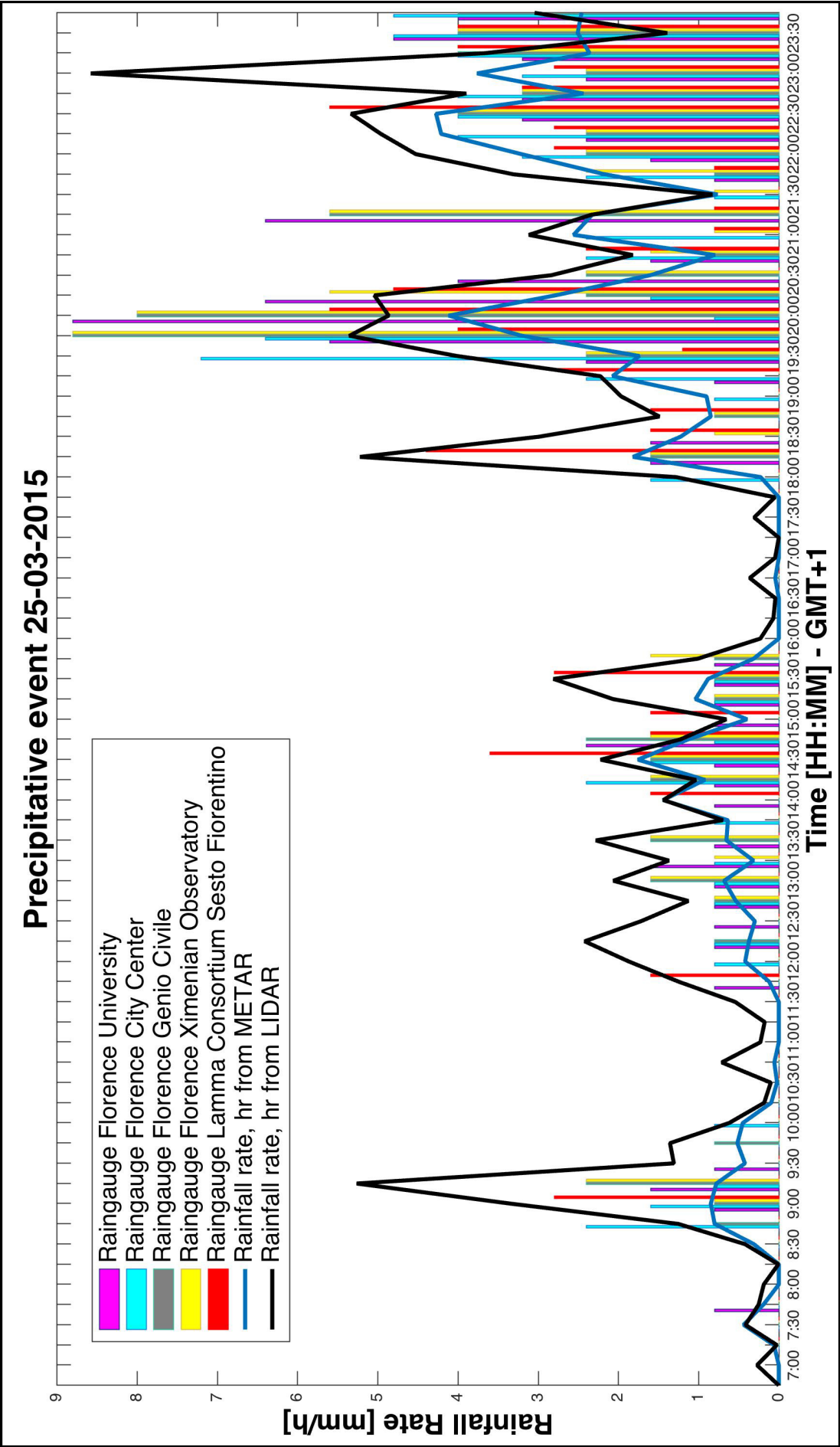


FIGURE 5.25: Rain rate measured by rain gauges vs estimated with RET-AB

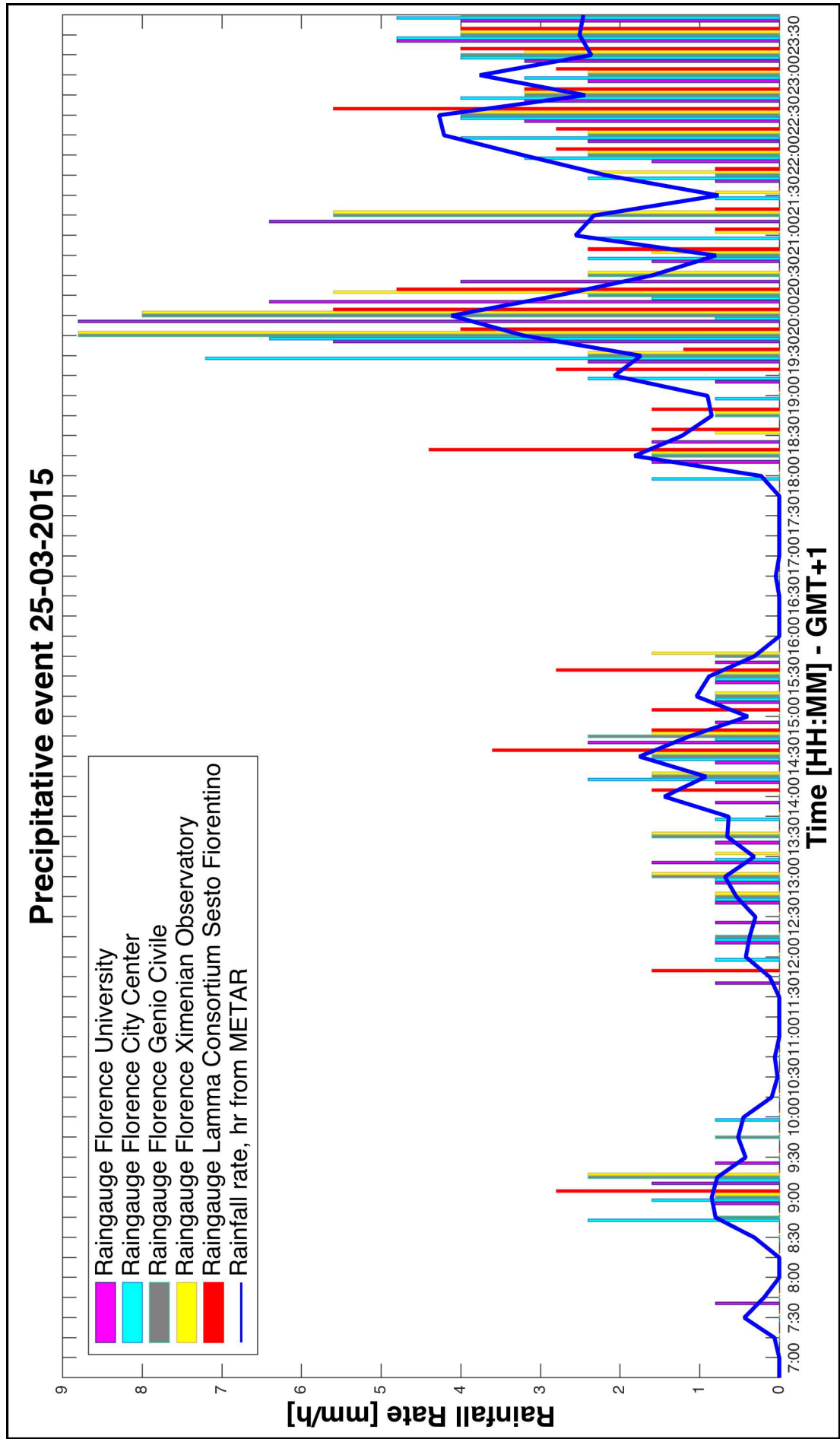


FIGURE 5.26: Rain rate measured by rain gauges vs estimated with RET-AB

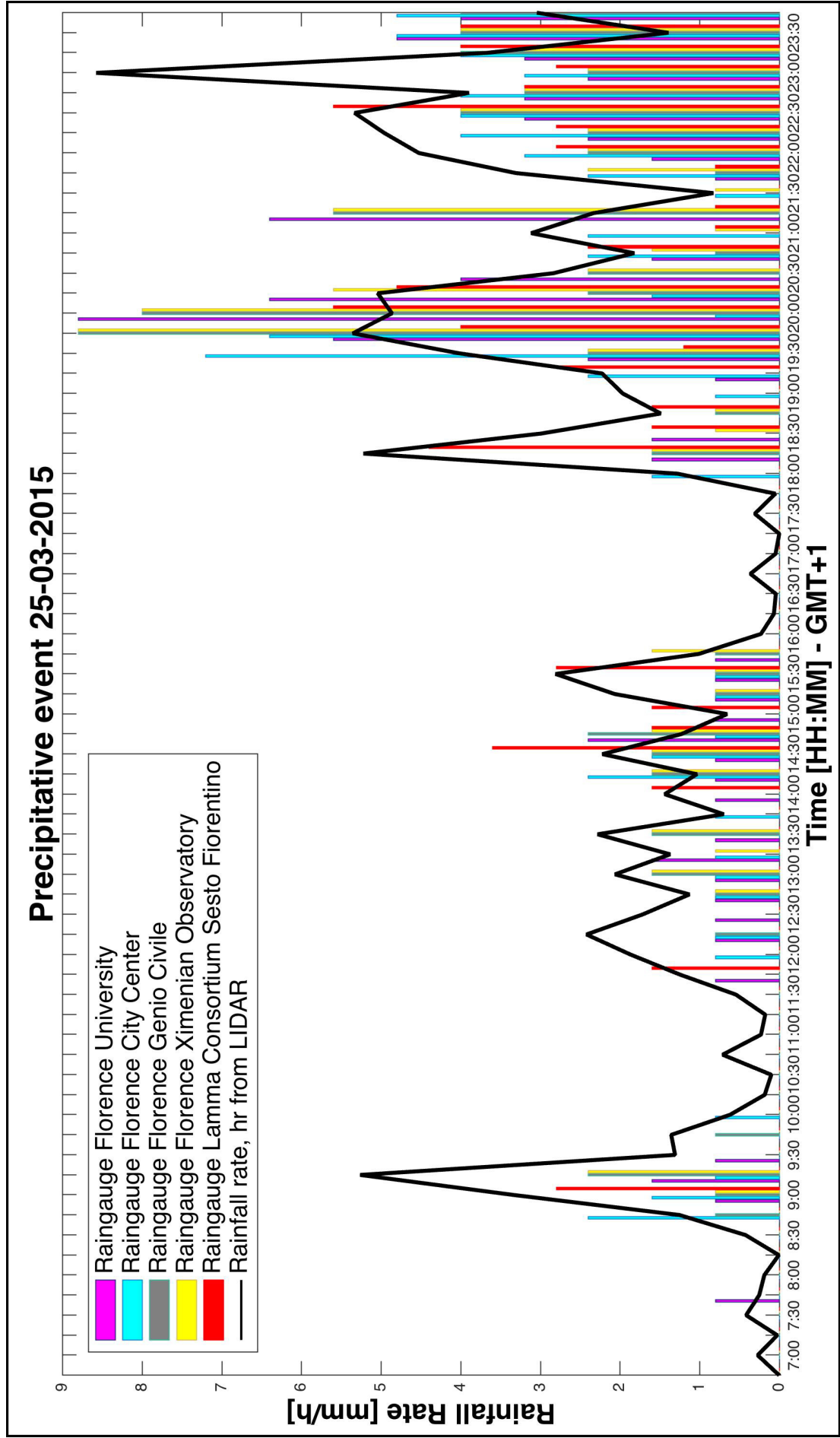


FIGURE 5.27: Rain rate measured by rain gauges vs estimated with RET-AB

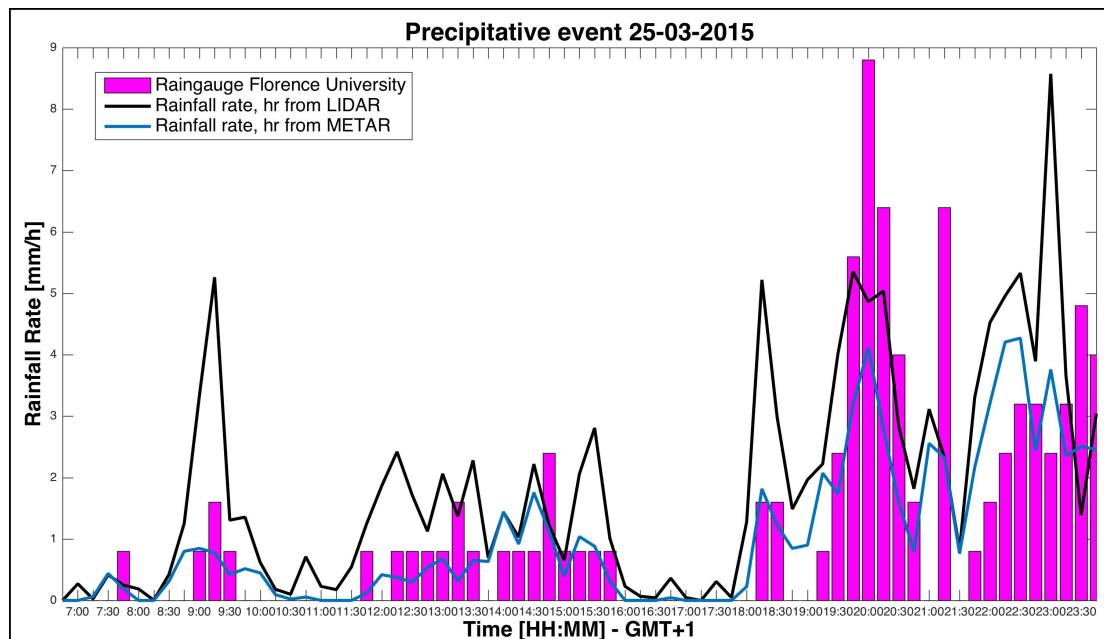


FIGURE 5.28: Rain rate measured by Florence University rain gauge vs estimated with RET-AB

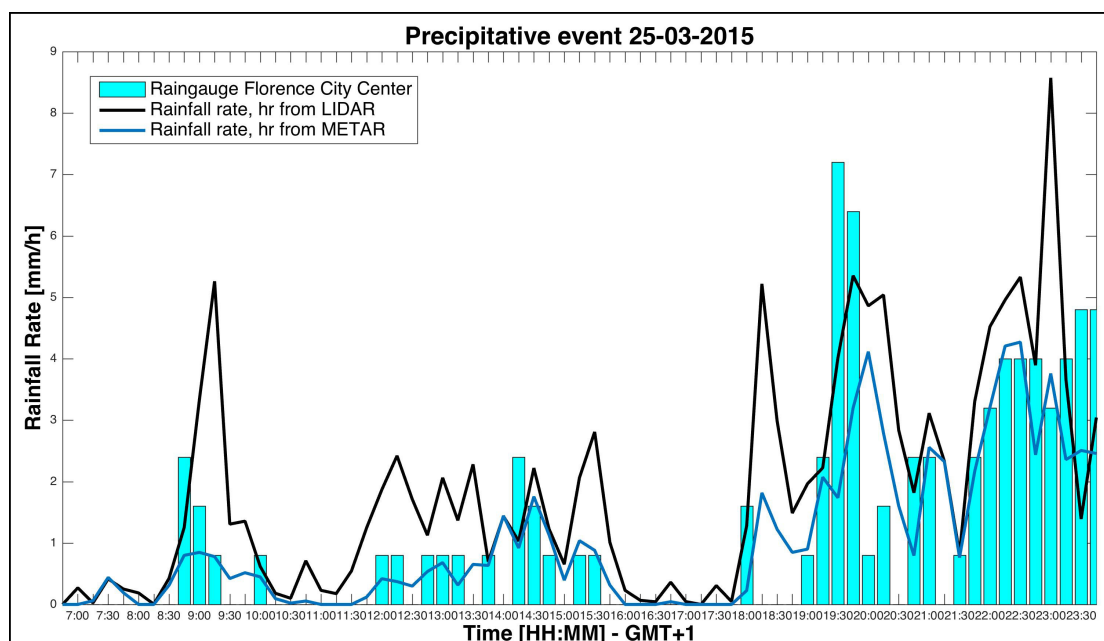


FIGURE 5.29: Rain rate measured by Florence City Center rain gauge vs estimated with RET-AB

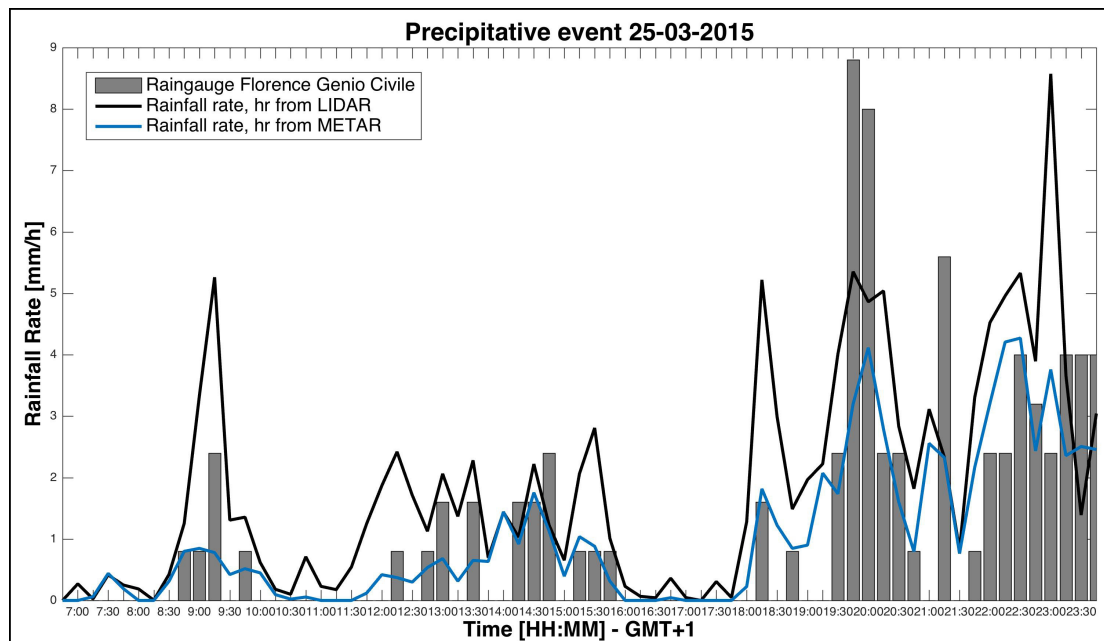


FIGURE 5.30: Rain rate measured by Florence Genio Civile rain gauge vs estimated with RET-AB

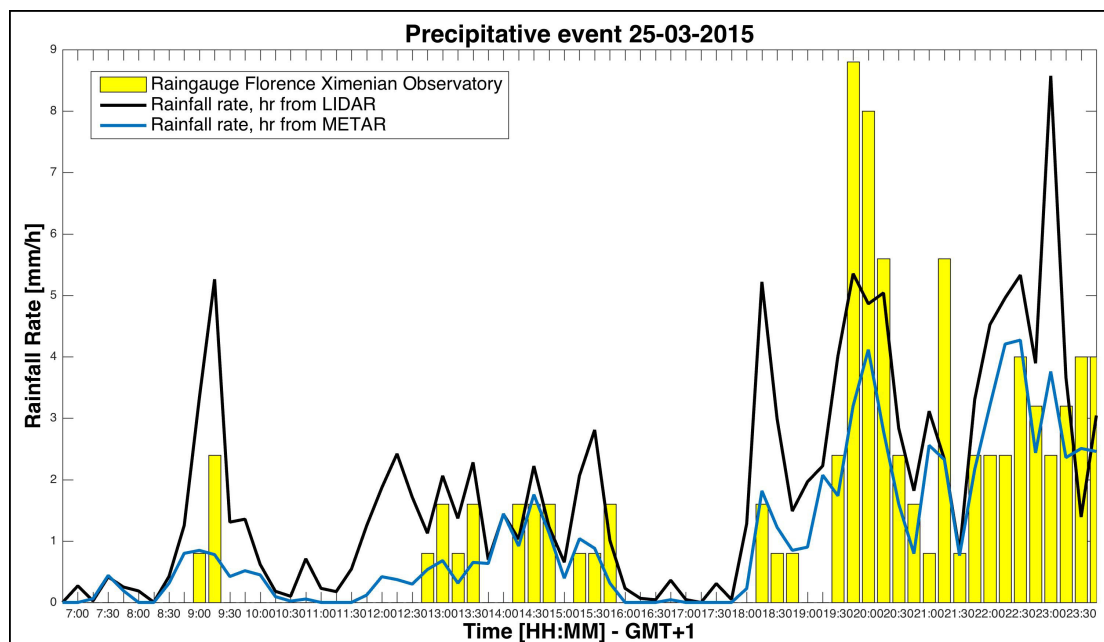


FIGURE 5.31: Rain rate measured by Florence Ximenian Observatory rain gauge vs estimated with RET-AB

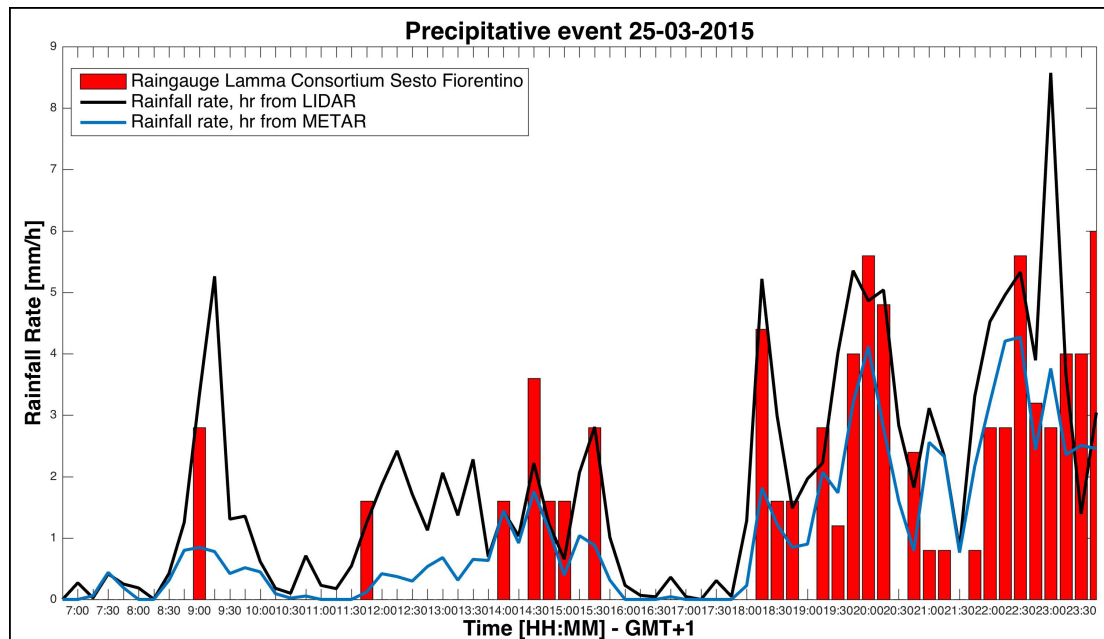


FIGURE 5.32: Rain rate measured by LaMMA Consortium Sesto Fiorentino rain gauge vs estimated with RET-AB

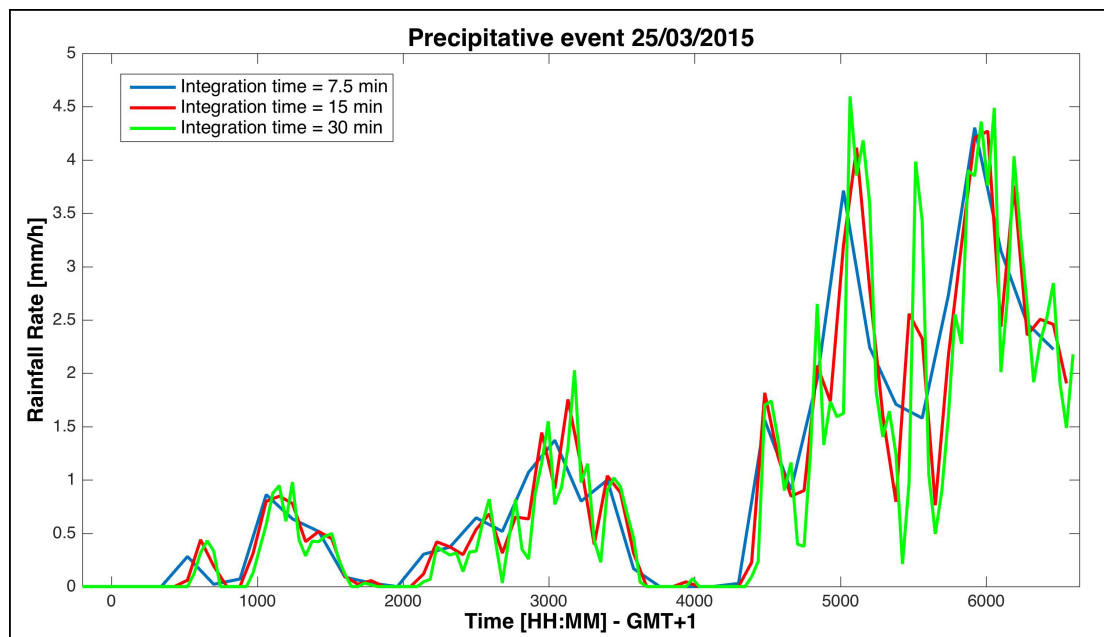


FIGURE 5.33: Rainfall rate evaluated at three different integration times

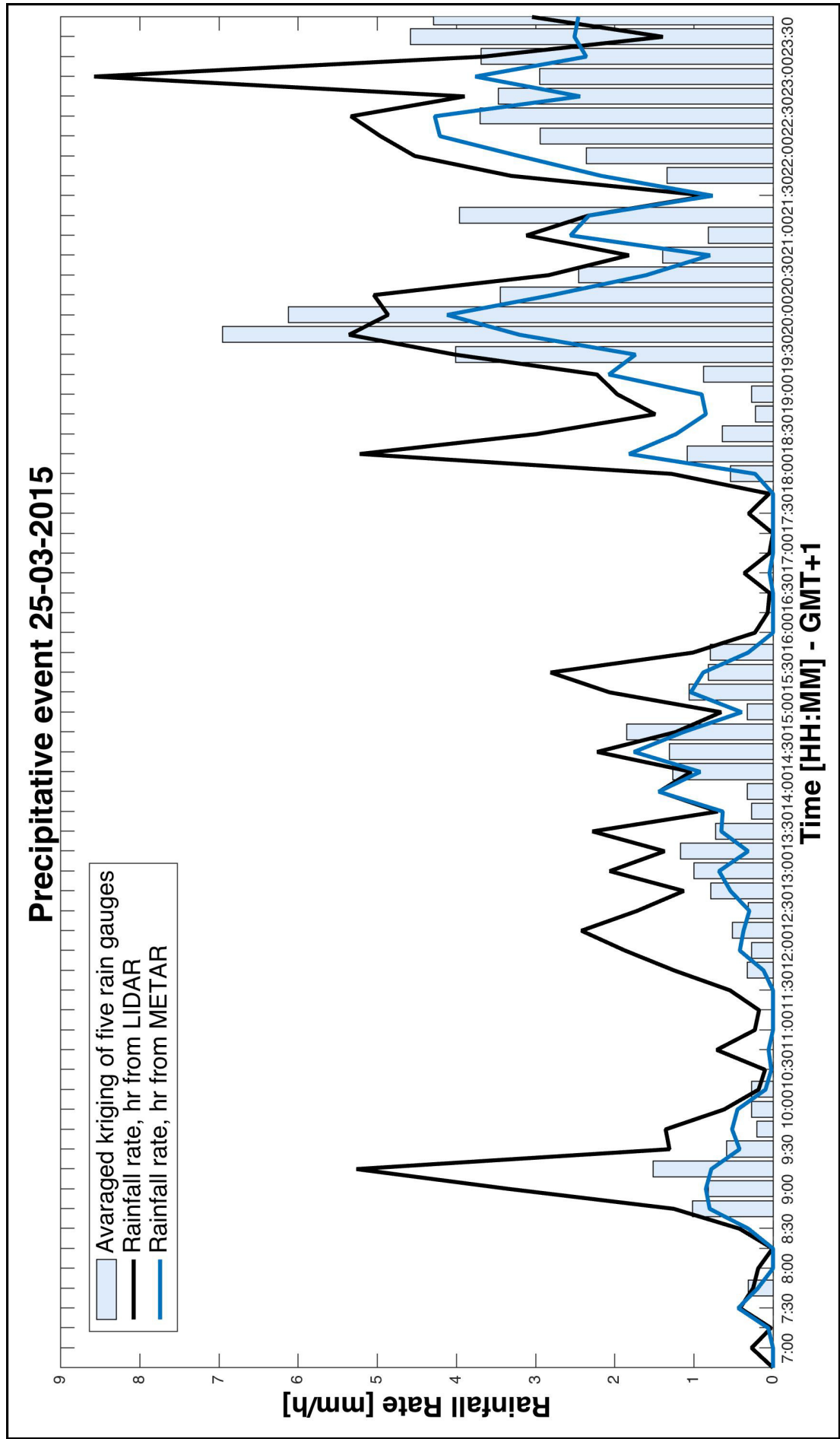


FIGURE 5.34: Comparison of rain rate: estimation with RET-AB vs interpolation with kriging technique

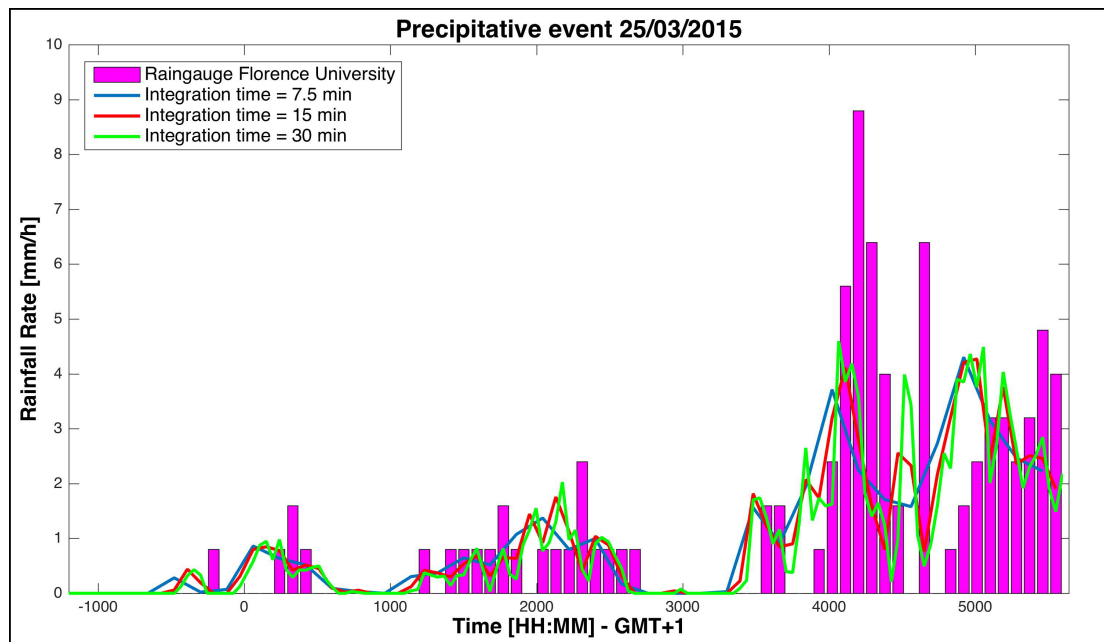


FIGURE 5.35: Rainfall rate evaluated at three different integration times vs measurement by Florence University rain gauge

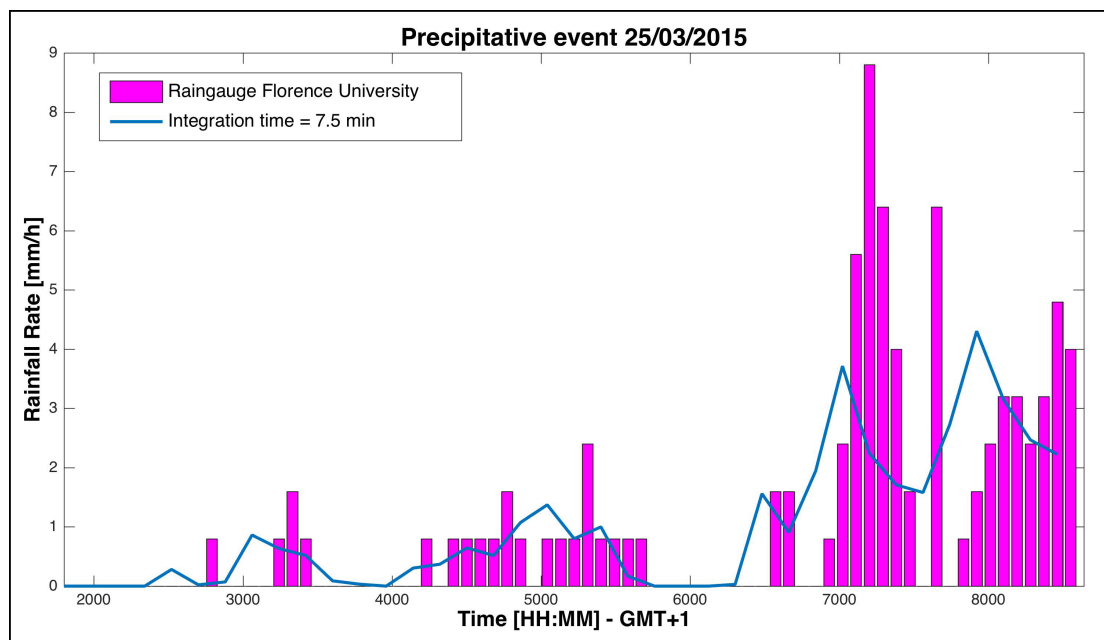


FIGURE 5.36: Rainfall rate evaluated with 7.5' integration times vs measurement by Florence University rain gauge

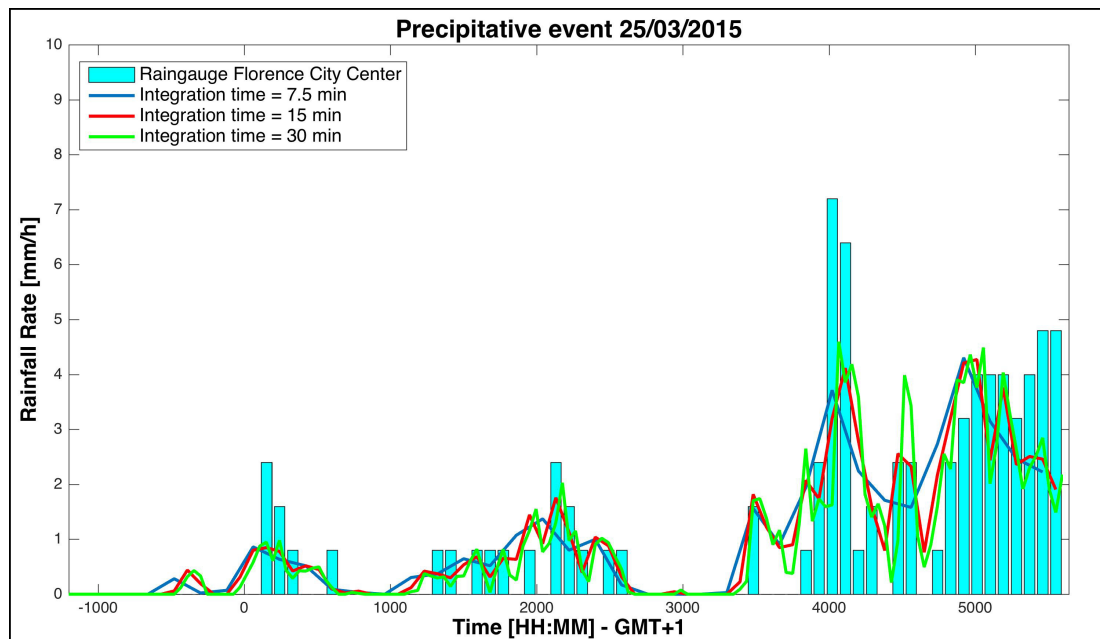


FIGURE 5.37: Rainfall rate evaluated at three different integration times vs measurement by Florence City center rain gauge

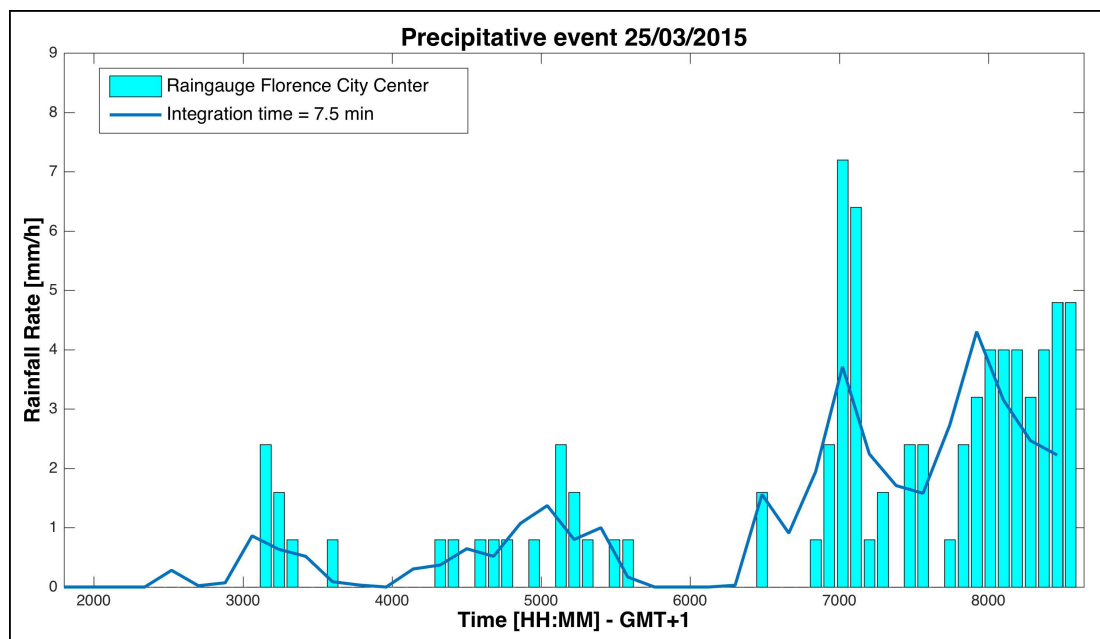


FIGURE 5.38: Rainfall rate evaluated with 7.5' integration times vs measurement by Florence City center rain gauge

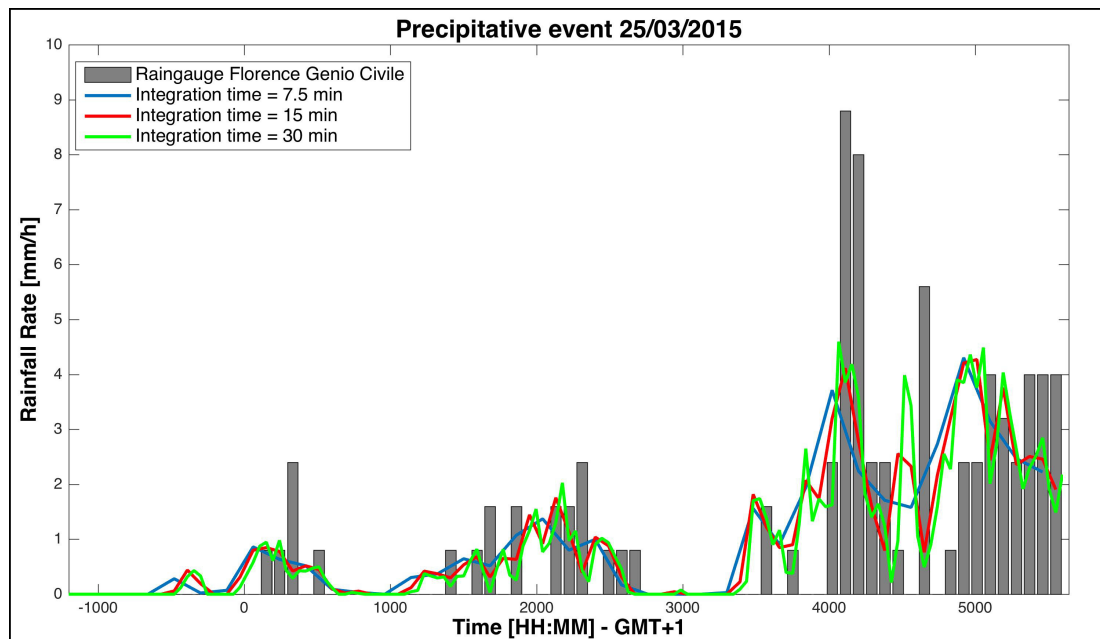


FIGURE 5.39: Rainfall rate evaluated at three different integration times vs measurement by Florence Genio Civile rain gauge

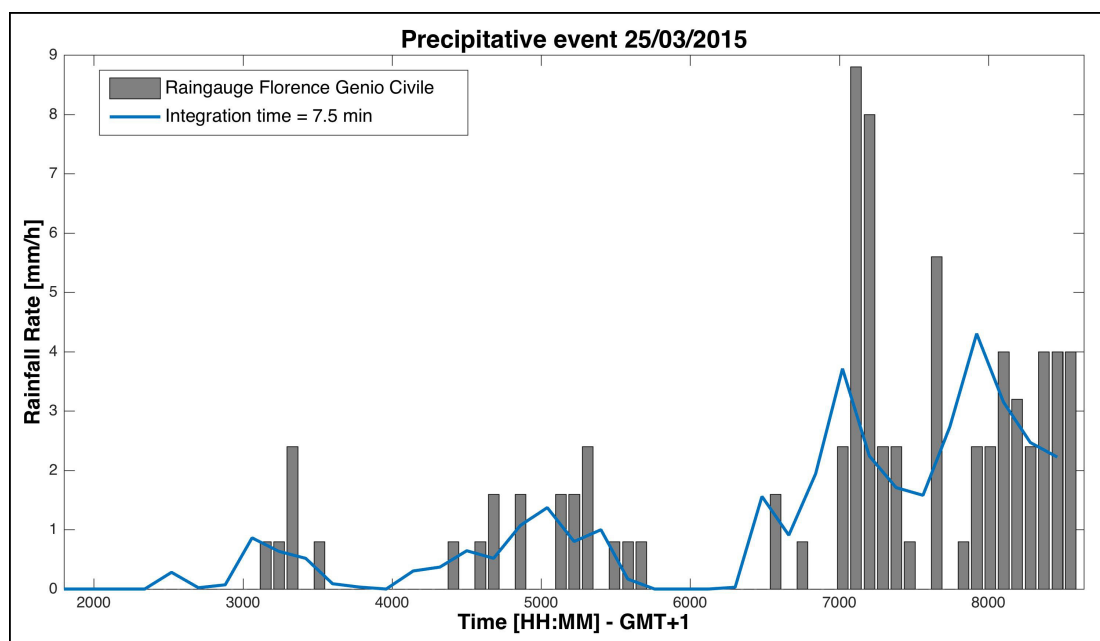


FIGURE 5.40: Rainfall rate evaluated with 7.5' integration times vs measurement by Florence Genio Civile rain gauge

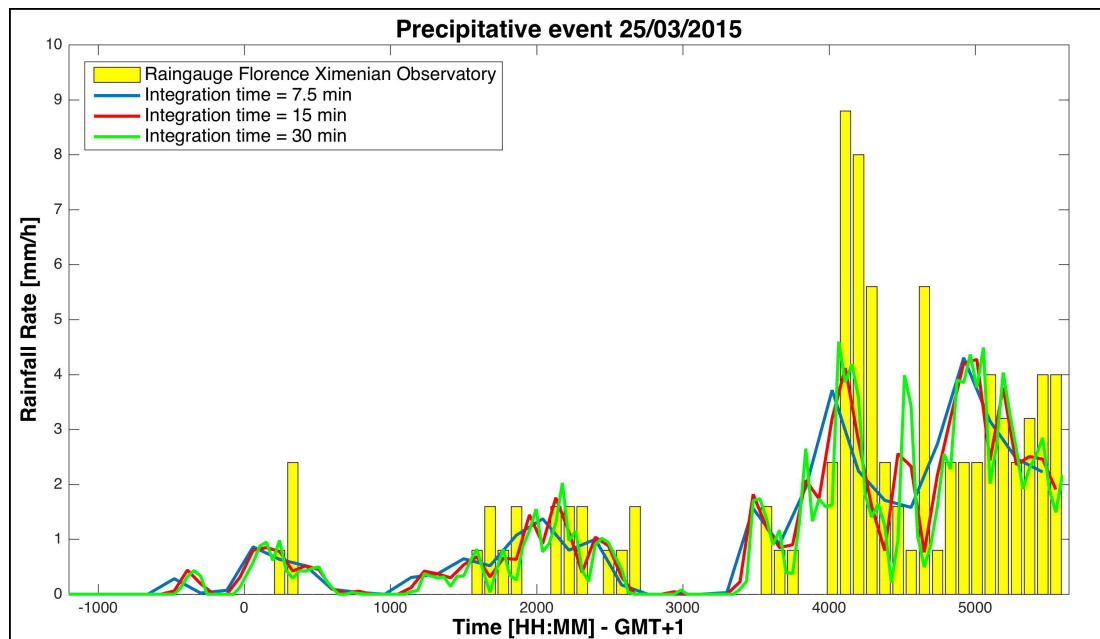


FIGURE 5.41: Rainfall rate evaluated at three different integration times vs measurement by Florence Ximenian Observatory rain gauge

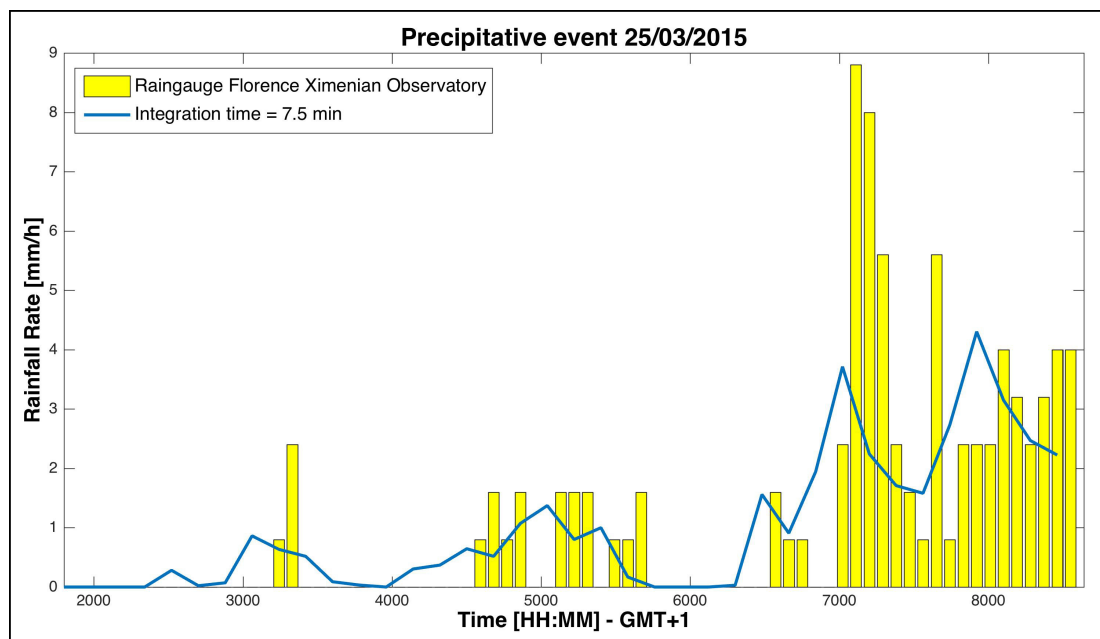


FIGURE 5.42: Rainfall rate evaluated with 7.5' integration times vs measurement by Florence Ximenian Observatory rain gauge

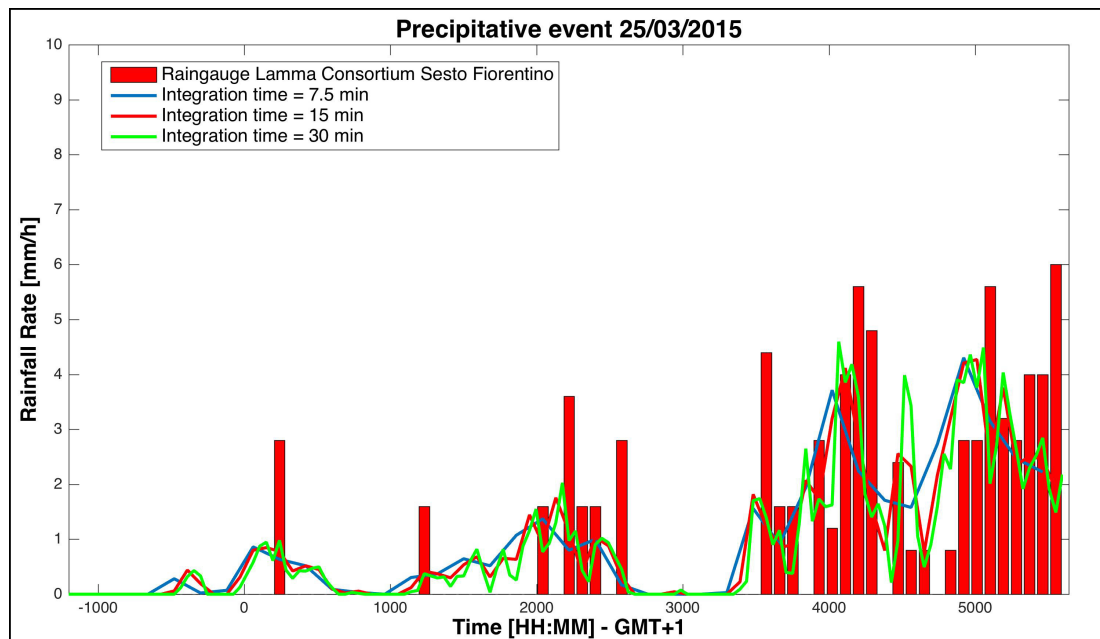


FIGURE 5.43: Rainfall rate evaluated with 7.5' integration times vs measurement by LaMMA Consortium Sesto Fiorentino rain gauge

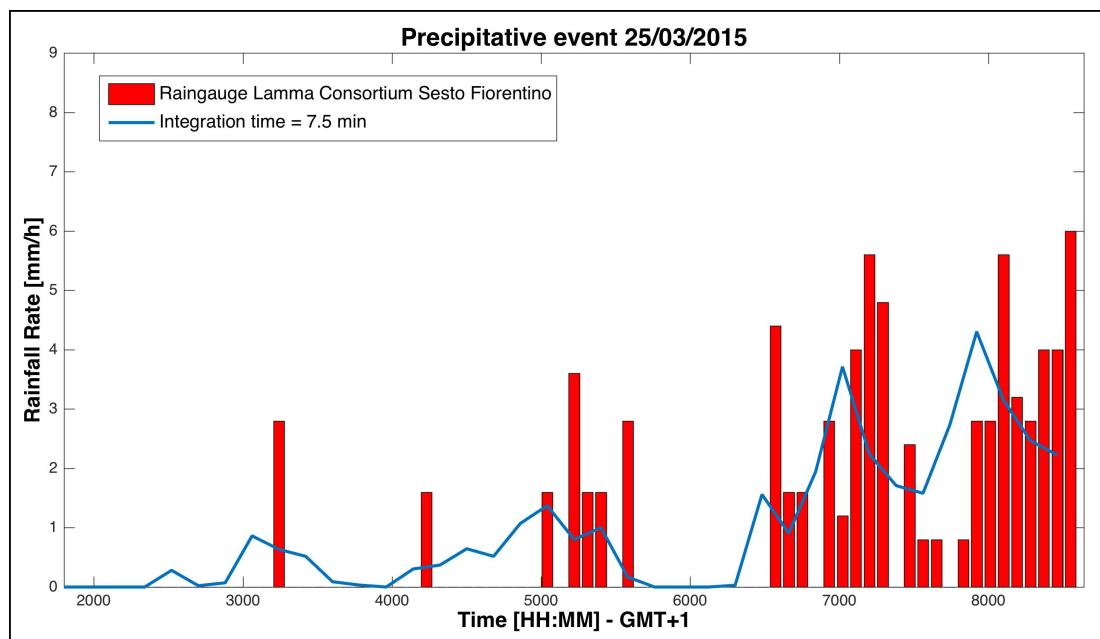


FIGURE 5.44: Rainfall rate evaluated with 7.5' integration times vs measurement by LaMMA Consortium Sesto Fiorentino rain gauge



FIGURE 5.45: The map of the urban area. Rain gauges, Florence airport, Earth station and satellite link are pointed out

### 5.3 4 April 2015

This is a long-temporal event, from 13:00 to 23:00. During the storm the window of CNR was dry by raindrops, so LIDAR could not record cloud data and, the following figures refers just to the rainfall rate retrieved considering only the altitude of cloud layer from METAR bulletins. Figures 5.46 and 5.48 show the values of cumulated rain recorded by regional rain gauges with and without the rainfall rate estimated by RET-AB algorithm. In figure 5.47 the results of processing algorithm are compared: since the  $h_R$  is lower when obtained by METAR bulletins, the corresponding amount of rain is higher.

By splitting the figure 5.48 is it possible to compare in detail every single measure with the value of rainfall rate retrieved by the algorithm.

In all the figures 5.49, 5.50, 5.51, 5.52, 5.53 a disagreement is evident: the peak at 13:30 is not detected by the receiver and, consequently, data processing cannot retrieve such peak. This is possibly due to the fast developing and locally concentrated strong precipitation.

Retrieved amount of rain is then compared with data merged by kriging and, obviously, the peak at 13:30 is still present and evident (figure 5.55).

Since the new algorithm permit to choose the time integration, figure 5.54 outlines the difference between three integration times (7.5', 15' and 30').

To better understand the advantages of a real time estimation, the following figures (5.56 - 5.65) show the benefits by using a real time algorithm such as RET-AB, instead of measurement devices affected by time delay as rain gauges. This advantage is more clear in figures where only the 7.5' integration is superimposed on the rain gauges data (5.57, 5.59, 5.61, 5.63, 5.65).

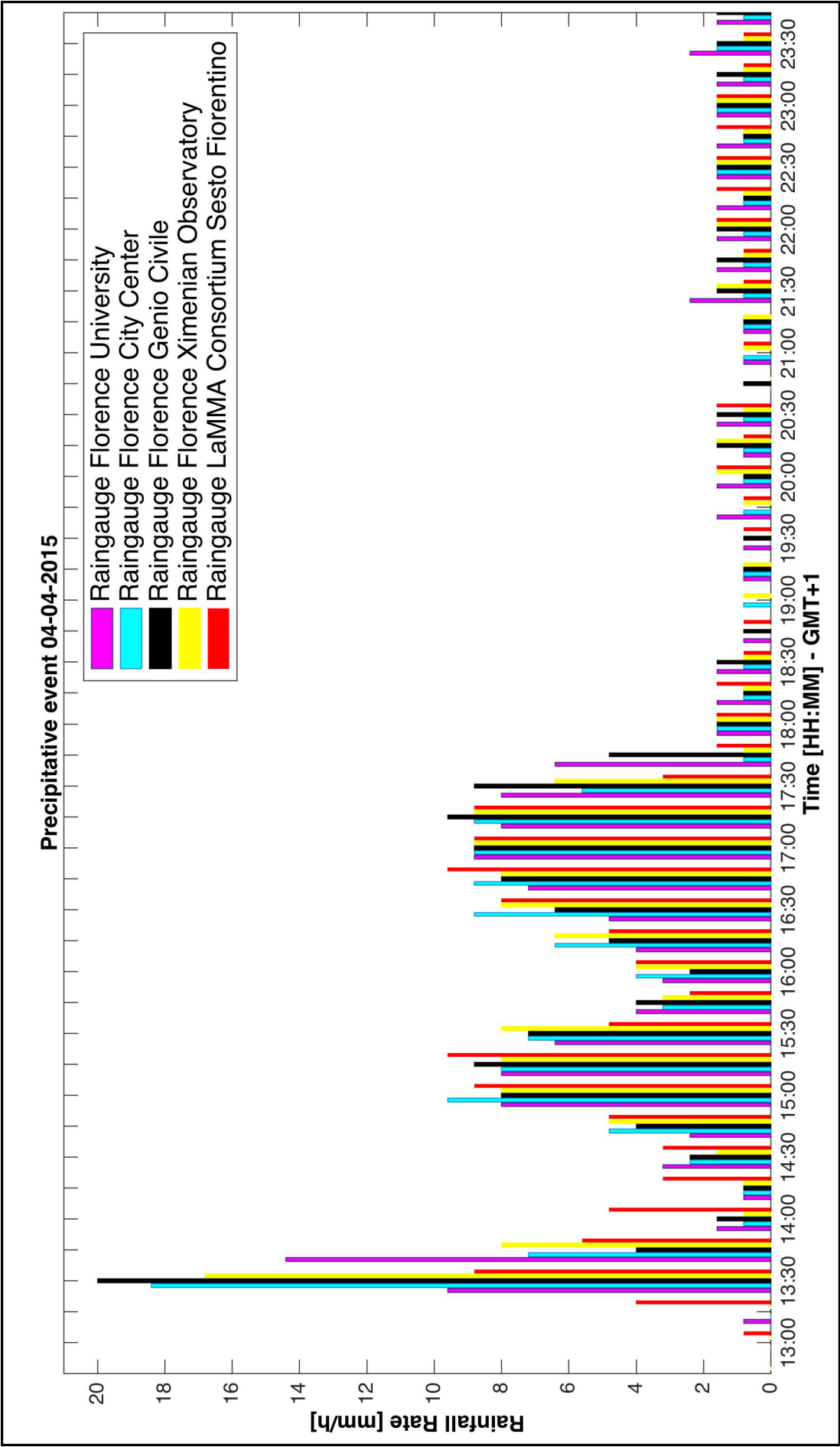
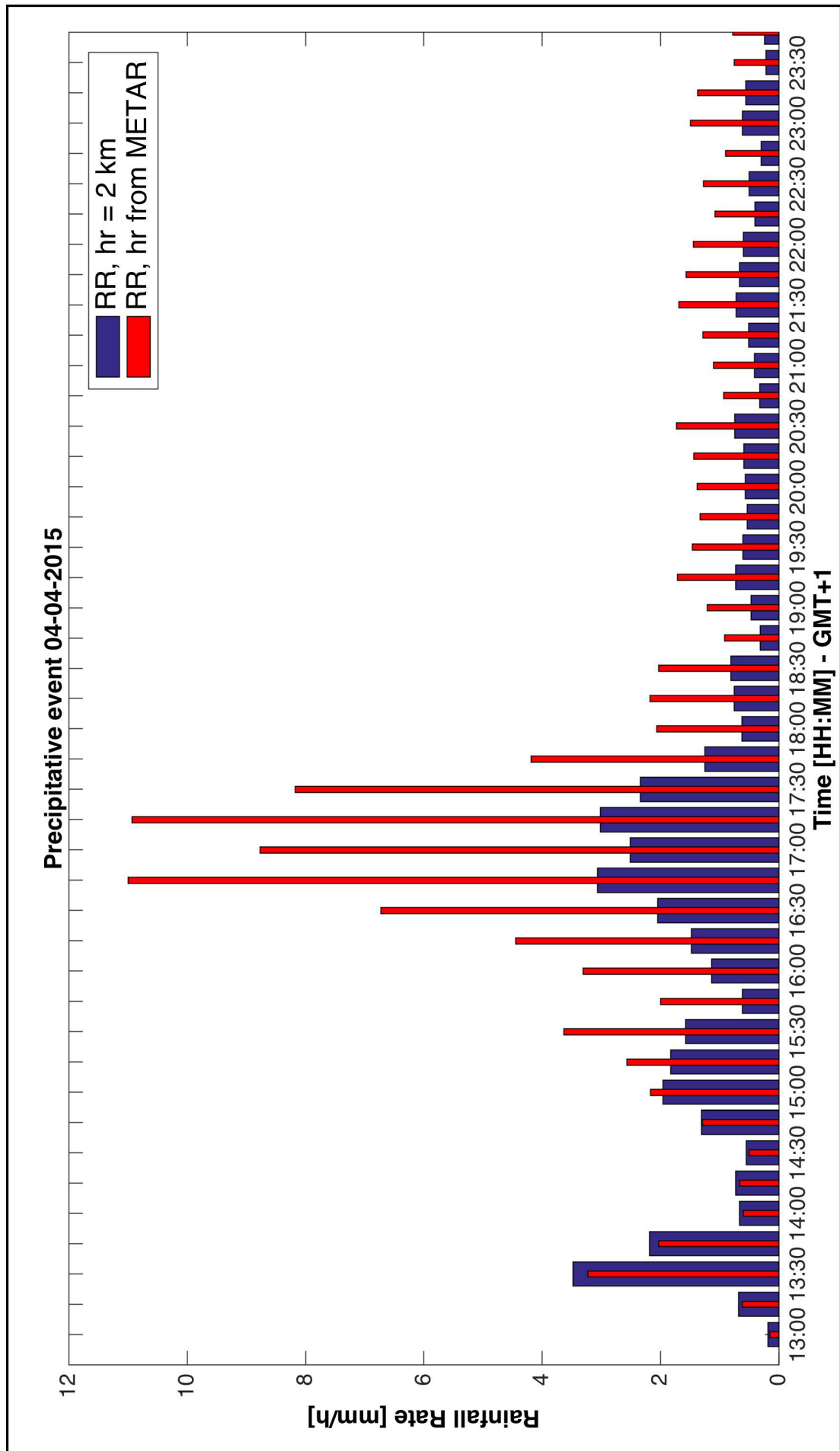


FIGURE 5.46: Rain rate measured by rain gauges

FIGURE 5.47: Rainfall rate: variation of cloud layer  $h_R$  - Fixed vs METAR

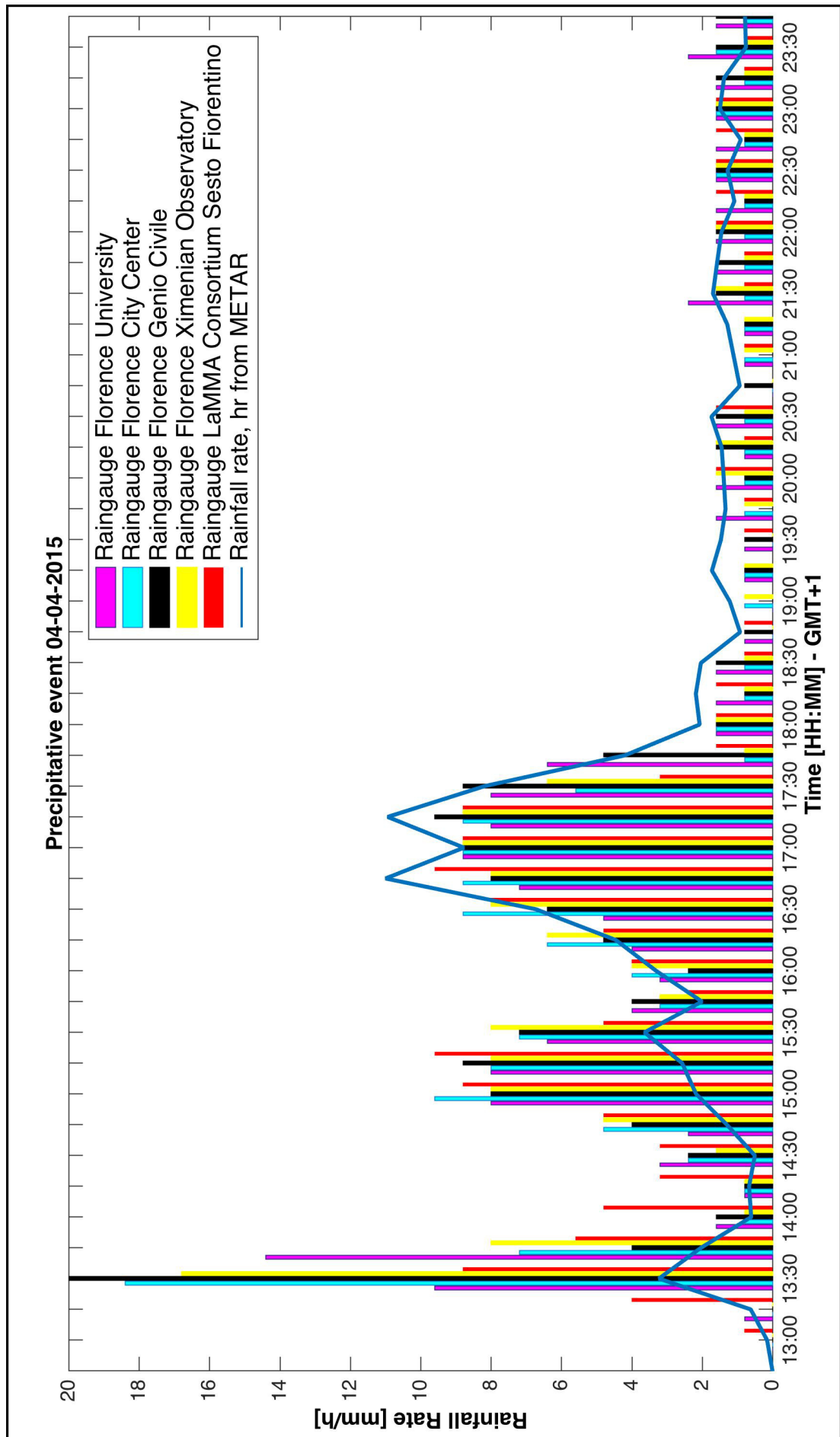


FIGURE 5.48: Rain rate measured by rain gauges vs estimated with RET-AB

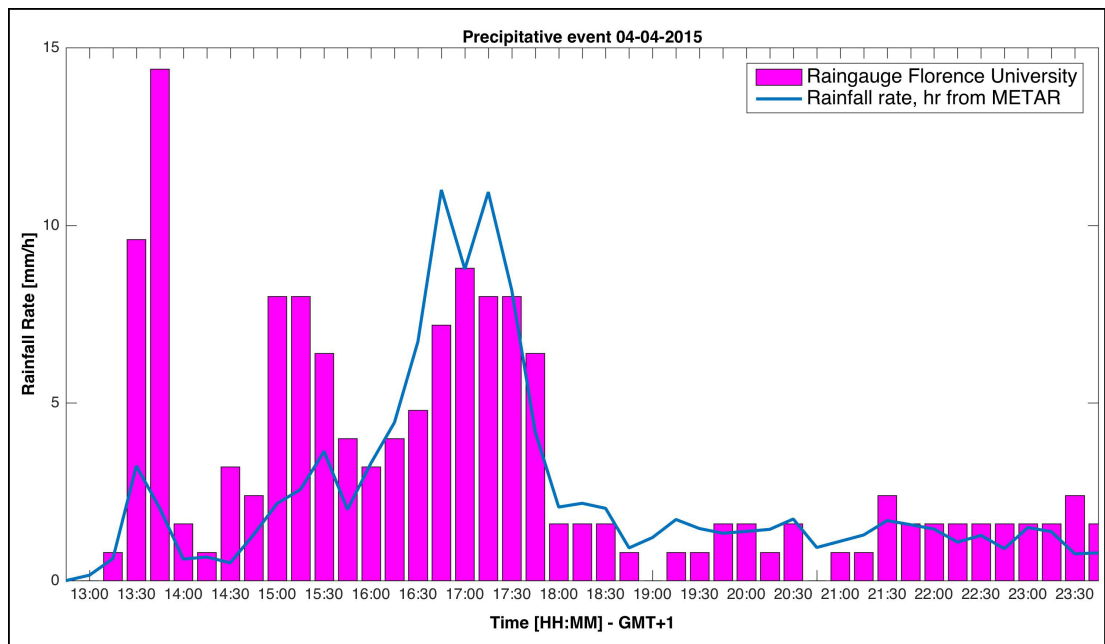


FIGURE 5.49: Rain rate measured by Florence University rain gauge vs estimated with RET-AB

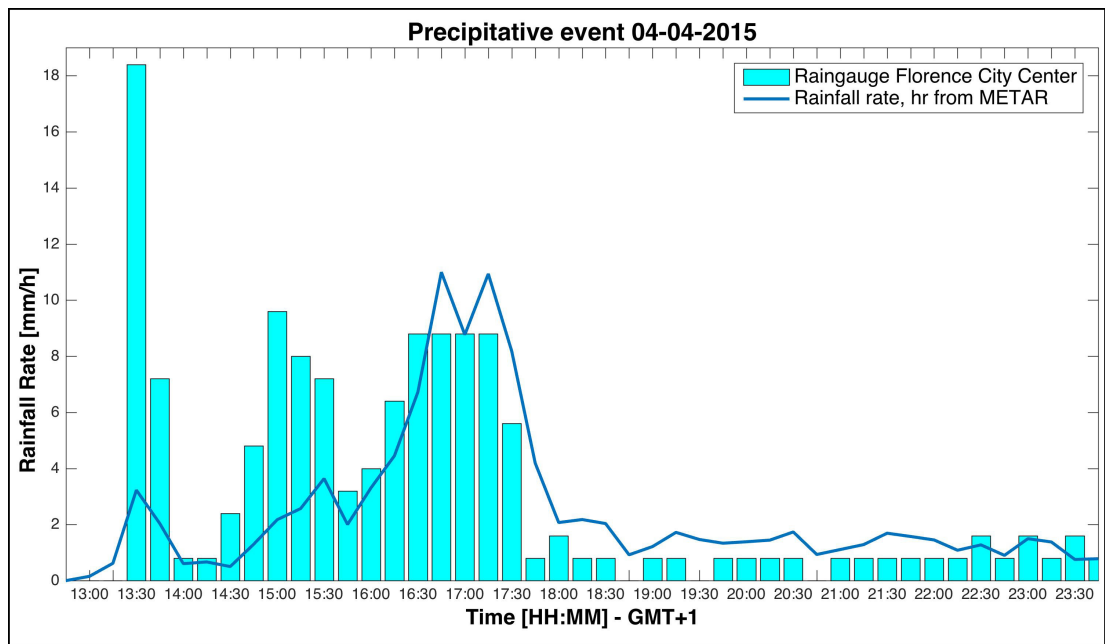


FIGURE 5.50: Rain rate measured by Florence City Center rain gauge vs estimated with RET-AB

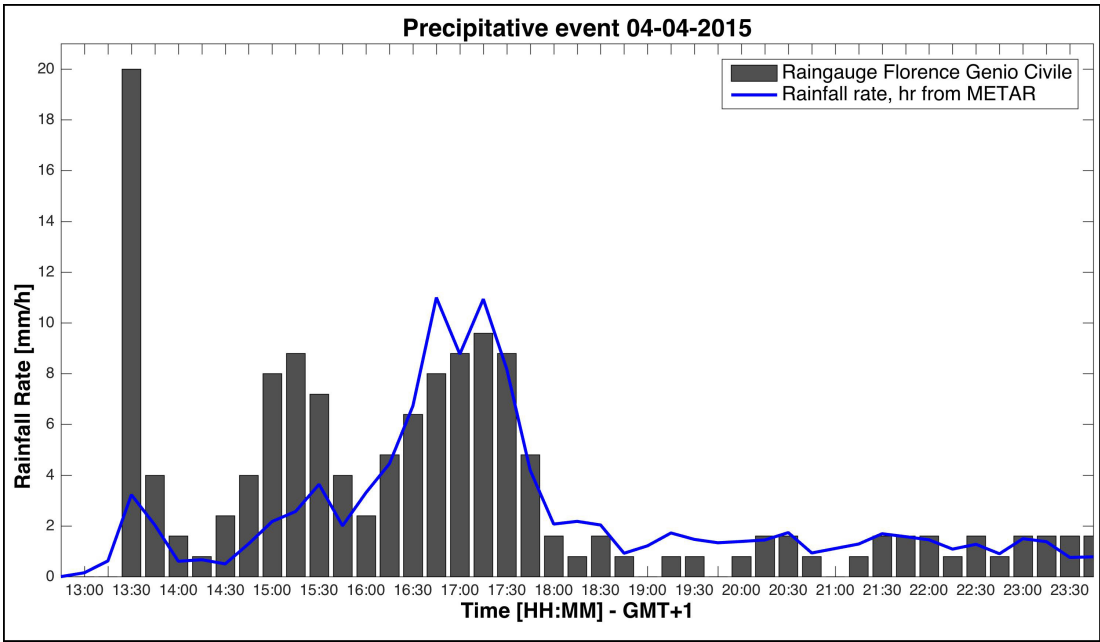


FIGURE 5.51: Rain rate measured by Florence Genio Civile rain gauge vs estimated with RET-AB

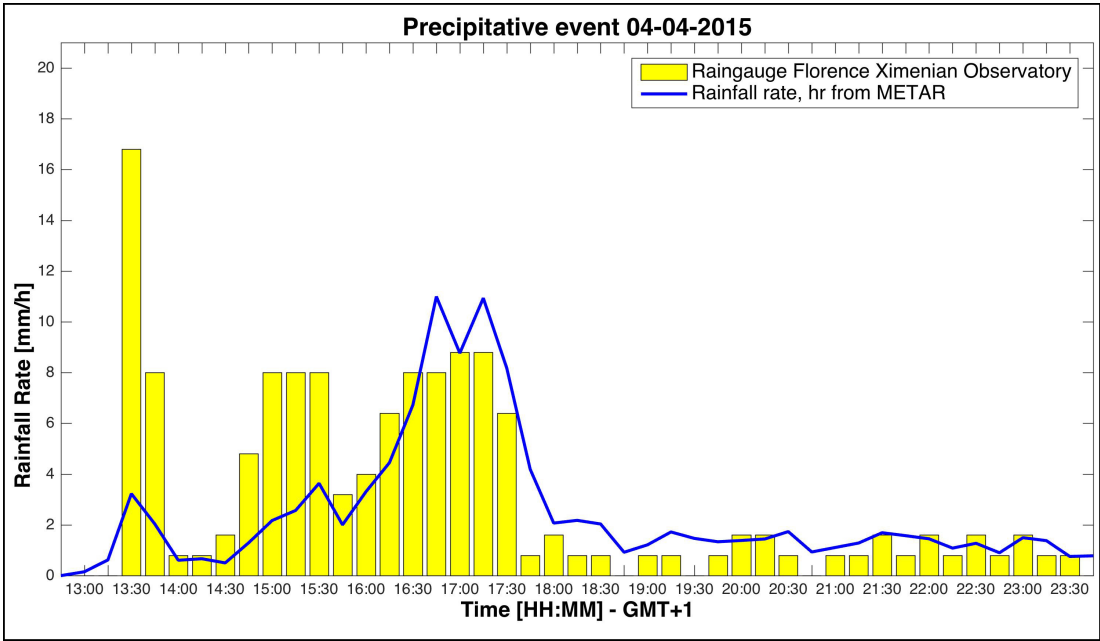


FIGURE 5.52: Rain rate measured by Florence Ximenian Observatory rain gauge vs estimated with RET-AB

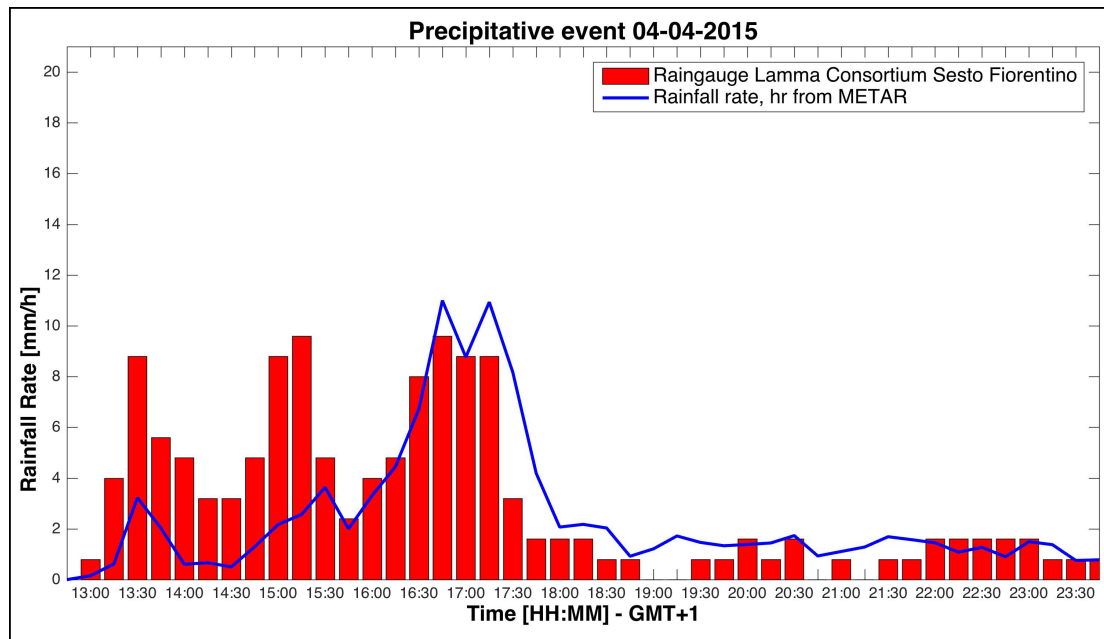


FIGURE 5.53: Rain rate measured by LaMMA Consortium Sesto Fiorentino rain gauge vs estimated with RET-AB

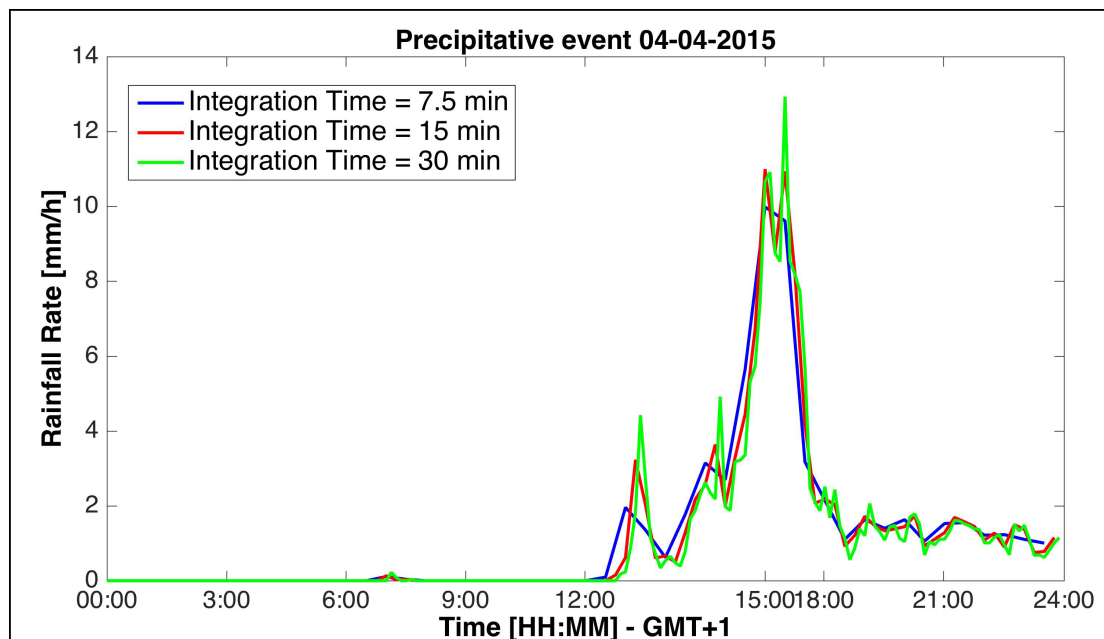


FIGURE 5.54: Rainfall rate evaluated at three different integration times

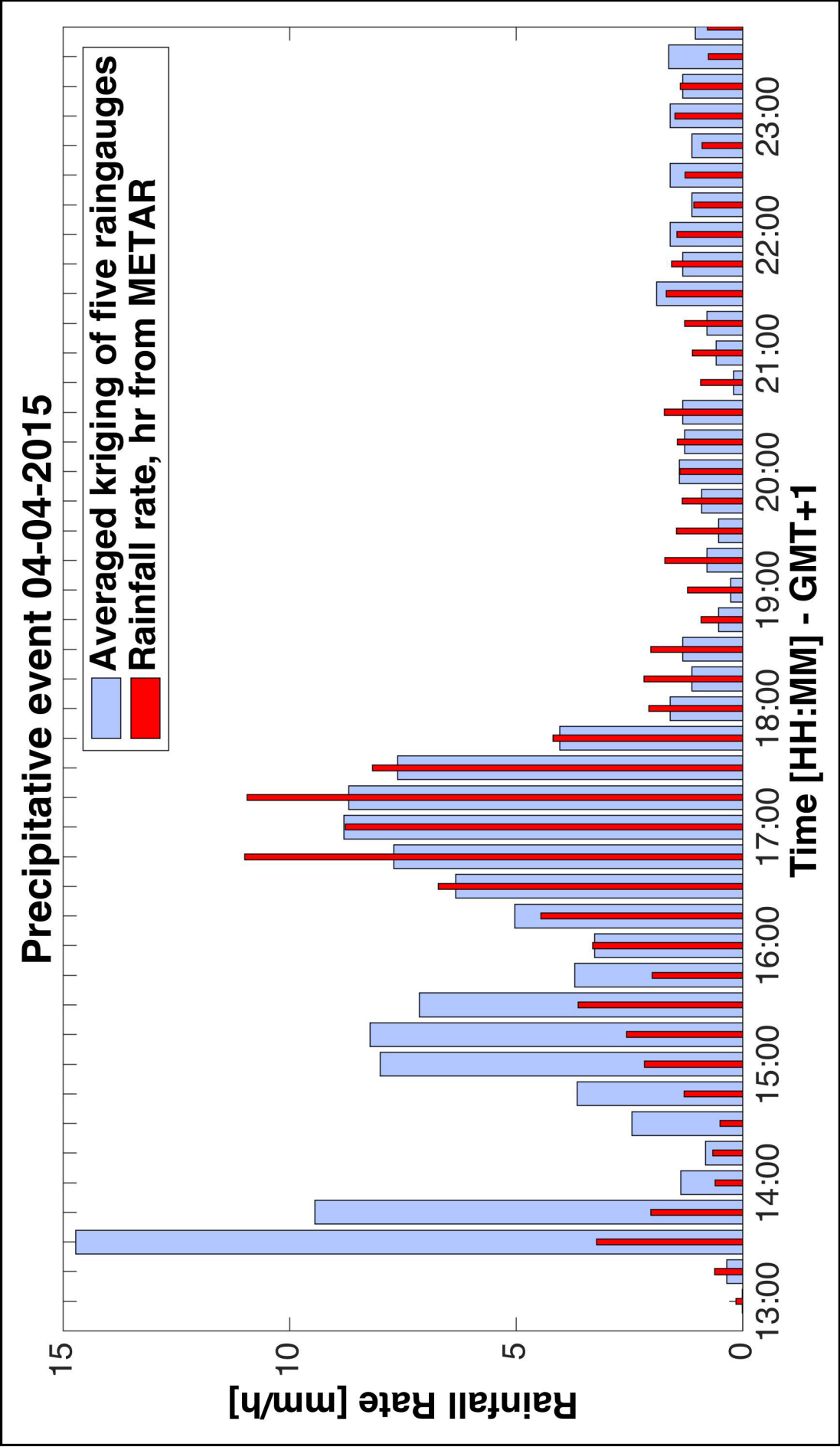


FIGURE 5.55: Comparison of rain rate: estimation with RET-AB vs interpolation with kriging technique

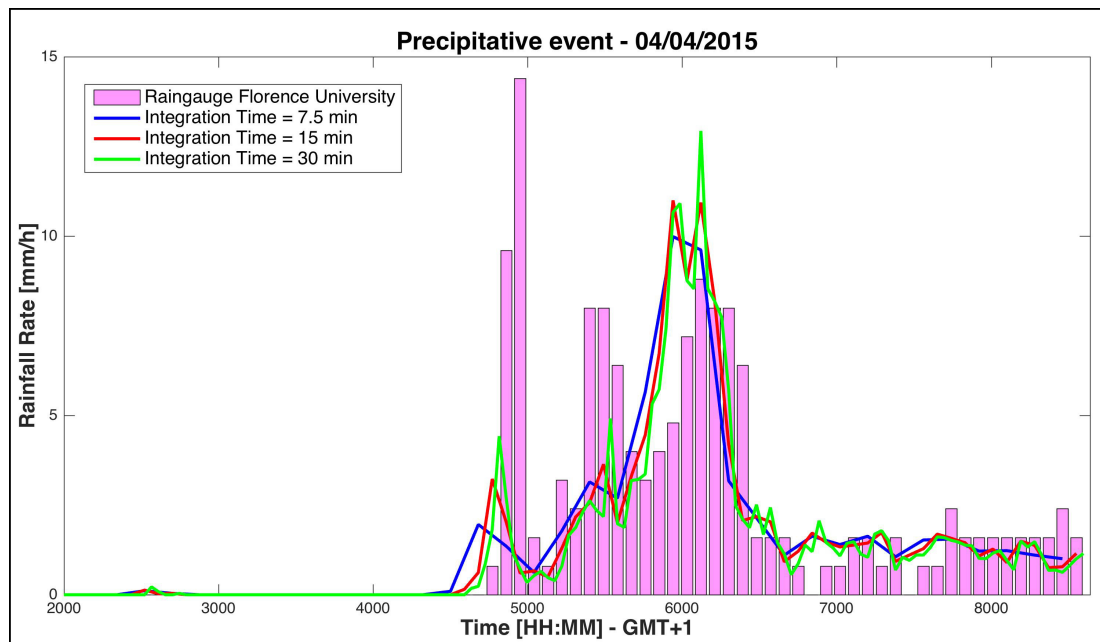


FIGURE 5.56: Rainfall rate evaluated at three different integration times vs measurement by Florence University rain gauge

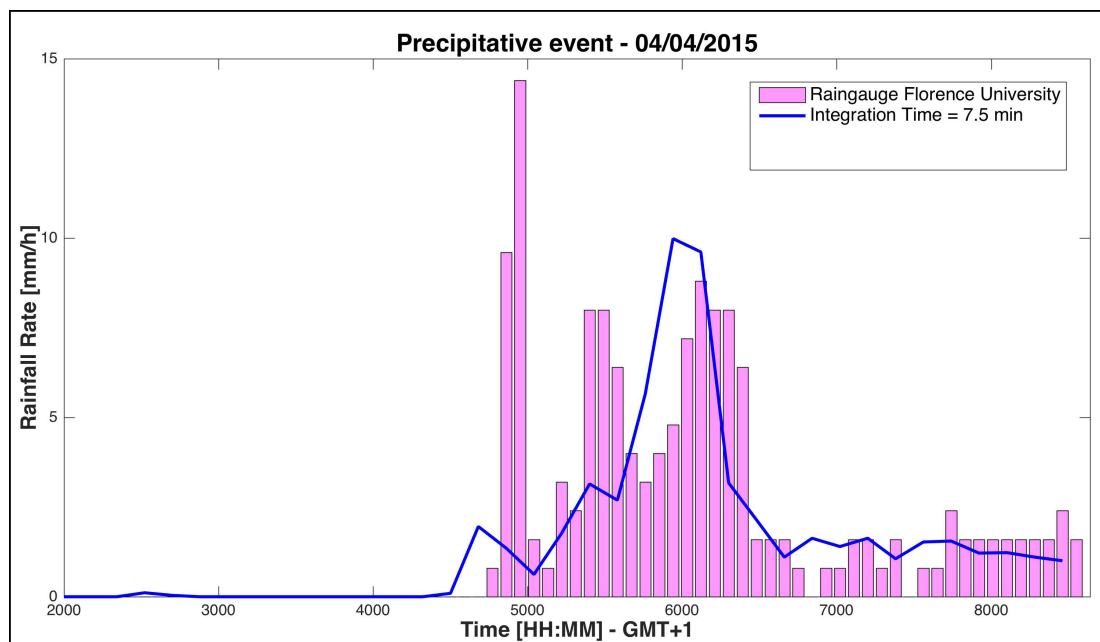


FIGURE 5.57: Rainfall rate evaluated with 7.5' integration times vs measurement by Florence University rain gauge

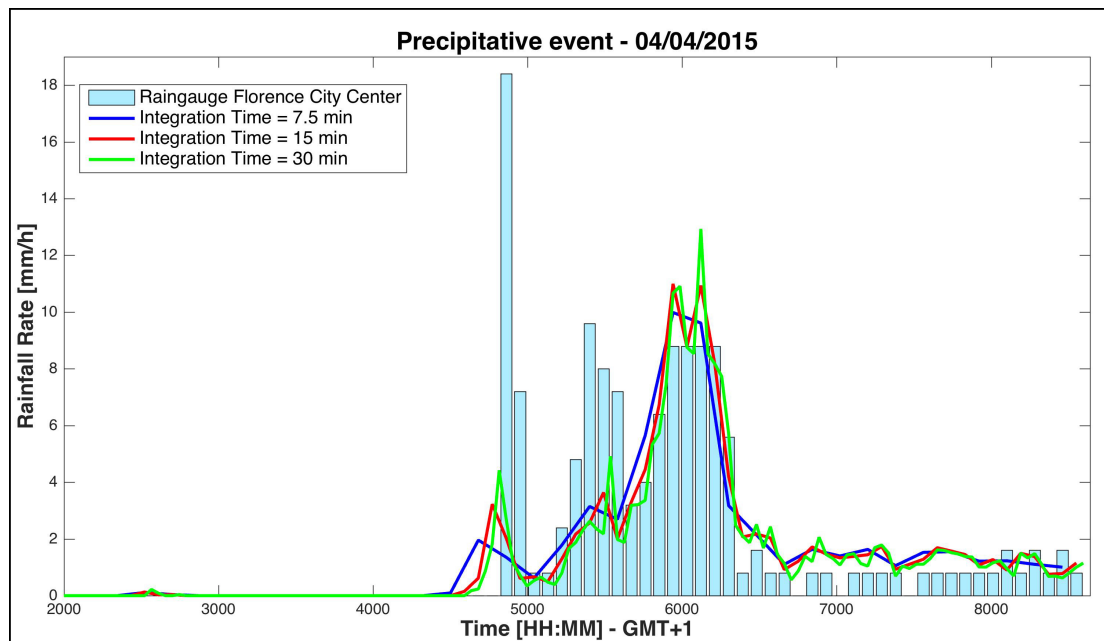


FIGURE 5.58: Rainfall rate evaluated at three different integration times vs measurement by Florence City center rain gauge

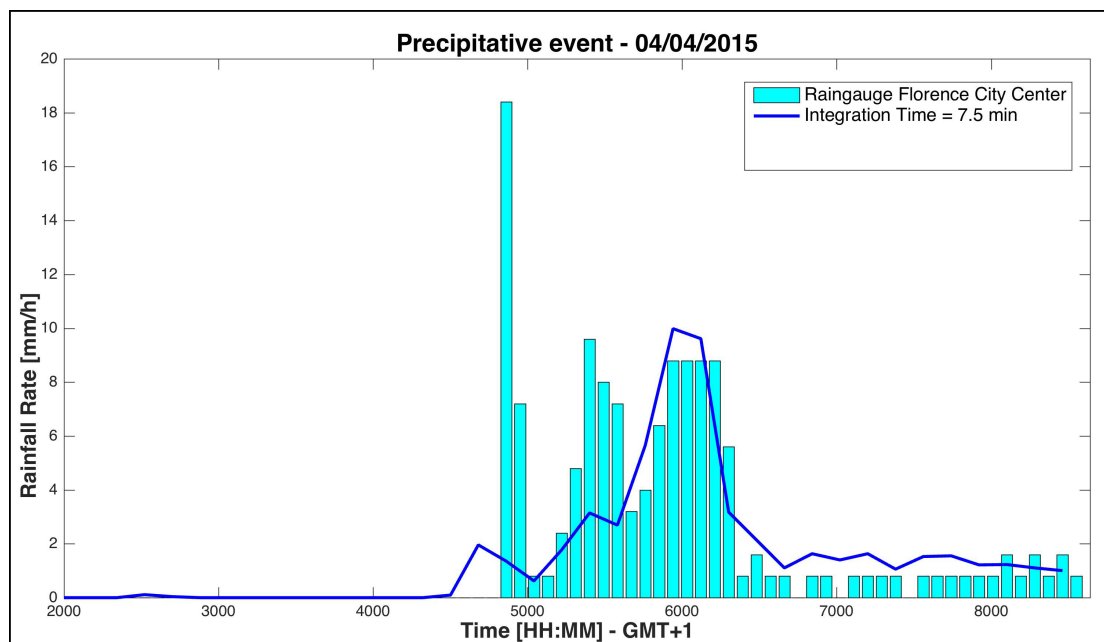


FIGURE 5.59: Rainfall rate evaluated with 7.5' integration times vs measurement by Florence City center rain gauge

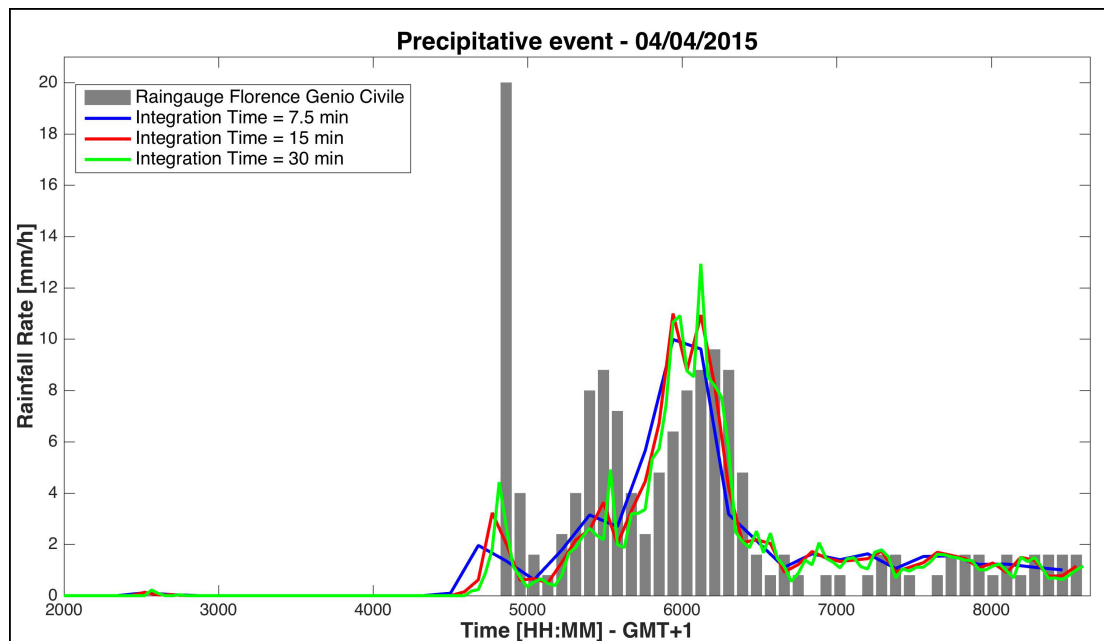


FIGURE 5.60: Rainfall rate evaluated at three different integration times vs measurement by Florence Genio Civile rain gauge

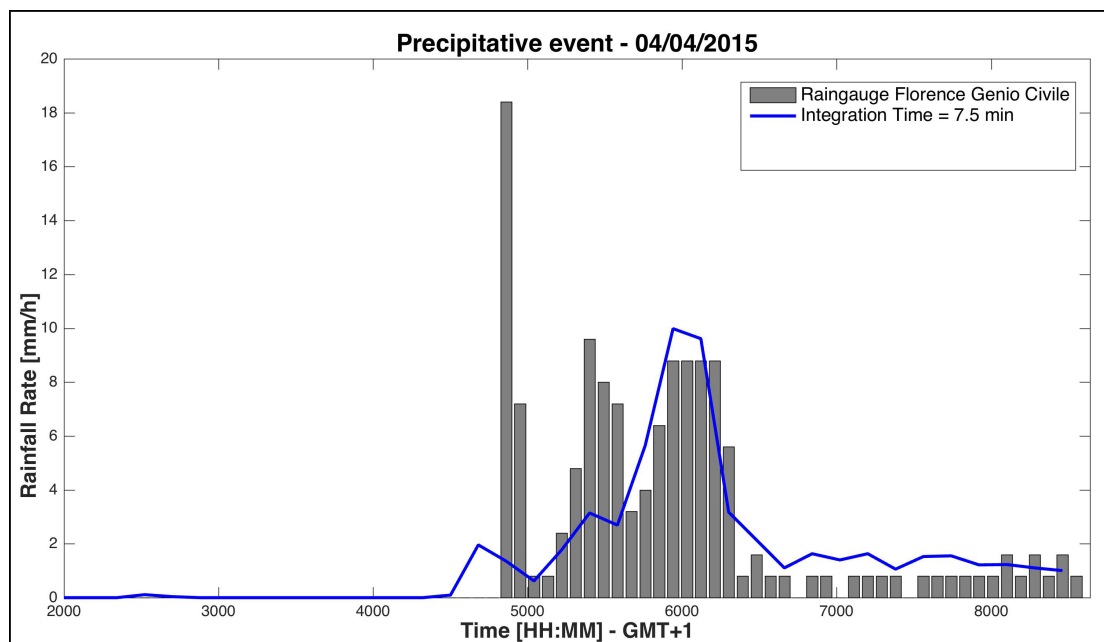


FIGURE 5.61: Rainfall rate evaluated with 7.5' integration times vs measurement by Florence Genio Civile rain gauge

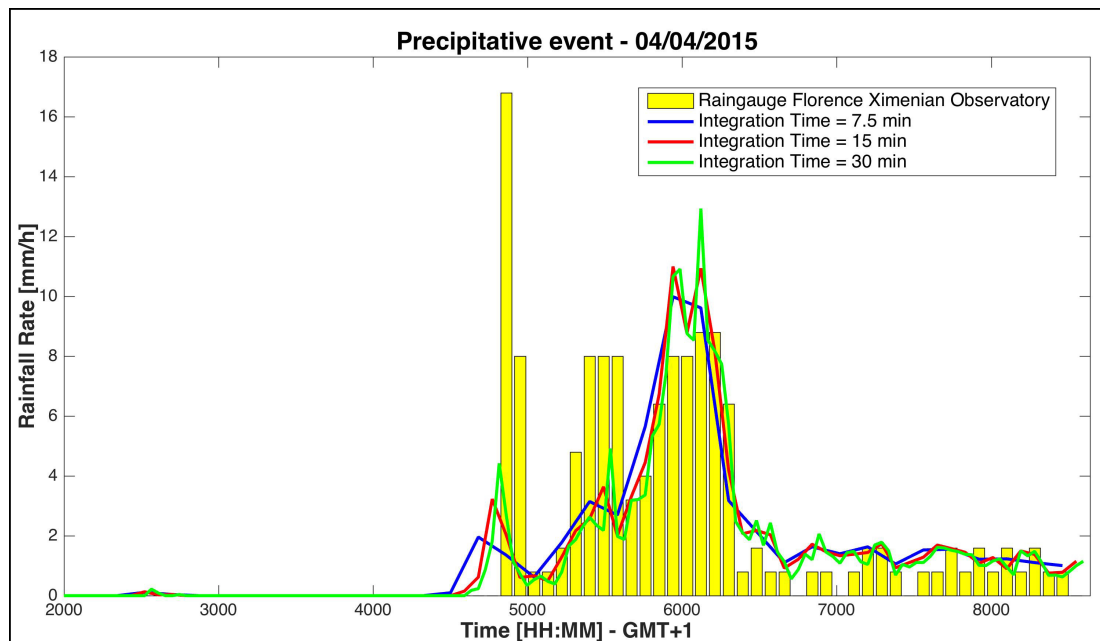


FIGURE 5.62: Rainfall rate evaluated at three different integration times vs measurement by Florence Ximenian Observatory rain gauge

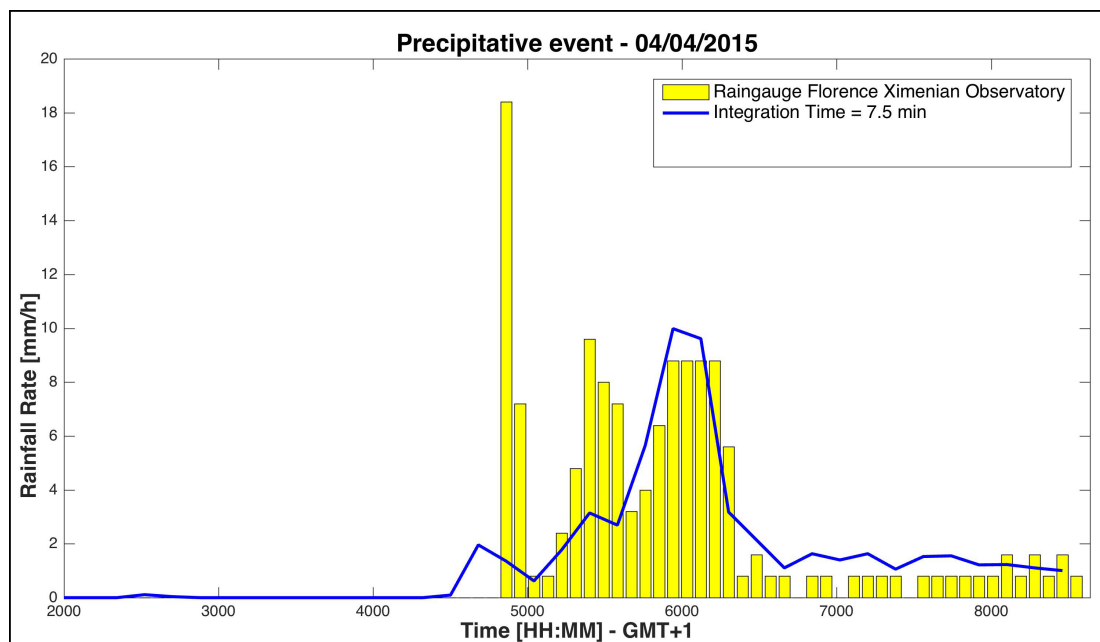


FIGURE 5.63: Rainfall rate evaluated with 7.5' integration times vs measurement by Florence Ximenian Observatory rain gauge

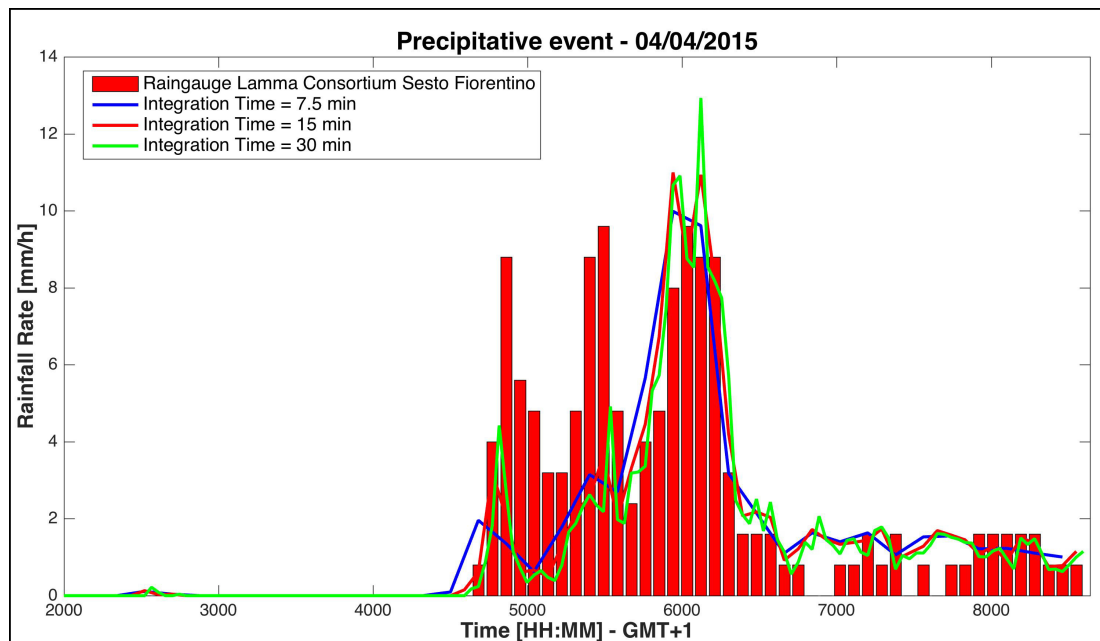


FIGURE 5.64: Rainfall rate evaluated with 7.5' integration times vs measurement by LaMMA Consortium Sesto Fiorentino rain gauge

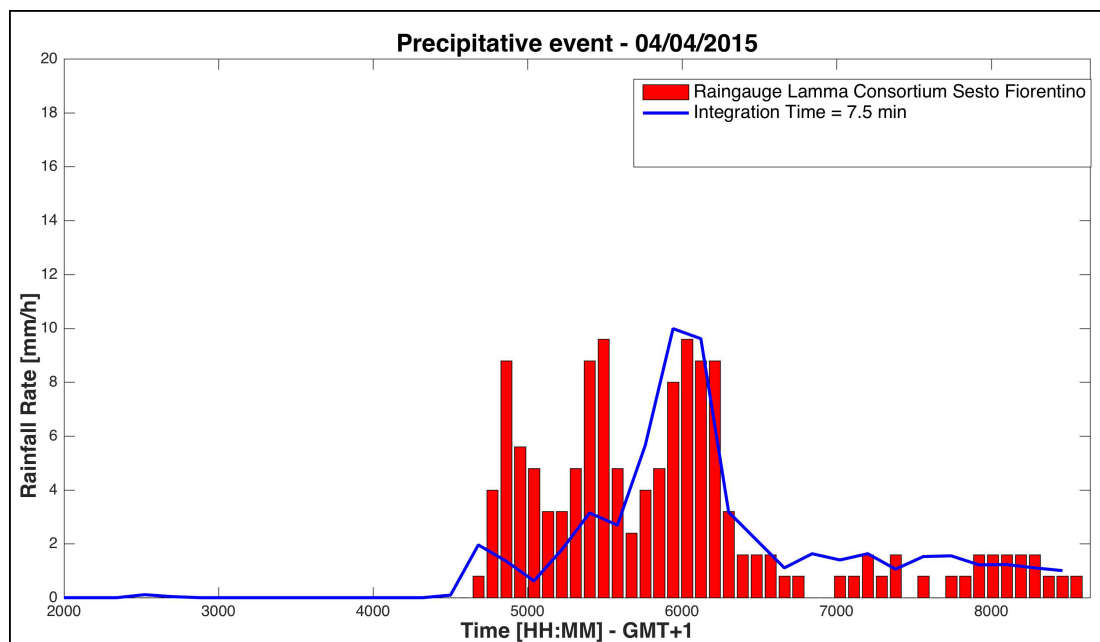


FIGURE 5.65: Rainfall rate evaluated with 7.5' integration times vs measurement by LaMMA Consortium Sesto Fiorentino rain gauge

In conclusion, the results obtained by the measurement campaign could be summarized as follow:

- The main parameter that more affects the results is the altitude of rain height  $h_R$ ;
- two possible methods to retrieve the value of  $h_R$  are data from LIDAR or METAR bulletins (both available online);
- the products of RET-AB algorithm are in agreement with data provided by Regional Authorities;
- the computational cost of the algorithm is low and it can permit a real time processing;
- by changing the integration time it is possible to verify immediatly (dependind on the integration time chosen) a potential threat.

## Chapter 6

# Conclusions and Further Developments

In this thesis a novel inexpensive, remote and automated real-time technique for rainfall estimation over large areas is proposed, based on the opportunistic use of a commercial tool for K<sub>A</sub>-band satellite DSL. In principle, the approach can be applied also in regions characterized by a complex orography that makes it impossible the employment of different methods. The considered method exploits the attenuation introduced by rain on a satellite-ground signal in K<sub>A</sub>-band in order to evaluate the rain rate. The proposed system is composed by instrumentation (parabolic antenna and modem) and an algorithm for data processing. The algorithm, RET-AB, processes data relating to transmitted power (transmitted power is adjusted in case of precipitation in order to guarantee continuous internet services) and retrieves the rainfall rate by inverting the value of attenuation with power law relationship.

Two measurement campaign were held in 2014 and 2015, respectively, which could permit to evaluate the goodness, the reliability and the feasibility of the whole system. By analyzing the results, it clearly appears that, accounting for a few inaccuracies (probably due to the sparse nature of the sensor network employed to validate the results and to the distributed and heterogeneous characteristics of the considered meteorological events) the processed data are quite consistent with that collected by the rain gauges from the competent Regional Authority.

The method relays on a scenario model with a dynamic value of the cloud base height (derived from the suggestion by ITU recommendations in a first approach, from METAR bulletins of the nearest airport and from LIDAR measurements in the second version of the algorithm) and, thanks to the relatively reduced computational load, it allows achieving a quasi-real-time estimation of the rain rate. An integration of the data over

a given time period has been necessary in order to interpret the results with the data from a small network of rain gauges deployed in the surroundings. Finally, a technique to merge the measurements from rain gauges (kriging) has been employed to better evaluate the comparison with the rain rate evaluated along the tract of the satellite link behind the clouds.

## 6.1 Limits of the system

Obviously, the adopted model both the meteorological event and the signal attenuation due to hydrometeors introduce several limits to the accuracy of the proposed approach. In fact, many important physical and environmental factors were not taken into account. Among these aspects, the main to be recalled are:

- the geographical heterogeneity of the precipitation event;
- the time evolution characteristic of a the precipitation event;
- the multilayer structure of the precipitation event;
- the real altitude of the precipitation  $h_R$ ;
- the variability of Drop Size Distribution from a rain event to another and within the same event;
- the different nature of the considered precipitation events;
- the water content of the cloud layer crossed by the satellite link;
- the sparse nature of the rain-gauges network employed for the result's validation.

Despite these necessary considerations, the employment of opportunistic K<sub>A</sub>-band satellite links for the rainfall estimation above urban areas seems quite promising.

## 6.2 Validation of the results

Measurement campaigns lead to the following considerations:

- the estimated rainfall rate trend is quite consistent with data gathered by regional rain gauges;

- the disagreement are probably due to the position of sensors: the devices that measures the cloud altitude (LIDAR installation and sensor generating data for METAR bulletins) are located in an area out of the city center, so far from the direction of the link and, in any case, the estimation can be distorted.

### 6.2.1 Ad-hoc rain gauges network

In order to obtain a correct validation of results, the better solution is the employment of an ad-hoc rain gauges network. The area interest by the link should be equipped with calibrated sensors, spatially displaced along the projection of the link. When all of the sensors measure the same value of rain rate, it means that the precipitation, at that time, has a uniform distribution. The results of data processing could be then compared with the ones measured by sensors in order to proceed to an exact validation of the system products.

### 6.2.2 Computation of $a$ and $b$ parameters

Another important aspect to take into account is the characterization of precipitation in order to define the best value of  $a$  and  $b$  parameters in the power law equation. In fact, the inhomogeneity in DSD within the same precipitation event and especially from an event to another, leads to not negligible errors in the application of the power law expression that bounds the rain-rate and the signal attenuation. A possible method to understand the exact nature of precipitation is the employment of a polarimetric weather radar. Since the weather radar measures, in the same direction of the link, reflectivity and the other polrimetric parameters, it is possible to define the main characteristic of precipitation event. Consequently, it permits to have all the needed information in order to retrieve the values of  $a$  and  $b$  parameters.

## 6.3 Future developments

The proposed method could be improve by employing additional instrumentation or other sources of information (i.e. new data for cloud height).

### 6.3.1 Frequency diversity techniques

In order to improve the system other considerations should be done. Frequency diversity techniques could be adopted. In fact, the possibility to install in proximity of the link a

KU-band receiver for satellite video broadcasting could represent a resource: it can be useful for a complete and more exact estimation, but also to compare the data evaluated at two different band of frequencies.

### 6.3.2 Investigation of other estimation methods for clouds height

In this research many sources to retrieve the exact value of clouds height have been considered.

- Fixed value of  $h_R$ , suggested by recommendation;
- $h_R$  retrieved METAR bulletins, emitted by Florence Peretola airport every 30 minutes and measured by a sensor station located near the airport;
- $h_R$  derived by LIDAR for automatic cloud detection operated by the Institute of Applied Physics - National Research Council (IFAC-CNR), located in Sesto Fiorentino (in the same direction of Florence's airport).

These method produced different results: in fact, since LIDAR and METAR data provide lower measures of  $h_R$ , especially in winter, the corresponding rain rate will be higher than the estimation calculated assuming a fixed and constant value of cloud altitude. In future work some alternative methods could be evaluated. In particular, a relatively inexpensive method is based on stereo-photography with two digital camera [42].

### 6.3.3 Data fusion

Moreover, the possibility of data fusion from different information sources could represent an interesting challenge for designing a complete monitoring system. For example, the recent increase in satellite-DSL users in Europe raises the probability to dispose of multiple overlapping satellite links above the same area, which could be employed to conduct a more accurate assessment of the rainfall intensity. A hypothetical evolution of the system consists in the employment of multiple satellite link overlapped above the urban area, in order to achieve a more accurate characterization of the precipitation and of its time-evolution. Another possible solution could be represented by the integration of multiples and different data to be processed: beside to satellite links measurements, other information sources, like cellular networks or weather radar (when available) or other devices for rainfall evaluation, could be essential in order to create a system as complex as accurate for a whole monitoring of extended areas.

#### 6.3.4 Other improvements

The water content of the clouds-layers interested by the satellite link is responsible for a certain attenuation of the signal, that, in a first approach, have been neglected: that is due to the fact that it is not directly related to the cumulated rainfall measured by the rain gauges. The proposed system does not account for the thickness and the consistency of the clouds above the considered area, than the accuracy of the results decreases whenever the meteorological event is characterized by a clouds layer thicker and richer of water vapor.

A future purpose to improve the whole system is to take in account for these factors and produce a more reliable set of results: a suggestion is to provide the system with a digital camera pointed in the direction of the link, so that, during daytime, it can provide visual information about the clouds layer. This way the processed rainfall data can be interpreted relatively to the characterization of the overall meteorological event. At the same time, another significant parameter that could be considered is the trend and strength of the wind within the area: in fact, during particular events (such as the event of 29 June 2014) wind has played a significant role in evolution of the event, that caused a high variation of the rainfall rate in the same area.

In fact, we are actually working to improve the presented approach by including different sensors such as a digital camera, that provides information about the characteristics of the cloud layers, and an anemometer placed at the Earth station, in order to formulate hypothesis relative to the temporal evolution of the rain event above the city area.

In conclusion, it is possible to affirm that the proposed system, composed by the instrumentation for internet services operating in  $K_A$  and the RET-AB algorithm for data processing, can be considered a valid resource for real time rainfall estimation in order to guarantee a continuously monitoring of areas that can not be monitored by other measurement devices, such as weather radar or rain gauges.

# Bibliography

- [1] Mugnai C., Sermi F., and Cuccoli F. Rainfall estimation with a commercial tool for satellite internet in ka band: concept and preliminary analysis. *SPIE Remote Sensing*, 9239, 2014.
- [2] Mugnai C., Sermi F., Cuccoli F., and Facheris L. Rainfall estimation with a commercial tool for satellite internet in ka band: model evolution and results. *Geoscience and Remote Sensing Symposium (IGARSS)*, pages 890 – 893, July .
- [3] Australian Government Bureau of Metrology. URL <http://www.bom.gov.au/climate/cdo/about/rain-measure.shtml>.
- [4] J. R. Probert-Jones. The radar equation in meteorology. *Quarterly Journal of the Royal Meteorological Society*, 88:485–495, 1962.
- [5] Olsen R. L., Rogers D. V., and Hodge D. B. The arb relation in the calculation of rain attenuation. *IEEE Transactions On Antennas and Propagation*, 26:318–329, 1978.
- [6] J. Marshall and W. Palmer. The distribution of raindrops with size. *Journal of Meteorology*, 5:165–166, 1948.
- [7] V. N. Bringi and V. Chandrasekar. *Polarimetric Doppler Weather Radar: Principles and Applications*. Cambridge University Press, 1st edition edition, 2001.
- [8] Zinevich A., Alpert P., and Messer H. Estimation of rainfall fields using commercial microwave communication networks of variable density. *Advances in Water Resources*, 31:1470–1480, 2008.
- [9] Zinevich A., Messer H., and Alpert P. Frontal rainfall observation by a commercial microwave communication network. *Journal of Applied Meteorology and Climatology*, 48:1317–1334, 2009.
- [10] Messer H., Goldeshtein O., Rayitsfeld A., and Alpert P. Environmental monitoring by wireless communication networks. *Science*, 312:713,.

- [11] Ostrometzky J., Cherkassky D., and Messer H. Accumulated mixed precipitation estimation using measurement from multiple microwave links. *Advances in Meteorology*, 2015.
- [12] Leijinse H., Uijlenhoet R., and Stricker N.M. Rainfall measurement using radio links from cellular communication networks. *Water Resources Research*, 43, 2007.
- [13] Chwala C., Kunstmann H., Hipp S., Siart U., , and Eibert T. Precipitation observation using commercial microwave communication links. *Geoscience and Remote Sensing Symposium (IGARSS)*, 5:2922–2925, July 2012.
- [14] Giuli D., Facheris L., and Tanelli S. A new microwave tomography approach for rainfall monitoring over limited areas. *Physics and Chemistry of the Earth*, 22: 265–273, 1997.
- [15] Giuli D., Facheris L., and Tanelli S. Microwave tomographic inversion technique based on stochastic approach for rainfall fields monitoring. *IEEE Transaction on Geoscience and Remote Sensing*, 37:2536–2555, 1999.
- [16] Minda H. and Nakamura K. High temporal resolution path-averaged raingauge with 50-ghz band microwave. *Journal of Atmospheric Oceanic Technology*, 22:165–179, 2005.
- [17] Holt A. R., Kuznetsov G. G., and Rahimi A. R. Comparison of the use of dual frequency and single frequency attenuation for the measurement of rainfall along a microwave links. *IEEE Proc. Microwave Antenna Propagation*, 150:315–320, 2003.
- [18] Berne A. and Uijlenhoet R. Path-averaged rainfall estimation using microwave links: Uncertainty due to spatial rainfall variability. *Geophys. Res. Lett.*, 34, 2007.
- [19] Kharadly M. M. Z. and Ross R. Effect of wet antenna attenuation on propagation data statistic. *IEEE Trans. Antenna Propagation*, 49:1183–1191, 2001.
- [20] Levizzani V. Satellite rainfall estimates: new perspectives for meteorology and climate from the eurainsat project. *Annals of Geophysics*, 46:363–372, 2003.
- [21] Kistawal C. M. Satellite remote sensing and gis. *Application in agriculture meteorology*, July 2003.
- [22] Arslan C. H., Aydin K., Urbina J., and Dyrud L. P. Rainfall measurement using satellite downlink attenuation. *Geoscience and Remote Sensing Symposium (IGARSS)*, pages 4111–4114, July 2014.
- [23] Malinga S. J., Owolawi P.A., and Afullo T. J. O. Estimation of rain attenuation at c, ka, ku, and v bands for satellite link in south africa. *Progress in Electromagnetics Research Symposium (PIERS)*, pages 948–958, March 2013.

- [24] Sudarshana K. P. S. and Samarasinghe A. T. L. K. Rain rate and rain attenuation estimation for ku band satellite communication over sri lanka. *International Conference on Industrial and Information System*, pages 1–6, August 2011.
- [25] Maitra A. and Chakravarty K. Ku band rain attenuation observation on an earth space path in the indian region. *IEEE Trans. On Antennas and Wireless Propag. Letter*, 3:180–181, 2004.
- [26] Barthès L. and Mallet C. Rainfall measurement from opportunistic use of earth-space link in ku band. *Atmospheric Measurement Techniques*, 6:2181–2193, July 2013.
- [27] Rogers D. V., Ippolito L. J., and Davarian F. System requirement for ka-band earth satellite propagation data. *IEEE preceedings*, 85, June 1997.
- [28] ITU-R p.618 8. Propagation data and prediction methods required for the design of earth-space telecommunication systems. In *International Telecommunication Union*, Geneve, 2003-04.
- [29] ITU-R p.676 10. Approximate estimation of gaseous attenuation in the frequency range 1-350 ghz. In *International Telecommunication Union*, Geneve, 2013.
- [30] ITU-R p.840 5. Attenuation due to clouds and fog. In *International Telecommunication Union*, Geneve, 2012.
- [31] Crane P. K. Prediction of the effects of rain on satellite communication system. *IEEE Proc*, 65(3):456–474, 1977.
- [32] Bhattacharya R., Das R., Guha R., Deb Barman S., and Battacharya A. B. Variability of millimetrewave rain attenuation and rain rate prediction: A survey. *Indian Journal of Radio and Space Physics*, 36:325–344, August 2007.
- [33] Capsoni C., Fedi F., Magistoni C., and Paraboni A. Data and theory for a new model of horizontal structure of rain cells for propagation applications. *Radio Science*, 22(3):395–404, 1987.
- [34] Goldhirsh J. and Katz I. Useful experimental results for earth-satellite rain attenuation modeling. *IEEE Transactions on Antennas and Propagation*, page 413, 1979.
- [35] Karasawa Y. and Maekawa Y. Ka-band earth space propagation research in japan. *IEEE preceedings*, 85, June 1997.
- [36] ITU-R p.838 3. Specific attenuation model for rain for use in predicting methods. In *International Telecommunication Union*, Geneve, 2003.

- [37] Venema V., Russchenberg H., Apituley A., van Lammeren A., and Ligthart L. Cloud boundary height measurements using lidar and rada. *Physics and Chemistry of the Earth*, 25:129–134, July 2000.
- [38] Del Guasta M. URL <http://lidarmax.altervista.org/lidar/Lidaronline.php>.
- [39] Baglioni A. and Del Guasta M. Image processing for automatic cloud detection from lidar data. *25th International Laser Radar Conference*, July 2010.
- [40] Sideris I.V., Gabella M., Erdin R., and Germann U. Real-time radar–rain-gauge merging using spatio-temporal co-kriging with external drift in the alpine terrain of switzerland. *Quarterly Journal of the Royal Meteorological Society*, 140:1097–1111, April 2014.
- [41] Berne A., Delrieu G., Creutin J.D., and Obled C. Temporal and spatial resolution of rainfall measurements required for urban hydrology. *Journal of Hydrology*, 299: 166–179, 2004.
- [42] Andreev M., Chulichkov A.I., Medvedev A.P., and Postylyakov O.V. Estimation of cloud base height using ground-based stereo photography: Method and first results. *SPIE Remote Sensing*, 9242, 2014.